Europa's Surface Composition

R. W. Carlson
NASA Jet Propulsion Laboratory/California Institute of Technology

W. M. Calvin
University of Nevada

J. B. Dalton
NASA Jet Propulsion Laboratory/California Institute of Technology

G. B. Hansen
University of Washington

R. L. Hudson
Eckerd College

R. E. Johnson
University of Virginia

T. B. McCord
Bear Fight Center

M. H. Moore
NASA Goddard Space Flight Center

Europa is unique in the solar system, having a young, icy surface bombarded by high-energy radiation and possessing many possible sources of surface material. One possible source is Europa's putative subsurface ocean, from which material may be emplaced through cryovolcanic activity or effusive flows. Impact ejecta from Io and implantation of iogenic sulfur, oxygen, sodium, potassium, and chlorine ions on Europa's trailing hemisphere are likely sources, as well as direct meteoritic and cometary impacts and outer-satellite-derived impact ejecta that spiral toward Jupiter. While we cannot yet answer the central question of where the non-ice material on Europa's surface comes from, we can identify and quantify the species that are known or thought to be present: H_2O, a hydrate, SO_2, elemental sulfur, O_2, H_2O_2, CO_2, Na, and K. Europa, like many satellites, has a hemispherical dichotomy, in this case a reddish trailing hemisphere (in the sense of orbital motion) and a brighter, leading hemisphere. The purest H_2O is found on the leading hemisphere while the trailing hemisphere contains the highest concentration of the next most prevalent species, a hydrated material of unknown composition. The H_2O ice on the leading side is amorphous on the upper surface, with crystalline ice present at submillimeter depths. The trailing hemisphere contains ice plus a hydrated component that may be hydrated salts, derived from the ocean as brine, and/or hydrated sulfuric acid, the major equilibrium product from radiolysis of sulfurous material and H_2O. The source of sulfurous material could be endogenic or from implantation of iogenic sulfur, or both. Sulfur dioxide and sulfur are thought to be present, mainly on the trailing hemisphere. This is consistent with ion implantation, but the sulfur distribution and that of the hydrate show correlations with geological features, so there must be some endogenic control of these constituents, either as a source or modification process. All the species in the ~1-m regolith are affected by radiation, but the archetypal radiolytic species, observed on both hemispheres, are molecular oxygen and hydrogen peroxide. These are certainly radiolytic products since continuous production is required, with O_2 being volatile and escaping easily, while H_2O_2 is quickly destroyed by sunlight. Carbon dioxide is present and poses a mystery. It could be outgassing from the interior or a photolytic or radiolytic product of micrometeorite-derived carbonaceous material. Sodium and potassium atoms are found in the tenuous atmosphere and arise from sputtering of surface material. These atoms can be derived initially from the iogenic plasma and from endogenic salts, but the implantation flux rates are not known well enough to establish the source.

1. INTRODUCTION

1.1. Introduction

Europa is a fully differentiated planet-sized satellite with a Fe or Fe-FeS core, a silicate mantle, and a 100- to 160-km-thick outer layer consisting of an icy crust covering a probable ocean (see chapter by Schubert et al.). Like Io, Europa is tidally heated and is currently (or recently) geologically active, exhibiting a crater age of 40 to 90 m.y. (*Zahnle et al.,* 2003; see chapter by Bierhaus et al.). While the surface is smooth on a large scale, at higher spatial detail it is modified everywhere by cracking of the brittle surface and possible convective motions within its ductile icy shell, producing lineae (long ridge systems often with a bright center band and dark margins), lenticulae (termed pits, spots, and domes), and chaos regions suggestive of partial melting. An active Io-like body may be hidden below the ice cover with possible hydrothermal activity at the ocean-mantle interface (*Kargel et al.,* 2000) and oceanic material may be emplaced on the surface. Other sources of surface material include exogenic material from Io and possibly other satellites, from the jovian magnetosphere, and from comet and meteorite impacts. These impacts also churn and mix the surface, producing an icy regolith. In addition, Europa is irradiated by high-energy particles that radiolytically modify the surface material and produce a tenuous sputtered atmosphere with species that are indicative of the surface composition. Impact gardening and micrometeoric deposition occurs predominantly on the leading side (in the sense of orbital motion), while plasma implantation and bombardment by high-energy electrons are strongest in the trailing hemisphere. These processes can lead to the observed hemispheric albedo differences, producing the "white" and "red" hemispheres (*Johnson and Pilcher,* 1977) shown in Fig. 1. Nonsynchronous rotation of Europa's shell, if occurring, would moderate these influences. While the surface appears geologically younger, brighter, and much icier than the other icy Galilean satellites, it does show the presence of non-ice materials, and these materials can provide clues to Europa's formation and evolution. Distinguishing between exogenic or endogenic source(s) of Europa's non-ice material is of particular interest. This is a question that we cannot yet answer, but is a guiding theme of this chapter.

In this chapter we first discuss the possible sources of surface species (section 1.2) and then chemical and physical alteration processes that can change the composition or distribution (section 1.3). The observational methods are briefly described (section 1.4) and a listing of known and suggested species is presented. Supporting laboratory studies are briefly discussed (section 1.5), followed by detailed discussions of each species (section 2). Some recommendations for future observations and experiments conclude the chapter.

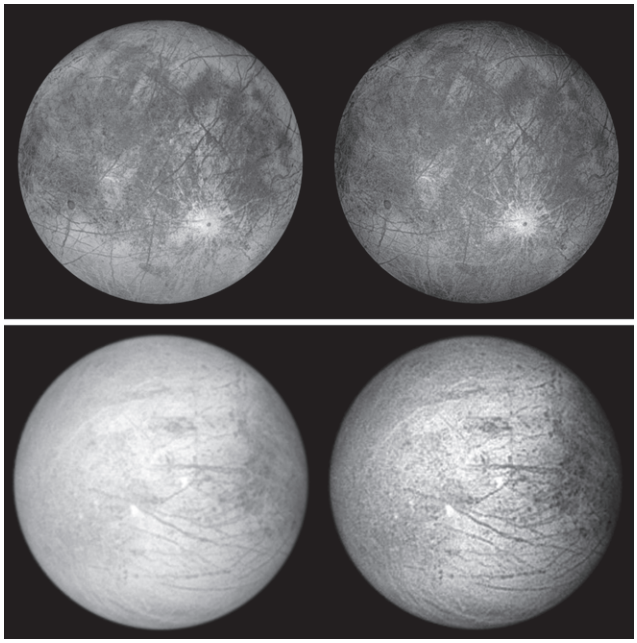

Fig. 1. See Plate 15. Europa's trailing and leading hemispheres (top and bottom panels, respectively), as imaged by Galileo's Solid State Imaging camera, illustrating the differences between the two sides and the association of the brownish material with geological features. The images at left are natural color, while the images at right are enhanced to show structural detail. The resolutions (and JPL Photojournal number) are 6.9 km/pixel (PIA00502) for the trailing sides and 12.7 km/pixel (PIA01295) for the leading side.

1.2. Sources of Surface Species

1.2.1. Endogenic sources. Jupiter's satellites formed from either a warm and dense protojovian nebula or a thin and cold disk (*Schubert et al.,* 2004; chapter by Canup and Ward). Thermochemical reactions in a warm nebula would have hydrated the silicates to serpentine, oxidized the iron to Fe_3O_4, and reduced the C and N compounds to CH_4, NH_3, and small amounts of HCN (*Prinn and Fegley,* 1981, 1989). Methane is too volatile to have condensed appreciably in the protojovian nebula, and ammonia would not have condensed at Europa's likely formation temperature. In the thin and cold nebula case, little thermochemical processing occurs before formation; unaltered silicates, Ni-Fe alloy, iron sulfide, organic matter, and water ice are retained and incorporated into the satellite. If the ice grains' compositions are similar to that of the interstellar medium (*Gibb et al.,* 2004), then CO_2, CH_3OH, OCS, H_2CO, HCOOH, NH_3, and OCN^- and perhaps CO and CH_4 may have been incorporated into the forming satellite, perhaps as clathrates. Some of the more volatile species may be outgassing at the present time, with the molecules diffusing to the surface and forming a tenuous atmosphere before being ionized and lost to the magnetosphere.

If Europa has an ocean (see chapter by McKinnon et al.), it is plausible that oceanic material could be emplaced on the surface. The young surface age and the absence of a dark meteoritic blanket, such as that covering Callisto, suggest recent replenishment of the surface. Whether or not the brownish material originates from the ocean is unknown, but there are tantalizing associations of non-ice material

TABLE 1. Estimated exogenic fluxes on Europa's surface, expressed in 10^6 atoms cm^{-2} s^{-1}; outer satellite ejecta sources are not included.

Element	Micrometeoroid (cometary)*	Io Plasma Torus (as ions)†	Io impact ejecta‡				
			Tholeiite basalt	Alkali basalt	Komatiite	Dunite	B1 CAI
H	8.2						
C	1.2	0.05, <0.14§,¶					
N	0.31						
O	2.7	~300**	9.6	9.4	9.8	9.4	9.4
Na	0.011	>5.3††	0.36	0.36	0.053	0.034	0.021
Mg	0.11		0.41	0.97	2.6	3.8	0.9
Al	0.0072	<0.05‡‡	1.0	0.96	0.28	0.056	2.1
Si	0.20	<0.6§	3.0	2.6	2.8	2.4	1.7
S	0.077	140					
Cl		1.8–5.6§,§§					
K	0.00021	~0.5¶¶	0.058	0.082	0.0067	0.0075	0.0075
Ca	0.0067	<0.006‡‡	0.56	0.64	0.34	0.51	1.81
Fe	0.056	<0.2‡‡	0.67	0.61	0.57	0.65	0.30

*Average mass influx from *Cooper et al*. (2001). Relative composition from *Anders and Grevasse* (1989).
†Sulfur flux value from *Johnson et al*. (2004) for trailing side apex and based on *Bagenal* (1994). No plasma deflection is included.
‡Equatorial mass influx rate averaged over 10-m.y. simulation, from *Zahnle et al*. (2008). The impactors' elemental composition is estimated for four models of Io basalts and an Allende-type calcium aluminum ceramic (B1 CAI), all from *Schaefer and Fegley* (2004).
§*Feldman et al*. (2004). Their C flux could be of solar wind origin.
¶Assumed a C/S ratio of 10^{-3} for Io plumes (*Schaefer and Fegley,* 2005), consistent with Voyager upper limits (*Pearl et al.,* 1979).
**O:S ~2:1 (*Hall et al.,* 1994) or higher at Europa (*Bagenal,* 1994).
††Lower limit for Na^+ from *Hall et al*. (1994). Note: comparable to Cl flux.
‡‡Neutral atom source limits relative to sodium, from *Na et al*. (1998).
§§*Kuppers and Schneider* (2000); *Feldman et al*. (2001).
¶¶*McGrath et al*. (2004) give a [Na]/[K] ratio of 10 ± 5 for atoms at 10–20 Io radii. We assume this ratio will be preserved in the plasma torus.

with geological features, suggestive of emplacement from below (Fig. 1). However, there is no direct evidence for surface-ocean exchange and other processes can produce geological and compositional associations (see below).

Europa's putative ocean overlies the silicate mantle, and may chemically react with it (see chapter by Zolotov and Kargel). Two different pathways are possible, depending on whether chemically evolved H_2 escapes or is trapped in the ocean by the icy shell. In the latter (closed) case, the presence of H_2 limits oxidation and species such as sulfates are not formed. If H_2 escapes, a likely scenario, the ocean initially evolves to an alkaline solution of (in order of concentration) OH^-, Na^+, $NaHSiO_3$, Cl^-, Ca^{2+}, NaOH, K^+, $HSiO_3^-$, H_2, $CaOH^+$, . . . (*Zolotov and Mironenko,* 2007). Cations (Na^+, Ca^{2+}, . . .) are supplied to the ocean through dissolution of the rock's silicates. Subsequent dissolution and long-term hydrothermal reactions may lead to a sulfate-bearing salty or acidic ocean (*Kargel et al.,* 2000; *Zolotov and Shock,* 2001; *Marion,* 2002; *Zolotov and Shock,* 2003; *Marion and Kargel,* 2008; chapter by Zolotov and Kargel). However, *McKinnon and Zolensky* (2003) have argued that sulfate is not easily formed in Europa's early ocean, which would have been sulfidic (e.g., *Zolotov and Mironenko,* 2007), but small amounts of sulfate introduced into the ocean from the mantle could overwhelm the initial sulfidic state (W. McKinnon, personal communication, 2008). It has also been suggested that SO_2 (*Kargel et al.,* 2000; *McKinnon and Zolensky,* 2003) could be vented into Europa's ocean. The SO_2 can form sulfurous acid or a clathrate (*Prieto-Ballesteros et al.,* 2005; *Hand et al.,* 2006) or, under oxidizing conditions, could form sulfuric acid. High-temperature decomposition of accreted organic compounds could also have supplied C, N, and S species to the ocean and icy shell (see chapter by Zolotov and Kargel). Finally, primary or modified organic matter may be transported toward the surface (*Kargel et al.,* 2000; chapter by Zolotov and Kargel).

1.2.2. Exogenic sources. Three sources are thought to be providing material to Europa's surface, the first being delivery of material from outside the jovian system through direct impacts of comets, asteroids, meteorites, and micrometeorites. Numerical estimates of the globally averaged elemental fluxes from micrometeoroid impacts are given in Table 1 using the flux from *Cooper et al*. (2001) and cometary abundances (*Anders and Grevasse,* 1989). The flux distribution on the surface will be nonuniform; orbital motion increases the flux striking the leading hemisphere and decreases the trailing-side flux (*Zahnle et al*., 1998) (see section 1.3.2).

The second source of material for the Galilean satellites' surfaces is material ejected from the outer irregular satellites of Jupiter. This source was discussed by *Pollack et al*. (1978), inferring from the low albedo of these small bodies that they are composed of carbonaceous-chondritic-like

material. These authors thought that this source is more potent than micrometeoroid bombardment due to the lower impact velocities, but no fluxes were estimated. It is also possible that ejecta from the outer Galilean satellites could contribute material to Europa. We can estimate this source strength as roughly equal to the iogenic impact ejecta source discussed below (K. Zahnle, personal communication, 2008); however, we do not further consider outer satellite contributions.

The third source is the neighboring inner satellite Io, from which material is brought to Europa by Io's thermal plasma torus, by higher-energy iogenic ions, and by impact ejection of crustal material from Io (*Alvarellos et al.,* 2008; *Zahnle et al.,* 2008, see also chapter by Zolotov and Kargel). Thermal plasma from Io deposits material mainly on Europa's trailing hemisphere. Implantation of more energetic ions occurs uniformly over the surface and, for sulfur, the flux is about 10% of the maximum flux of thermal S ions at the trailing antapex. An estimate of the undeflected trailing-side sulfur plasma flux from *Johnson et al*. (2004) is used with relative ion density measurements to generate the plasma input in Table 1. Plasma deflection could reduce the implantation flux. *Ip* (1996) predicted a 20% reduction, whereas modeling by *Saur et al*. (1998) suggested a factor of 5 reduction. Using Galileo data, *Paranicas et al*. (2002) and *Volwerk et al.* (2004) have estimated that only 10% of the impinging plasma is diverted around Europa. These plasma effects are discussed in the chapter by Kivelson et al., but no further estimates are currently available.

Io's impact ejecta, suggested to consist largely of basaltic spall fragments (*Alvarellos et al.,* 2008; *Zahnle et al.,* 2008), strike Europa at high velocities and will be largely vaporized and undergo reactions in the plume. The fluxes are given in Table 1 for five models of Io's magma composition. Io's volcanos are dust sources (*Postberg et al.,* 2006), but their contribution to Europa's surface is inconsequential (*Kruger et al.,* 2003).

Exogenic material will accumulate on the surface and be buried by micrometeoroid gardening. We can crudely estimate the expected concentrations by assuming that the resurfacing age of the icy crust is the same as the ~50-m.y. cratering age (see *Zahnle et al.,* 2003) and ignoring the asymmetric flux rates and gardening patterns. We then find that a flux of 10^6 atoms cm^{-2} s^{-1} in a nominal 1-m-deep regolith (see Fig. 2) will result in a longitudinally and vertically averaged volume mixing ratio relative to H_2O of

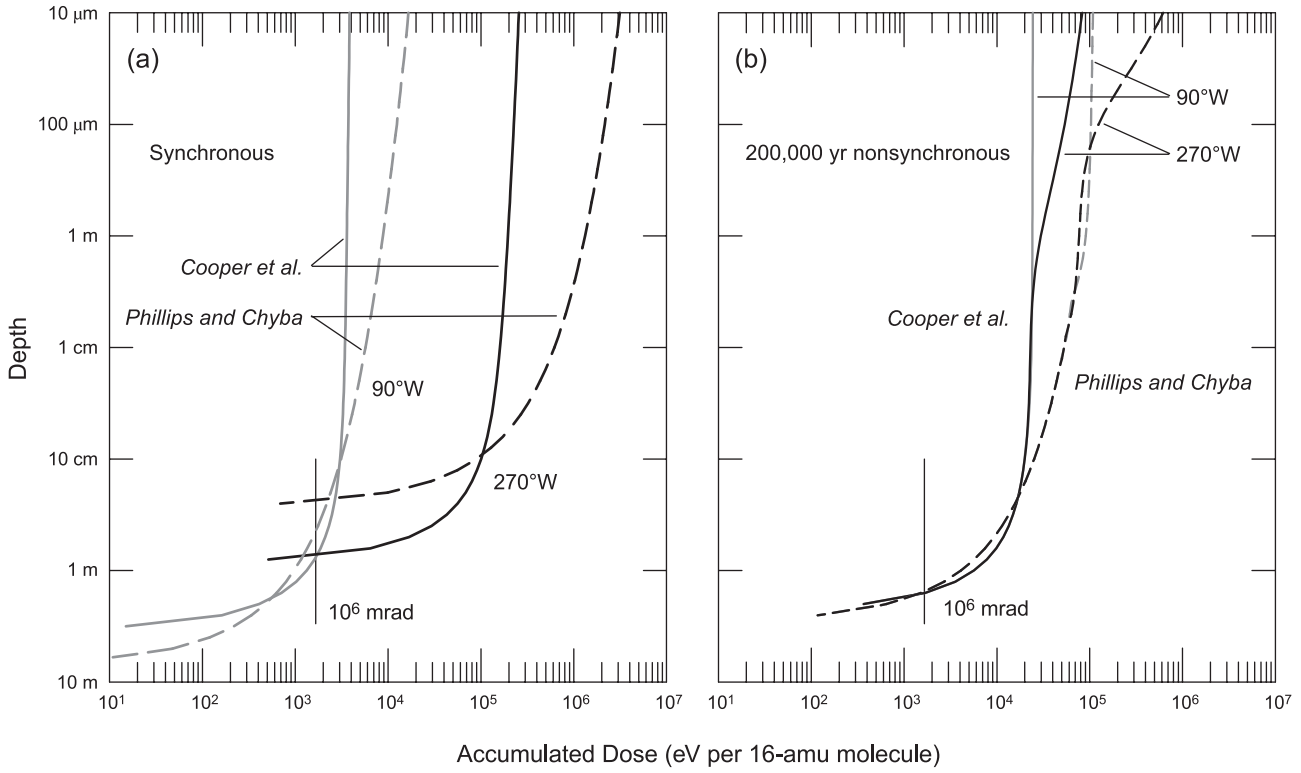

Fig. 2. Radiolytic dose for molecules as a function of their current depth for a 50-m.y. surface. The doses for the leading-side apex and trailing-side antapex are shown as gray and black lines, respectively. This vertical variation will also approximate the relative distribution of implanted iogenic sulfur, sodium, and other thermal plasma atoms since their longitudinal flux distrubutions are somewhat similar to the ionizing radiation distribution. Gardening models of *Cooper et al*. (2001) (solid lines) and *Phillips and Chyba* (2001) (dashed lines) are shown for **(a)** synchronous rotation and **(b)** a 200,000-yr nonsynchronous rotation period. The trailing-side enhancement of dose is due to the higher electron flux contribution and lower gardening rate for that hemisphere. Remote optical sensing samples approximately the top 100 μm to 1 mm. Porosity is neglected in these calculations.

roughly 500 ppm. If Io were the only source of non-ice material to Europa's surface and no loss occurred, then using the flux values from Table 1, sulfur compounds could be present on the surface at ~7% (molar abundance) relative to H_2O, while Na and Cl could reach 0.3%. Silicon and magnesium could be comparable or slightly less than Na and Cl. These estimates assume uniform mixing and ignore hemispherical flux and gardening rate differences, which can produce surface concentrations that are a factor of 10 or more different between the leading and trailing sides (see Fig. 2 and caption).

1.3. Chemical and Physical Processes

In the following subsections we briefly describe various processes that can chemically or physically alter the surface composition.

1.3.1. Radiolysis. The Galilean satellites are imbedded in an intense radiation environment, with their surfaces being constantly bombarded by energetic electrons, protons, and heavy ions (see chapter by Paranicas et al.), along with a lesser-energy flux of solar ultraviolet (UV) photons (the mean solar UV energy flux that can dissociate H_2O is ~2% of the magnetospheric flux). *Burns* (1968) and *Morrison and Burns* (1976) were the first to point out that the surfaces of the Galilean satellites could be modified by magnetospheric irradiation, causing albedo and color variations, but the magnitude of radiation effects was not fully appreciated until two definitive radiolytic species, molecular oxygen and hydrogen peroxide, were discovered on Europa (see sections 2.5 and 2.6).

A single keV to MeV electron or ion passing through an icy molecular solid produces a trail of ionizations and excitations as the original particle's energy is degraded. Each ionization event along the track will produce secondary electrons that, in turn, travel through the ice, creating separate tracks of yet more ionizations, excitations, and subsequent reactions and chemical changes. In this way, the direct chemical action of the incident particle is overshadowed by the chemistry produced by the secondary electrons. This implies that, to a first approximation, the chemical reactants produced by various ionizing radiations (e^-, H^+, He^+, X-rays, γ-rays) are identical, although product yields may depend on specific doses, dose rates, and the linear energy transfer rate of the primary particle. The average penetration depth for magnetospheric electrons at Europa is 0.6 mm (*Cooper et al.,* 2001) but high-energy electrons and bremmstrahlung can deposit energy to meter depths. Ions have a much shorter range. Protons at Europa's orbit have an average range of 0.01 mm (see chapter by Paranicas et al. for dose vs. depth curves). Range and stopping power data for electrons and ions are available from *ICRU* (1984) and *Ziegler et al.* (1985), respectively. The time-integrated particle or energy flux incident on a surface is termed the fluence, and the absorbed energy density in the material is the dose, expressed in various units including eV molecule^{-1}, eV 16-amu^{-1}, rads (1 rad = 100 erg g^{-1}), and grays (1 Gy = 1 J kg^{-1}). Additional information can be found in standard references on general radiation chemistry (e.g., *O'Donnell and Sangster,* 1970; *Swallow,* 1973; *Spinks and Woods,* 1990; *Mozumder,* 1999) and charged-particle interactions with planetary surfaces (*Johnson,* 1990; *Johnson et al.,* 2004). A pre-Galilieo summary of photolysis and radiolysis on icy satellites is found in *Johnson and Quickenden* (1997) and a special section of the *Journal of Geophysical Research* is devoted to photolysis and radiolysis in the outer solar system (*Domingue and Allamandola,* 2001).

The chemical composition of Europa's regolith is profoundly influenced by jovian magnetospheric radiation. At the same time, this radiation can also alter the molecular environment, and therefore the positions and shapes of spectral bands (see section 2.2.3). It also can produce defects and disorder in the ice and thereby alter the thermophysical and optical scattering properties. The dominant ionizing particles at Europa are electrons and protons (and, to a lesser extent, multiply charged S and O ions) with energies ranging from <10 keV to >10 MeV and with average energies in the MeV range. Energetic particle observations from both flyby and orbiting spacecraft show that radiation doses of 1 eV per H_2O molecule (~600 Mrad) is achieved in three years or less at depths of ~100 μm, which is a typical remote-sensing depth (*Cooper et al.,* 2001). Extremely energetic electrons and bremmstrahlung X-rays will penetrate more deeply, while micrometeoroid-induced gardening simultaneously buries the radiation products and brings material from depth. Irradiated material will be vertically mixed throughout the regolith (Fig. 2). Significant changes occur for doses of only a few eV per molecule (the dose often expressed as eV per 16-amu), so most molecules in the regolith will have been altered many times over the age of the surface.

A measure of the initial radiolytic production or destruction rate is given by the G value, the number of molecules produced or destroyed per 100 eV of absorbed energy. As an example, from the compilation by *Johnson et al.* (2004), CO_2 in H_2O ice is destroyed at a rate $G(-CO_2) = 0.55$ per 100 eV. Therefore, at an accumulated dose of about 5×10^4 eV 16-amu^{-1} (a rough global average in the upper millimeter for the 200,000-yr nonsynchronous rotation case; see Fig. 2) a CO_2 molecule would have been destroyed 800-fold. The alkaline Earth sulfates and their hydrates are among the most radiolytically stable molecules. They can be dehydrated and decomposed by producing SO_2 with $G(SO_2) = 0.004$ (*Johnson et al.,* 2004), so hydrates such as epsomite ($MgSO_4 \cdot 7H_2O$) will have suffered ~30 destructive events for the conditions considered above. For newly emplaced or exposed material, it is of interest to know the time required to accumulate a dose of 1 eV 16-amu^{-1}, a typical dose to establish new products. For a typical optical sampling depth of 100 μm, and using the dose values from the chapter by Paranicas et al., the time for a pristine sample to generate these new species and to reach radiolytic equilibrium is ~20 months on the trailing side (at the anta-pex) and 40 months on the leading side (apex).

Because Europa's ice is dominated by water molecules, it is appropriate to briefly consider their radiation chemistry (*Buxton,* 1987; *Spinks and Woods,* 1990). A keV to MeV electron encountering an H_2O molecule will cause either an excitation or ionization. These will yield, in turn, a set of primary products that include charged species, radicals, and closed-shell molecules, summarized as

$$H_2O \rightarrow H_2O^+ + e^- \rightarrow H + OH \rightarrow H_2 + H_2O_2$$

H_2 molecules rapidly escape from the surface and even the satellite, so the surface becomes oxidizing. Some reduction can occur from energetic magnetospheric proton implantation, as on Mercury, the Moon, and asteroids (*Hapke,* 2001) from the solar wind, but this will be a secondary effect due to the relatively low proton flux.

The incident radiation also decomposes peroxide, so equilibrium concentrations will be achieved where production equals destruction. This decomposition, and other secondary reactions, will make HO_2, HO_3, O_2, and O_3, and electron attachment to OH (hydroxyl) will produce OH^- (hydroxide). Given these radiation products from H_2O, subsequent reactions with other molecules in the original ice may include H^+ transfer (acid-base reaction), e^- transfer (oxidation-reduction), and free-radical reactions, such as radical combinations, H and OH addition, disproportionation, and atom abstraction by H and OH. In general, all these reactions are sufficient to explain many chemical species identified on Europa (e.g., H_2O_2, H_2SO_4 hydrates, O_2). The dissociation products of H_2O_2 are species such as OH, OH^-, HO_2, O_2, H_2, and H_2O. Since H_2 readily diffuses out of the ice at Europa's temperature, the ice surface is permanently modified and becomes more oxidized as the $H_2O \leftrightarrow H_2O_2$ reaction cycle continues and H_2 is lost.

Sulfur species thought to be present in Europa's ice, elemental sulfur, SO_2 and the SO_4^{2-} ion, are part of the dynamic sulfur cycle driven by interactions with the jovian magnetosphere on relatively short timescales. In Europa's water ice, sulfur, SO_2, and other sulfur species are oxidized to SO_4^{2-} with radiation processing. Some of the species formed are

$$H_2O + SO_2 \rightarrow SO_3, HSO_3^-, HSO_4^-, SO_4^{2-}, H_3O^+$$

Reactions of SO_2 with H_2O_2 can form sulfates. Irradiation of possible hydrated salts, e.g., $Mg_2SO_4 \bullet 7H_2O$ and $Na_2 \bullet 10H_2O$, yields metal oxides, the SO_4^{2-} ion in the form of sulfuric acid and sulfate salts, and SO_2. Based on laboratory experiments (*Moore et al.,* 2007), it is estimated that these radiolytic processes form the observed abundances of SO_4^{2-} on Europa in $<10^4$ yr. The radiolytic cycle on Europa continues as H_2SO_4 and its hydrates are dissociated, resulting in species such as SO_3, HSO_4^-, SO_2, H_2, and S. Thus the sulfur cycle, $S \rightarrow H_2SO_4 \rightarrow SO_2 \rightarrow S$, results in a dynamic equilibrium where the relative abundances are established by production and loss mechanisms. The largest reservoir of sulfur on Europa is thought to be in the more stable sulfate and other sulfur-containing ions, 93–98%, compared to 1.5–6.9% as SO_2 [abundances relative to total sulfur (*Moore et al.,* 2007)]. Note that the starting point for these cycles is immaterial; one could start with sulfur, sulfide, or a sulfate, eventually reaching equilibrium with sulfate (as acid and salts, if the metal cations are present), SO_2, and sulfur allotropes.

The carbon volatile, CO_2, identified in Europa's H_2O ice and discussed further in section 2.7, probably takes part in the radiolytic carbon cycle. Some of the species formed by irradiation are

$$H_2O + CO_2 \rightarrow CO_3, CO, O_2, O_3, H_2CO_3$$

On Europa, it is estimated that CO_2 will convert to CO and H_2CO_3 (carbonic acid) with a half-life <2000 yr. With further irradiation, H_2CO_3 is destroyed reforming CO_2

$$H_2CO_3 \rightarrow CO_2 + H_2O$$

A large destruction rate for H_2CO_3 has been measured in laboratory studies, so at equilibrium ($H_2O + CO_2 \leftrightarrow H_2CO_3$) most of the carbon will be as CO_2. Europa's surface is an open system and CO_2 can slowly enter the atmosphere and escape to space. Thus, a continuing source of carbon may be required. The carbon cycle is discussed in more detail in section 2.7.

1.3.2. Sputtering redistribution. When high-energy ions strike a surface, they eject atoms and molecules through both elastic collisions and through localized electronic excitation (see *Johnson,* 1990). While electrons and photons also sputter material, the most efficient particles are heavy high-energy ions. Jupiter's magnetosphere contains energetic protons, sulfur ions, and oxygen ions, with the latter two species producing most of the sputtering at Io. Because of their large gyroradii, these ions strike Europa fairly uniformly in longitude. Relevant features are sputtered Na and K atoms that form a tenuous ballistic atmosphere and a flux of escaping atoms. Europa also has an O_2 and presumably H_2O atmosphere (see chapters by Johnson et al. and McGrath et al.), formed by the sputtering products of water — H_2O, O_2, and the light molecule H_2 that directly escapes. Measurement of the sputtered atmosphere offers a means of exploring the surface composition. This process also redistributes material over the surface, as discussed in the following.

Tiscareno and Giessler (2003) computed the globally averaged erosion rate of 0.0147 μm yr, in agreement with prior calculations by *Cooper et al.* (2001). Of these molecules, 42–86% of the molecules restrike the surface. There is more sputtering on the trailing hemisphere and the net transfer, mainly of water molecules, from the trailing to leading side is <0.003 μm yr^{-1}. This rate is small compared to *Cooper et al*.'s (2001) vertical gardening rate of 1.2 μm yr^{-1}. In the 50-m.y. age of the surface, a maximum net of transfer of 15 cm of material will be mixed into the nominal 1-m leading-side regolith (see below). While unimportant for H_2O, this process may be important in redistributing

the Na and K atoms to explain the orbital behavior of the Na and K clouds (*Leblanc et al.,* 2005; but see *Cipriani et al.,* 2008).

1.3.3. Impact-induced chemistry. Hypervelocity impacts on ice produce high-temperature shock waves, vaporization, electronic excitation, light emission, and ionization (*Eichhorn and Grun,* 1993; *Burchell et al.,* 1996; *Kissell and Krueger,* 1987) and there will be chemical changes produced in this highly energetic process. Although the average power in micrometeoroid impacts is about a factor of 10^5 less than that for energetic particles, and therefore not globally significant, large impacts may produce localized effects (*Cooper et al.,* 2001).

The chemical effects of impact heating and shock-wave generation may be simulated by a variety of processes (*Kissell and Krueger,* 1987; *Scattergood et al.,* 1989) including pulsed lasers. Laser ablation experiments on mixed ices to simulate Europa have been performed by *Nna-Mvondo et al.* (2008). For example, for H_2O:CO_2 ices they find H_2O_2, CO, and CH_3OH being produced, while H_2O ice with Na_2CO_3 generates CO and CO_2. Irradiation of water ice containing methanol yields more complex products, indicating that large impacts may produce a quantity of diverse and interesting compounds. Additional quantitative work is needed to assess the importance of this process for icy satellites.

1.3.4. Micrometeoroid gardening. The formation of regoliths, the fragmented, porous "rock blankets" produced by meteoritic impact, directly influences the surface composition. Meteoritic impacts introduce new material and produce craters, excavating the existing surface and covering the adjacent surface. As Europa's surface is being implanted with sulfur ions and bombarded by high-energy radiation that forms new molecules, gardening simultaneously buries these products, and brings fresh (and previously irradiated) material to the surface where the implantation and bombardment process continues. Regoliths can also present large areas for chemical and physical interaction with atmospheric species (*Cassidy et al.,* 2007).

The volume of material ejected by impacts is 10 to 100 times greater for ice targets than crystalline rocks (*Lange and Ahrens,* 1987), so a thick, porous regolith may expected on Europa, depending on the surface age. This mixing ("gardening") extends to a depth that increases with time but can vary significantly over the surface due to statistical variations of the impactor's mass, velocity, and flux as well as location and orbital geometry. One of the first estimates of regolith growth on Europa is by *Varnes and Jakosky* (1999), who predicted 1- to 10-cm-deep regoliths for a 10-m.y.-old surface. *Cooper et al*. (2001) developed a depth vs. time relationship using lunar examples and Ganymede impact rates derived by *Shoemaker et al.* (1982) and *Shoemaker and Wolfe* (1982). The initial rate is about 1.2 μm per year, slowing as the regolith forms and penetration to deeper levels becomes progressively more unlikely. *Phillips and Chyba* (2001, 2004) developed two regolith growth models, the first normalized to large craters (*Phillips and Chyba,* 2001) and the second to small craters (*Phillips and Chyba,* 2004). Average regolith depths for an assumed 10-m.y.-old surface are 1.3 m and 0.7 m for the *Cooper et al.* (2001) and *Phillips and Chyba* (2001) formulations, respectively. These depths are averages over the satellite surfaces.

The micrometeorite impact rate and their velocities are greatest on the leading hemispheres (*Zahnle et al.,* 1998), so there will be differences between regoliths on the leading and trailing sides. If Europa is not tidally locked, but undergoes nonsynchronous rotation, then the hemispherical differences can average out, depending upon the rotation rate.

Carlson (2003) used two different gardening formulations and computed the mean vertical dose profile that a molecule, now at that depth, has received in a given time, subject to asymmetric charged particle irradiation (*Paranicas et al.,* 2001), asymmetric meteoritic erosion rates, and various cases of nonsynchronous rotation. The dose is normalized to a 16-amu molecule and shown in Fig. 2 for a 50-m.y. exposure [the crater age of the surface, from *Zahnle et al*. (2003)]. The gardening depth on the leading side is about 1 m for both models in the tidally locked case, but the trailing-side depths differ by a factor of ~10, from ~5 cm in the Phillips-Chyba model to ~50 cm using Cooper et al.'s formulation. In the nonsynchronous rotation case, the gardening depths are about the same due to the spin averaging.

The optical surface is overturned rapidly. Using *Cooper et al.*'s (2001) formulation the optical surface is gardened at a rate of 1.2 μm yr^{-1}, so for a nominal 100-μm remote sensing sampling depth, gardening excavation and overturning occurs in about 80 yr.

1.3.5. Thermal processes. The surface of Europa can be heated by solar insolation and by internal heat sources. We first consider the solar heating. While H_2O absorbs only weakly in the visible region, it does absorb infrared (IR) radiation, and this must be considered when computing thermal effects. For impure ice and hydrated material, additional absorption can occur, depending on the absorption properties, and can produce heating rates and temperatures greater than for ice. The increased temperature will promote greater H_2O sublimation from the impure ice. The sublimation rates of hydrates depend on the particular hydrate and can be less than for water ice. The net effect is to thermally segregate H_2O molecules from darker materials (*Spencer,* 1987a) and possibly "garden" the surface (*Grundy and Stansberry,* 2000). Since sublimation and recondensation occurs diurnally, with sublimated molecules condensing on both dark and icy regions, the segregation is probably not carried to completion. The surface of Europa contains amorphous ice (section 2.1), and amorphous ice has a higher vapor pressure than crystalline ice, so the local sublimation and condensation fluxes may be as high as 10^{12} molecules cm^{-2} s^{-1} at 120 K (*Sack and Baragiola,* 1993, their Fig. 5), to be compared to the average sputtering rate of ~1.5×10^9 molecules cm^{-2} s^{-1}. This amorphous ice sublimation rate is greater than the crystalline ice sublimation rates used by *Shi et al*. (1995) in their comparison of icy satellite sublimation and sputtering rates. However, there are different forms

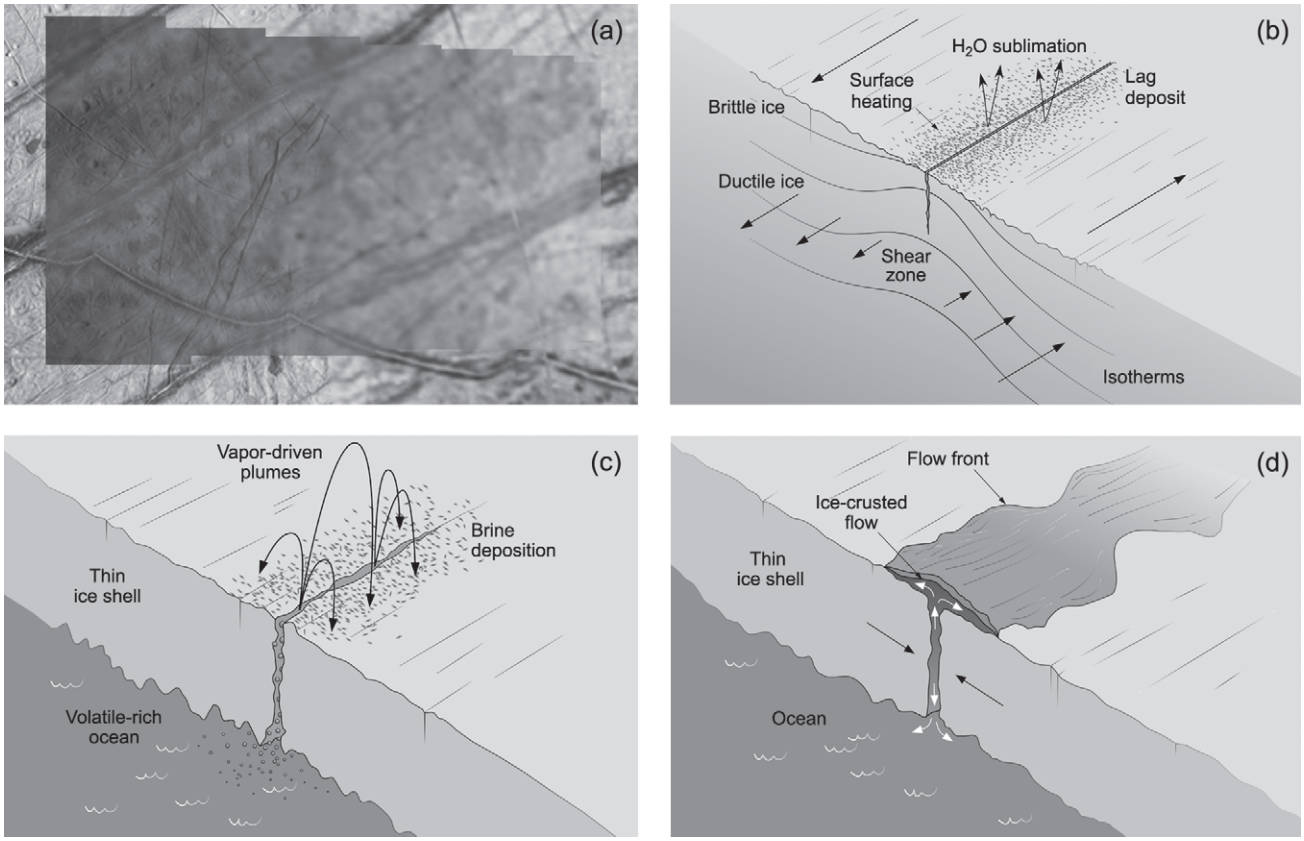

Fig. 3. See Plate 16. Association of Europa's dark material with lineae and possible geological mechanisms. **(a)** False-color Galileo NIMS observation 11ENCYCLOD01 overlaid upon visible imaging data. Red indicates hydrated materials while blue denotes more pure water ice and frost. Note correlation between red (hydrated) material and lineae. In higher-resolution spectral maps the bright central band of lineae are observed to be water ice (*Carlson et al.,* 2005a). **(b)** Thermal modification of the surface from shear heating of the surface in the region of the linea, sublimating H_2O and leaving enhanced concentrations of higher vapor pressure hydrate and darker, possibly sulfurous material. **(c)** Thin shell volatile-driven explosive cryovolcanism depositing oceanic brine. **(d)** Effusive emplacement of near-surface liquid by tide-induced opening and closing of a crack. Other mechanisms are possible.

of amorphous ice, so the sublimation rate of amorphous ice produced by irradiation needs to be measured.

Heating by geological processes can affect the surface through sublimation, by softening or melting of surficial material, and by the generation of plumes. The sources of heat can be rising diapirs and shear heating of cracks (*Nimmo and Gaidos,* 2002) (see Fig. 3b). Sublimation will produce local thermal segregation and lag deposits of more refractory material (*Head et al.,* 1999; *Fagents et al.,* 2000; *Fagents,* 2003). Diapiric heating can soften and mobilize the ice crust and even produce localized melting [brine mobilization (see *Head and Pappalardo,* 1999; *Fagents et al.,* 2000; *Fagents,* 2003)]. Europa exhibit some evidence for small-scale, low-viscosity flooding, which could be from liquid effusion to the surface (see below) or from heating and melting of surface material. While most sulfate salts (see section 2.2) depress the freezing point by less than 5°, one sulfate salt, ferric sulfate, has a low melting point (*Chevrier and Altheide,* 2008), although there is little evidence for iron compounds on the surface (section 2.9.5). Sulfuric acid-water solutions have a eutectic point as low as ~200 K (*Zeleznik,* 1991), forming a low-temperature liquid that may explain some observed features (*Collins et al.,* 2000; *Fagents,* 2003). Note, however, that significant quantities of sulfuric acid, ferric sulfate, or other low-melting-point material would have to be present in the upper icy shell to explain many of these geological features if they are not from effused liquids. The necessary quantities remain to be investigated.

Plumes created by shear heating will contain near-surface material that can be ejected at 450 m s^{-1} and rise to altitudes of 70 km (*Nimmo et al.,* 2007). The plumes can produce local resurfacing with a rate of ~50 μm yr^{-1} (*Nimmo et al.,* 2007).

1.3.6. Cryovolcanism. Cryovolcanism may be operating on Europa and introducing material from the icy shell and even from the ocean. There are two descriptions of the ice crust, thin or thick, and this parameter influences the cryovolcanic mechanisms. Thin crusts allow direct contact of the ocean to the surface by melt-through, explosive cryovolcanism, and through deep, tidally worked cracks. In the thick case, uprising diapirs can cause thermal modifications

of the surface, as discussed above, and can break through the surface. The icy shell thickness can vary over the surface and evolve with time. Mechanisms and examples are given below.

1.3.6.1. Explosive cryovolcanism: A crack penetrating through a thin shell to the ocean can be an energetic source of material (Fig. 3c) if the ocean contains volatiles such as CO_2, CO, SO_2, NH_3, and CH_4 (see analysis by *Fagents et al.,* 2000). Volatiles released by exposure to low pressure can erupt and spray gases and particulates (ice crystals, liquid droplets) at velocities of 30 to 250 m s^{-1} and form 1- to 25-km-high plumes. If multiple plumes occur along a crack, the deposited oceanic material will form a margin a few kilometers to tens of kilometers wide. This mechanism is consistent with observations, but *Fagents et al*.'s (2000) preferred explanation for the dark margins along lineae was the production of sublimational lag deposits [of possibly sulfurous material (see *Fagents,* 2003)].

1.3.6.2. Effusive flow: The flow of liquid onto a low-temperature icy surface has been analyzed in general by *Allison and Clifford* (1987) and specifically for effusion on Europa by *Fagents* (2003). This process may occur by direct, localized melt-through of a thin crust when the surface is below the water line and may form the smooth low plains found on Europa. Effusive flow can also be produced if cracks penetrate the thin crust to the ocean and partially fill with denser oceanic liquid. Tidally forced opening and closing of the crack extrudes liquid to the surface, probably under a thin frozen crust (Fig. 3d).

For thick icy shells, internal convection produces rising diapirs of warm ice that, in general, reach a "stagnant lid" and do not penetrate the surface. However, some positive relief features such as Murias Chaos (the "mitten") appear to show high-viscosity flow, suggesting that a large thermal diaper of warm plume pierced the crust. Other features such as bands may be indicative of processes similar to seafloor spreading. These high-standing features may be produced from compositionally and thermally buoyant ice (*Prockter et al.,* 2002). The relationship to the ocean and the composition of diapirs is not established.

1.3.7. Other processes.

1.3.7.1. Mass wasting: High-resolution imagery has shown evidence for downslope motions of dark material that we will show later is associated with hydrate material. These observations suggest that the dark material forms a thin veneer of unknown thickness. This mass wasting uncovers brighter ice and may be an explanation, along with others (*Carlson et al.,* 2002), for the brightening of lineae found by *Geissler et al.* (1998). The accumulation of dark matter at the base of ridges concentrates the material. Mass wasting may be assisted by charging and electrostatic levitation.

1.3.7.2. Impact exhumation: Impacts excavate material forming bright icy rays, and some impacts may have penetrated to the ocean: *Fanale et al.* (2000) investigated the Tyre and Pwyll impact sites and suggested that Europa's subsurface was laced with numerous liquid intrusions lying below a superficial ice veneer. They suggest that this thin ice layer, prominent on the leading hemisphere, is produced by sputtering, eroding the trailing side and depositing the material on the opposite hemisphere. However, as discussed in section 1.3.2, sputtering redistribution is too slow to build up such a surface.

1.3.7.4. Clathrate disruption: Clathrates have been suggested to be present in the ocean (*Prieto-Ballesteros et al.,* 2005). Bouyant clathrates may be incorporated into the ice crust and, through convective or other motions, be introduced to the surface where they are unstable. Explosive gas release could mechanically disrupt the surface and perhaps alter its composition (*Prieto-Ballesteros et al.,* 2005).

1.4. Observational Methods and Europa Surface Species

The primary source of our compositional information is remote sensing, by groundbased and Earth-orbiting telescopes and from spacecraft measurements. Earth-based spectra often are recorded at visible and near-IR wavelengths where there is efficient reflection of solar radiation. For groundbased observations, absorption by the Earth's atmosphere limits the accessible spectrum and the object's distance limits the spatial resolution. The majority of these telescopic observations observed reflected sunlight for wavelengths less than 3 μm, but some measurements have been performed at longer wavelengths (*Lebofsky and Freieburg,* 1985; *Noll and Knacke,* 1993) and in the thermal IR (*Mills and Brown,* 2000). Earth-orbiting telescopes such as the International Ultraviolet Explorer (IUE) and Hubble Space Telescope (HST) have been used to probe Europa's surface at UV wavelengths obscured by Earth's ozone and oxygen (0.2 to 0.3 μm). Both HST and ground-based telescopes are used to study Europa's tenuous atmosphere, which is formed by sputtering from the surface and therefore serves as a useful indicator of surface composition. Voyager provided thermal IR spectra (*Spencer et al.,* 2004) and the Galileo mission obtained UV and IR spectroscopic measurements, the former in the 0.2- to 0.3-μm range and the latter in the 0.7- to 5.2-μm region. A major limitation of the Galileo measurements is radiation-induced noise, which affects the UV and the long-wave IR measurements (wavelengths $\lambda >$ 3 μm). Consequently, some of the features seen on Ganymede and Callisto could not be investigated at Europa with sufficient sensitivity. Some long-wave features were detected by taking measurements from afar, near Ganymede's orbit. The deficiency of high-quality spectra for wavelengths greater than 3 μm is a major detriment to understanding Europa's surface composition. The New Horizons Jupiter flyby augmented Galileo's spectral mapping coverage of Europa in the 1.25- to 2.5-μm wavelength range.

The IR region senses vibration-rotation transitions of molecules, with the strongest transitions, the "fundamental bands," generally occurring at longer wavelengths, while the shorter-wavelength near-IR region contains weaker overtones and combination bands of two or more vibrational modes. The exception is hydrides such as H_2O, where the

low mass of the H atom moves the fundamental OH stretching vibration to ~3 μm. The visible and UV regions contain spectral features generally due to electronic transitions and there are some electronic transitions observed in the near-IR for Fe-containing compounds. In condensed matter, electronic transitions are often quite broad, so definitive identifications are difficult to make, but the absorptions can be strong, providing good sensitivity to minor species. There is a lack of laboratory UV reflectance spectra for materials of interest for Europa, particularly at relevant temperatures.

Ultraviolet, visible, and IR spectroscopy probes just the upper portion of the surface, and it is important to be able to estimate those depths (Z) and corresponding photon path lengths (L). These wavelength-dependent quantities are determined by the single scattering phase function, the grain diameter D and absorption coefficient α. We computed the reflectance, R, and the mean optical path length (MOPL) (*Clark and Roush,* 1984), for refractive scattering and various values of αD. Dividing the mean optical path length (MOPL ≡ –ln(R) = αL) by αD gives the path length-to-grain diameter ratio L/D as a function of reflectance. Assuming that the sampling depth is one-fourth of the mean photon path length, depths of a few grain diameters are probed in dark absorbing media and greater depths are sampled in bright materials (e.g., for reflectivity R = 0.1, 0.5, and 0.9, we find Z/D ~ 2, 5, and 30, respectively). These depths, uncorrected for porosity, are in good agreement with calculations by W. Grundy (personal communication, 2008), found using *Grundy et al.*'s (2000) Monte Carlo routine for irregularly shaped particles. They are also consistent with the MOPL calculations of *Clark and Lucey* (1984) for near-IR reflectance spectra of laboratory frost samples. Later we will use the above results with independently determined grain sizes to estimate absorption properties and abundances of minor species in the scattering grains.

Several approaches have been used to estimate concentration by comparing observed satellite spectra with laboratory-derived results such as (1) Spectral radiative transfer models employing optical constants for candidate materials. Linear mixing, granular mixing, and molecular mixing models are used in such models. (2) Laboratory reflectance spectra of pure or mixed species; the latter can be approximately simulated by numerical linear mixing of results for pure species. (3) Laboratory transmission spectra, inferring concentrations from band depths. (4) Comparing equivalent widths (integrated band areas expressed as the width times the continuum level) of Europa spectral features with experimentally determined integrated band strengths (e.g., *d'Hendecourt and Allamandola,* 1986; *Allamandola et al.,* 1988; *Gerakines et al.,* 1995, 2005; *Moore and Hudson,* 1998; *Kerkhof et al.,* 1999; *Moore et al.,* 2003; and others).

In addition to remote sensing methods, there are suggestive *in situ* plasma, plasma wave, and energetic neutral atom measurements (see chapter by Kivelson et al.). Probable and possible surface species from both remote sensing and *in situ* observations are collected in Table 2; however, this list must be considered incomplete, as there are likely numerous species awaiting discovery. Spectral features similar to those observed from Ganymede and Callisto by Galileo's Near-Infrared Mapping Spectrometer (NIMS) may be present on Europa. We also include the neutral Europa torus (Table 2, bottom) because remote observations of atomic and molecular emissions from this torus may be fruitful in determining minor species originating from Europa, as demonstrated by *Hansen et al.* (2005).

1.5. Laboratory Methods

It is often the case that new planetary observations provide unanticipated results, necessitating new laboratory measurements to aid interpretation. This situation is true for Europa's surface composition and particularly applicable for understanding radiolytic species and the reflectance spectroscopy of hydrates. These two efforts are briefly discussed below.

1.5.1. Radiation chemistry. Since samples retrieved from Europa's surface are not yet available, chemical compositions are determined most directly from spectral comparisons with laboratory analogs. Experimental samples of the volatile ices can be prepared by condensation of a vapor onto a precooled substrate inside a vacuum chamber. Substrate temperatures relevant to Europa are appropriate, but not always always used. In some cases, ices are made by flash cooling of a room-temperature liquid mixture or spraying from a nebulizer onto a cold plate. Following ice formation, the ice sample's transmission or reflection spectrum can be recorded at various temperatures and irradiation conditions.

Laboratory ice analogs also can be studied from the UV to IR, with each region carrying its own benefits and disadvantages. For example, UV and visible-light measurements often give only broadly sloping but otherwise generally featureless spectra, making unique chemical assignments difficult. Near-IR spectra can possess distinct absorptions, but usually only for the more abundant species since near-IR bands generally are due to combination and overtone transitions and are usually much weaker than the fundamental transitions. The most productive laboratory work, in terms of assigning molecular bands and unraveling chemical change, has been done with mid-IR spectroscopy (2.5–25 μm, 4000–400 cm^{-1}). Spectra in this region are from vibrations involving functional groups (groups of bonded atoms), with many functional groups having very diagnostic wavelengths. Relatively little work has been done in the far-IR, although this region can be useful for distinguishing the amorphous or crystalline phase and determining the clathrate nature of an ice. In general, all this suggests that using laboratory measurements to understand Europa's surface chemistry requires measurements over a wide spectral range.

1.5.2. Reflectance spectroscopy. Interpretation of spectral observations of icy satellites relies upon comparison to

TABLE 2. Known and suggested identifications of species on Europa (see individual sections for discussion).

Identification	Method	Wavelength or Region	Comments
H_2O ice	Solar reflectance	1.5, 2, 3 μm	Amorphous and crystalline
Hydrate or hydronium	"	1.3, 1.5, 2 μm	Salts and/or acid
S_μ, S_4, S_8	"	0.3–0.6, 0.53 μm	Trailing/leading-side differences
SO_2	"	0.25–0.32, 4 μm	Trailing-side enhancement
O_2	"	0.577, 0.628 μm	Radiolytic, surface and atmosphere
H_2O_2	"	3.5 μm, 0.2–0.3 μm	Radiolytic
CO_2	"	4.26 μm	
Possible transient NH_3 H_2O*	"	2.21, 2.32 μm	Possibly spurious*
Possible amide features $-NH_2$†	"	2.05, 2.17 μm	
Na, K	Atmospheric resonance scattering	0.589, 0.590, 0.766, 0.770 μm	In sputter atmosphere and escaping from Europa.
H_2O^+	Plasma mass spectra	M/Z = 18	Pickup ions‡
H_3O^+ or K^{2+}	"	M/Z = 19	§
O_2^+	Ion cyclotron waves		Possible trace pickup ions¶
Cl^+, Cl^-	"		"
Na^+ or Ca^+, Mg^+ or K^+	"		"
SO^+, Si^+	"		"
Water group atoms and molecules (inferred)	Energetic Neutral Atoms (H)	H^+ charge exchange	In gas torus around Jupiter**
H††	Emission spectra	0.12 μm	"

**Brown et al.* (1988).
†*Dalton et al.* (2003).
‡*Paterson et al.* (1999a).
§*McNutt* (1993).
¶*Volwerk et al.* (2001).
***Mauk et al.* (2003).
††*Hansen et al.* (2005).

reference spectra of candidate materials measured under controlled conditions. Reflectance spectra of water ice and ices of other volatiles at low temperatures have been performed since the 1970s and numerous minerals and ices and have been studied spectroscopically. While large spectral databases exist for many materials (*Clark et al.,* 1993, 2003, 2007; *Henning et al.,* 1999; *Christensen et al.,* 2000) and applications to Mars have prompted spectroscopic studies of sulfate minerals (*Cloutis et al.,* 2006), many measurements do not encompass Europa's entire solar reflection regime, which extends from the UV to the mid-IR, from 0.2 to about 7 μm (thermal emission will dominate at longer wavelengths). Furthermore, most of these measurements were not obtained at sample temperatures appropriate to the surface of Europa. At these low temperatures [~100–132 K for the dayside (*Spencer et al.,* 1999)] spectra of many materials can be quite different (*Pauling,* 1935; *Grundy and Schmitt,* 1998; *Hinrichs and Lucey,* 2002). Early reflectance spectroscopy measurements of frozen volatiles by *Kieffer* (1970), *Kieffer and Smythe* (1974), *Lebofsky and Fegley* (1976), *Clark* (1981a,b), and others established the field of planetary laboratory reflectance spectroscopy that continues today. Recent application of cryogenic reflectance spectroscopy to candidate Europa surface materials (*McCord et al.,* 2001; *Carlson et al.,* 2005a; *Dalton et al.,* 2005) has continued to improve our knowledge of possible hydrated compounds that may be on the surface. Hydrocarbon reflectance spectra, of potential use for Europa studies, are being obtained by *Clark et al.* (2008a).

2. SURFACE SPECIES

We begin this discussion with the two major constituents: water ice and a hydrated species. Sulfur compounds (sulfur dioxide and elemental sulfur) are then discussed. While all molecules on Europa are influenced by radiation, the two obvious radiolytic products, molecular oxygen and hydrogen peroxide, are presented in order of discovery. Carbon dioxide is then discussed, followed by sodium and potassium, and finally other suggested but as yet unobserved or unverified species.

2.1. Water Ice

2.1.1. Introduction. Water, present throughout the solar system (*Encrenaz,* 2008), is expressed on Europa's icy crust (see chapter by Schubert et al.) as relatively fine-grained frost, combined with the hydrated materials described in section 2.2. Other possible H_2O forms include clathrate hydrates, discussed in sections 2.4 and 2.6. Water ice is indicated on Europa by the appearance of prominent vibrational bands in spectra of Europa (Fig. 4). Early

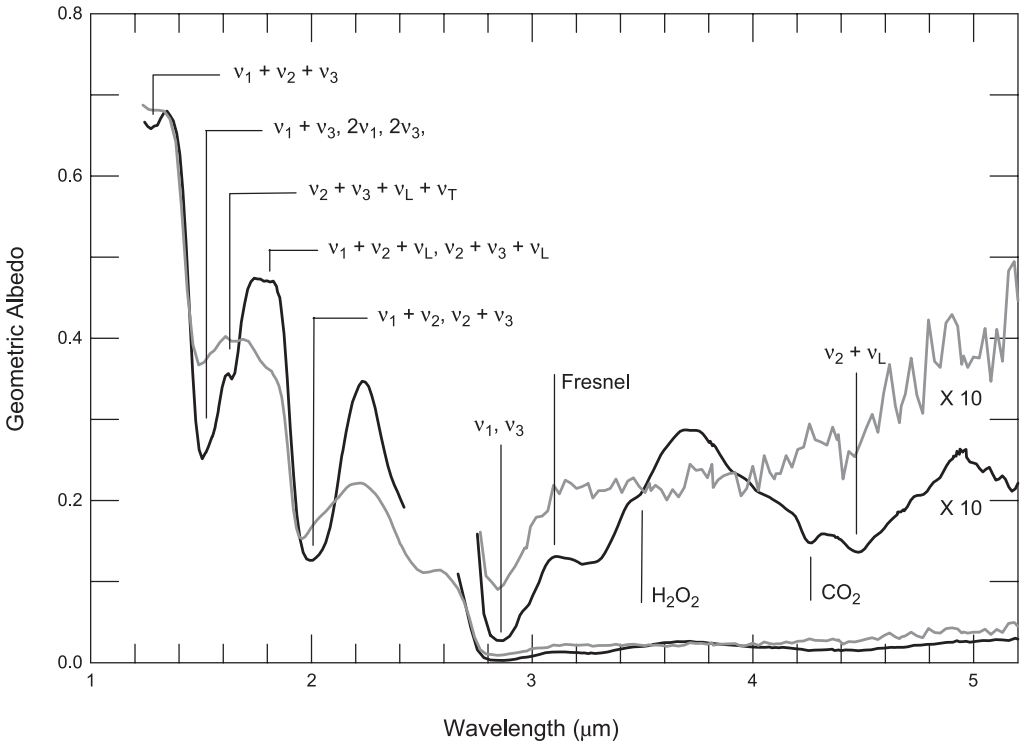

Fig. 4. Galileo NIMS near-IR spectra of Europa's leading (black line) and trailing (gray line) hemispheres. The leading-side spectrum indicates nearly pure H_2O ice with about ~30-μm grain size, along with H_2O_2 and CO_2. Band assignments are from *Ockman* (1958); ν_1 and ν_3 are the fundamental symmetric and asymmetric stetch modes and ν_2 is the fundamental bending mode. T denotes translational excitations, L denotes librational excitations. The HDO ν_3 fundamental occurs at 4.10 μm, but is not found yet in NIMS spectra. A Fresnel reflection feature (reststrahlen band) is found in at 3.1 μm where the ν_1 and ν_3 absorption is so strong that ice behaves like a metal (the reflection minima at 2.85 μm occurs where the real index crosses unity) The shape of Europa's diffuse reststrahlen feature indicates amorphous ice in the leading-side surface, but the feature at 1.65 μm that involves lattice excitations indicates crystalline ice at submillimeter sampling depths. The average trailing-side spectrum shows the asymmetric water bands of Europa's hydrated material. This spectrum, obtained during the G2 Galileo Europa flyby, is noisier than the leading-side spectrum, which was obtained during the E11 orbit at a large distance from Europa, outside its intense radiation environment.

telescopic observations of the Galilean satellites by *Kuiper* (1957) suggested the presence of water bands, confirmed by near-IR spectra obtained by *Moroz* (1965) and *Johnson and McCord* (1971) (see chapter by Alexander et al.). High-quality spectra were obtained by *Pilcher et al.* (1972) and *Fink et al.* (1973) and show Europa to have a predominantly H_2O covered surface with much more ice coverage than on Ganymede or Callisto. *Pollack et al.* (1978) obtained spectra of the Galilean satellites from airborne telescopic measurements and *Clark* (1980) obtained high-quality ground-based spectra. They both noted that the H_2O bands on the trailing hemisphere were distorted, and we now know that these distorted bands are due to a hydrate and not pure H_2O frost. Europa's trailing side contains hydrate and H_2O ice in variable proportions, whereas the leading hemisphere's surface is dominated by water ice.

2.1.2. Ice phases and their formation. The phases of ice are of interest because they indicate surface processes and likely play a role in trapping of volatile molecules such as O_2 and CO_2. The lowest-energy lattice arrangement of water ice at low pressures is hexagonal. Ice produced by freezing liquid water is this form except when flash frozen under very special conditions, forming amorphous ice (*Mayer,* 1985). Condensation from the gas phase produces different forms depending on the temperature (*Jenniskens et al.,* 1998; *Baragiola,* 2003). Water ice grown within about 100° of its 273 K melting point is hexagonal. A metastable cubic crystalline structure (in which the alternate planes of the hexagonal structure are shifted one position) is formed at temperatures of approximately 140 to 150 K, and disordered amorphous structures are made below 150 K. There are three known amorphous phases (see *Jenniskens et al.,* 1998), a high-density phase (I_ah) formed at temperatures <30 K, a low-density phase (I_al) formed at temperatures <100 K, and restrained amorphous ice (I_ar) that coexists with cubic ice and formed when either I_al is heated or irradiated, or when water molecules are condensed in the temperature range of 100 to 140 K.

Once formed, the various forms of ice will eventually become hexagonal ice, with the rates being very dependent on temperature. Observed europan temperatures range from <76 K at night to a dayside maximum of 132 K (*Spencer*

et al., 1999), but ice and darker materials may segregate by sublimation (*Spencer,* 1987a), leading to higher-albedo icy regions having low daytime temperatures of perhaps ~110 K (*Grundy et al.,* 1999). Even at these temperatures, amorphous ice will crystallize over short timescales, e.g., at 100 K it will crystallize within 10 yr to cubic ice (*Jenniskens et al.,* 1998; *Baragiola,* 2003) and perhaps within 20 yr to hexagonal ice [extrapolated from measurements by *Dowell and Rinfret* (1960)].

Amorphous ice on Europa can be continuously created from the condensation of previously sublimated or sputtered molecules (there may be deposition rate effects that favor the crystal formation (*Kouchi et al.,* 1994; but see *Baragiola,* 2003). Another likely amorphization mechanism is the disruption of crystalline ice by particle radiation. Ultraviolet, electron, and ion irradiation produce disorder in crystalline ice (*Kouchi and Kuroda,* 1990; *Baratta et al.,* 1991; *Moore and Hudson,* 1992; *Strazzulla et al.,* 1992; *Baragiola,* 2003; *Raut et al.,* 2004; *Baragiola et al.,* 2005; *Mastrapa and Brown,* 2006, *Leto and Baratta,* 2003; *Leto et al.,* 2005, and references therein). Note that a numerical cross-section error in *Kouchi and Kuroda* (1990) is corrected in *Leto et al*. (2003). Amorphization by irradiation is more effective at temperatures lower than those of Europa's surface. However, the decrease in efficiency with increasing temperature appears to depend on the type of incident particle. It may also depend on the dose rate and on the specific measurement, e.g., electron diffraction, the far-IR lattice bands, the 3.1-μm fundamental stretch band, or the 1.65-μm combination band, each of which may indicate different amorphous properties. *Moore and Hudson* (1992) first noted particle dependence when comparing the temperature dependence of the amorphization rate for proton irradiation with *Strazzulla et al.*'s (1992) results for helium ion bombardment. Similar conclusions are suggested by comparing *Leto and Baratta*'s (2003) and *Raut et al.*'s (2004) argon ion experiments conducted at 16 K and 70 K, respectively, for which there is only a factor of ~2 decrease in efficiency, compared to a factor of 200 for protons. (Note that the ion energies were somewhat different.) Amorphization by electrons exhibits a small rate decrease with temperature (*Strazzulla et al.,* 1992). It seems likely that electrons and the heavy energetic (keV to MeV) sulfur and oxygen ions produce the amorphous ice seen on Europa. We also note that irradiation of existing condensed amorphous ice increases its resistance to crystallization (*Baratta et al.,* 1994). The amorphization rate will decrease with depth and at some level below the surface the crystallization rate will exceed the amorphization rate and a transition from amorphous to crystalline will be formed.

2.1.3. Spectral properties. The water molecule has a fundamental H–O–H bending transition (ν_2) at 6 μm and O–H fundamental stretching bands (ν_1, ν_3) at 3 μm. Overtones and combination bands produce features at shorter wavelengths (Fig. 4). Ice exhibits lattice excitations (phonons) at ~45 μm and ~12 μm, corresponding to molecular translations (ν_T) or librations (ν_L), respectively. Many weak combination bands include these modes.

The spectrum of hexagonal and cubic ice are essentially indistinguishable from each other at near- and mid-IR wavelengths (*Bertie and Whalley,* 1964, 1967; *Bertie et al.,* 1969), and the difference of internal energy between cubic and hexagonal ice is small (*Handa et al.,* 1988). There is some evidence of absorptivity differences between cubic and hexagonal ice in the 60-μm region (*Bertie and Jacobs,* 1977; *Curtis et al.,* 2005). There are also possible differences between cubic and hexagonal ice absorption properties in the far UV (*Onaka and Takahashi,* 1968).

The amorphous forms have highly variable spectra, depending on their temperature history. "Annealed" forms of amorphous ice (that have been warmed above 100 K) have well-defined spectra that are distinct from the spectra of crystalline ice (*Hagen et al.,* 1981; *Schmitt et al.,* 1998). There are several features in the near-IR reflection spectrum of water ice that can be used to probe lattice order. These include the narrow combination band at 1.65 μm that involves lattice motions as well as molecular vibrations and exhibits a greatly reduced strength in warm crystalline or amorphous ice (*Hagen et al.,* 1981; *Grundy and Schmitt,* 1998; *Schmitt et al.,* 1998; *Mastrapa and Brown,* 2006). This band is temperature sensitive, and has been used as a thermometer for some outer solar system satellites, but has not been useful for determining Europa temperatures due to the presence of amorphous ice, hydrated mineral phases, and radiation-damaged crystalline ice (*Grundy et al.,* 1999). The fundamental absorption near 3.1 μm appears as a reflection peak in frost spectra. It is broad and weak for amorphous and warm ice (*Hagen et al.,* 1981; *Wood and Roux,* 1982), and narrower and stronger with a triplet structure for cold crystalline ice (*Bertie et al.,* 1969; *Bergren et al.,* 1978; *Hagen et al.,* 1981). Subtle band-center shifts and bandwidth changes are also apparent for all the IR bands as a function of temperature and crystallinity (*Hagen et al.,* 1981; *Grundy and Schmitt,* 1998; *Mastrapa et al.,* 2008; *Mastrapa and Sandford,* 2008), as well as other parameters such as grain size, purity, and illumination and observation geometry.

2.1.4. NIMS observations. Although several telescopic spectral studies of Europa were conducted earlier (see *Calvin et al.,* 1995), the spatial and spectral resolution needed to study the physical state of the ice and to separate the ice and hydrate components was not available until the Galileo Near Infrared Mapping Spectrometer (NIMS) (*Carlson et al.,* 1992) orbited Jupiter. *Hansen and McCord* (2004), using NIMS data, studied the balance between crystal disruption by radiation vs. crystal formation by thermal processes for the icy Galilean satellites' surfaces. They used the 3.1-μm reststrahlen or Fresnel reflection peak, which is formed by reflection off the facets of the water ice grains and is effectively from depths of approximately a wavelength. The strength and shape of the 3.1-μm peak does not vary significantly with grain size, as long as the grains are larger than about 10 μm.

Hansen and McCord (2004) found that the nearly pure ice on the uppermost surface of Europa's leading hemisphere appeared to be uniformly amorphous, implying that

radiation processes dominated thermal processes in that hemisphere. The trailing side contains predominantly hydrated material rather than pure ice, so no definitive statements about phase can be made, other than that there is some crystalline H_2O ice present, as indicated by the presence of a weak 1.65-μm band. The 2.71-μm dangling bond feature, formed in porous amorphous ice, is not apparent in NIMS spectra and is not expected to be present due to rapid compaction and pore closure by ion irradiation (*Palumbo,* 2006; *Raut et al.,* 2007). From the presence of the 1.65-μm band on the leading side, *Hansen and McCord* (2004) inferred that ice at ~1 mm depth was crystalline, so the transition zone from amorphous to crystalline must take place somewhere above 1 mm depth. This depth value can be refined somewhat. Using the sampling depth calculations of section 1.4 with a reflectivity of R (1.65-μm) ~ 0.4 (see Fig. 4) and a grain diameter D ~ 30 to 40 μm, then the sampling depth Z is about 120 to 160 μm. It is plausible that the ice phase is the restrained amorphous form. Within that depth, there will be both amorphous and crystalline ice and the relative amounts can be studied using the ratio of the 1.65-μm and 1.5-μm band areas. From Fig. 4, an area ratio of 0.025 is found and is about one-half or less than that for crystalline ice at a nominal Europa temperature of 120 K (*Grundy and Schmitt,* 1998; *Leto et al.,* 2005, *Mastrapa and Brown,* 2006). Leto et al. have studied the amorphization of cubic ice irradiated at 90 K by 200-keV protons, as indicated by these band ratios, and find that a dose of ~5 eV/16-amu will produce the observed value. They found that complete amorphization is accomplished at ~10 eV/16-amu. At the midpoint of the sampled depth (Z/2 ~ 70 μm) the heavy ion dose rate is ~0.05 eV/H_2O-molecule/year (see chapter by Paranicas et al.), giving a very crude estimate of amorphization timescales of ~100 yr. If protons are included in the dose rate, the timescale will be less. Note that Leto et al.'s results are different than *Mastrapa and Brown*'s (2006) measurements for the same band and the same ionizing particle (protons); the latter authors suggest that differences in experimental film thicknesses may be important. The phase state of the surface may be a useful indicator of age, but more experimental work on amorphization and crystallization at Europa-like temperatures is needed.

Since the vapor pressure of amorphous ice is up to 100 times that of crystalline ice (*Kouchi,* 1987; *Sack and Baragiola,* 1993), the preponderance of amorphous ice on the surface could increase the role of sublimation relative to sputtering and micrometeoroid impacts on producing an atmosphere, H_2O redistribution, and resurfacing (*Shi et al.,* 1995; *Tiscareno and Geissler,* 2003) (see sections 1.3.2 and 1.3.5).

Water ice grain diameters for the leading, icy hemisphere have been determined to be ~30–40 μm using theoretical water ice spectra and comparing them to the NIMS data (*Hansen and McCord,* 2004). In the trailing hemisphere, where there is both water and hydrate contributing to the absorption, the two different average grain sizes were determined using intimate mixing of these two materials (*Carlson et al.,* 2005a). Hydrate grain sizes are given in section 2.2; for H_2O, there is an equator-to-pole increase in H_2O grain sizes, at least for the northern hemisphere. H_2O grains of about 20 μm in diameter are found for equatorial regions, increasing to 50 μm at midlatitudes (45°). Mean diameters are about 100 μm at 60°N. The particle sizes are probably controlled by micrometeoroid-induced gardening and comminution, balanced by the sputter destruction of small grains (*Clark et al.,* 1983).

2.2. Hydrates

2.2.1. Introduction. Europa exhibits H_2O absorption bands that are distorted and asymmetric compared to pure H_2O (Fig. 4). These bands were first noted by *Pollack et al.* (1978), who suggested that the bands were broadened by magnetospheric particle bombardment, as found in laboratory measurements of irradiated silicates (*Dybwad,* 1971). *Clark* (1980) found similar features in trailing-side spectra and remarked that they were most unusual spectra among the four objects he studied (Europa, Ganymede, Callisto, and Saturn's rings), and possibly due to ice mixed with other minerals as studied in his laboratory (*Clark,* 1981b). He presciently noted that no hydrated minerals could be ruled out. These distorted bands, noted in early NIMS spectra and found to be similar over much of the trailing side, were initially considered to be from water in clays, which can contain interlayer H_2O molecules, or in natural zeolites such as chabazite and copiapite that can trap H_2O and other molecules. In both cases distorted and asymmetric water bands are found (*Clark et al.,* 1990, 1993) but the band shapes did not provide good matches to Europa spectra (*McCord et al.,* 1998b). Spectra of OH-bearing minerals, particularly phyllosilicates, also bear resemblance to those of Europa's dark terrain. However, lacking the H–O–H stretching plus bending combination bands ($\nu_1 + \nu_2$, $\nu_2 + \nu_3$) at 2 μm, they do not exhibit all the combination features observed in Europa's 1- to 3-μm spectrum (*Hunt and Ashley,* 1979; *Clark et al.,* 1990). Attempts to reproduce the distorted Europa spectral features using varying grain sizes of water ice frosts and glazes, as well as neutral scattering elements such as bubbles or dust, achieved only limited success (*Carlson et al.,* 1996; *McCord et al.,* 1999; *Dalton,* 2000). The remaining possibility was hydrates.

Two explanations for the asymmetric bands were proposed, based on two different classes of hydrated molecules: hydrated salts (possibly sulfates) (*McCord et al.,* 1998b) and hydrated sulfuric acid (*Carlson et al.,* 1999b). In the first case, the initial source of the salts is considered to be upwelled material from the ocean, while the second, sulfuric acid, is the major equilibrium product of the radiolysis of sulfurous material and H_2O. In the latter case the initial source of sulfur is masked by radiolytic chemistry, and could be iogenic sulfur ions or endogenic sulfate salts, sulfides, or sulfoxides. It is important to note that the hydrate bands are from vibrations of water molecules, distorted in

the hydrate structure, and this alteration can produce non-unique spectra. Thus, it is difficult to establish unambiguous identification with the current data, and there is presently no definitive, unequivocal evidence for either acids or salts on Europa.

2.2.2. Spectroscopy of hydrates. Hydrated compounds are molecules or ions with surrounding shells of water molecules that are held in place by polar bonds. (Hydrates should not be confused with clathrate hydrates, which are crystalline arrangements of H_2O molecules that form cages surrounding trapped "guest" molecules.) Hydrated molecules exist in aqueous solutions, in mixed amorphous ices, and as stoichoimetric crystals. In crystalline hydrates, water molecules are bound at specific sites (*Bauer,* 1964; *Hunt and Salisbury,* 1970; *Hunt et al.,* 1971a,b; *Hunt,* 1977; *Crowley,* 1991) and comprise part of the crystal lattice. This configuration allows for some but not all of the normal water vibrational modes (*Herzberg,* 1950; *Whalley and Bertie,* 1967; *Hunt and Salisbury,* 1970; *Hunt et al.,* 1973). The electrostatic influence of the other molecules leads to distortion of the crystal lattice and hydrogen bonds (*Pauling,* 1935; *Herzberg,* 1945) and consequently shifts the allowed vibrational frequencies and alters the corresponding features' shapes (*Whalley,* 1968; *Bertie et al.,* 1969; *Hunt and Salisbury,* 1970; *Hobbs,* 1974; *Hunt,* 1977). These shifts are illustrated by the near-IR spectra of hydrated magnesium sulfates ($MgSO_4 \bullet nH_2O$; n = 0, 1.5, 2, 3, 4, 5, 6, 7) shown in Fig. 5. The spectrum of anhydrous $MgSO_4$ (top) is nearly featureless, because $MgSO_4$ has no vibrational features in this wavelength range (*Gaffey et al.,* 1993; *Chaban et al.,* 2002; *Dalton,* 2003). The two small absorptions seen in the anhydrous $MgSO_4$ spectrum in Fig. 5 are actually caused by adsorbed water, which is virtually impossible to remove even under stringently controlled laboratory conditions because of the hygroscopic nature of the $MgSO_4$ (*Bauer,* 1964; *Crowley,* 1991; *Dalton,* 2003). Magnesium sulfate readily accepts water molecules, and $MgSO_4 \bullet H_2O$ (kieserite) has features at ~1.0, 1.25, 1.5, and 2.0 μm whose positions correlate with those in the water ice (compare Fig. 4 and Fig. 5) and, indeed, arise from the bound water. As water content increases, more vibrational modes become possible, and several smaller features become apparent in the spectrum. As the number of waters of hydration increases, the magnesium sulfate hydrate spectra become more complex, while various small bands overlap and blend to give rise to broader absorption features. In a very general sense, as the number of water molecules of hydration increases, the spectrum of hydrated magnesium sulfate begins to more closely resemble the spectrum of the non-icy material on Europa.

At the low temperatures that prevail on icy satellites of the outer solar system, many hydrated compounds exhibit markedly different spectral behavior compared to spectra obtained at "room" temperature (*Dalton and Clark,* 1999; *McCord et al.,* 1999; *Dalton et al.,* 2005). In the 100–132-K range of dayside surface temperatures observed at Europa by Voyager and Galileo (*Spencer,* 1987b; *Spencer et al.,* 1999), the decreased thermal motion lowers the intermolecular coupling and causes the individual bands to narrow, reducing their overlap and producing several discrete, fine absorption features. This is illustrated in Fig. 6 for hexahydrite ($MgSO_4 \bullet 6H_2O$) and bloedite [$Na_2Mg(SO_4)_2 \bullet 4H_2O$]. The effects are most pronounced within the complexes that make up the 1.5- and 2.0-μm absorption features. At 300 K, these features are smooth and broad. At 120 K, however, these and other minor absorption features become much more pronounced. Several very fine absorption features, with widths ranging from 10 to 50 nm, can be observed within the 1.5-μm feature in both species.

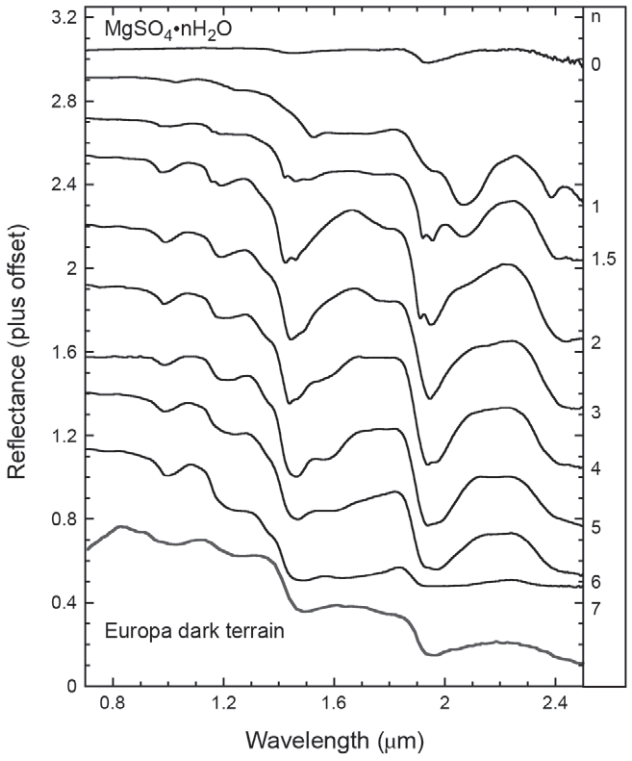

Fig. 5. Spectra of magnesium sulfate hydrates, $MgSO_4 \bullet nH_2O$, for n = 0–7. The addition of each water of hydration produces additional absorption features. As n reaches higher values, the absorptions overlap and blend together, producing broader features. These spectra were measured for samples at room temperature. Adapted from *Dalton* (2003); pentahydrite spectrum from *Crowley* (1991).

Near-IR reflectance spectra of numerous hydrated materials have been studied in the laboratory (*Hunt et al.,* 1971b; *Crowley,* 1991; *Carlson et al.,* 1999b, 2005a; *Dalton,* 2000, 2003, 2007; *McCord et al.,* 2001, 2002; *Crowley et al.,* 2003; *Dalton et al.,* 2003, 2005; *Orlando et al.,* 2005) and many hydrates show diagnostic absorptions in their spectra. A great number of these features are of sufficient strength and depth to be distinguishable at the Galileo NIMS resolution (25 nm), yet have not been detected in any examination of the NIMS observations to date, nor in high-resolution, high-signal-to-noise, spatially resolved telescopic spectra of Europa's trailing side obtained by *Spencer et al.* (2005). Experiments with flash-frozen brines (*Dalton and*

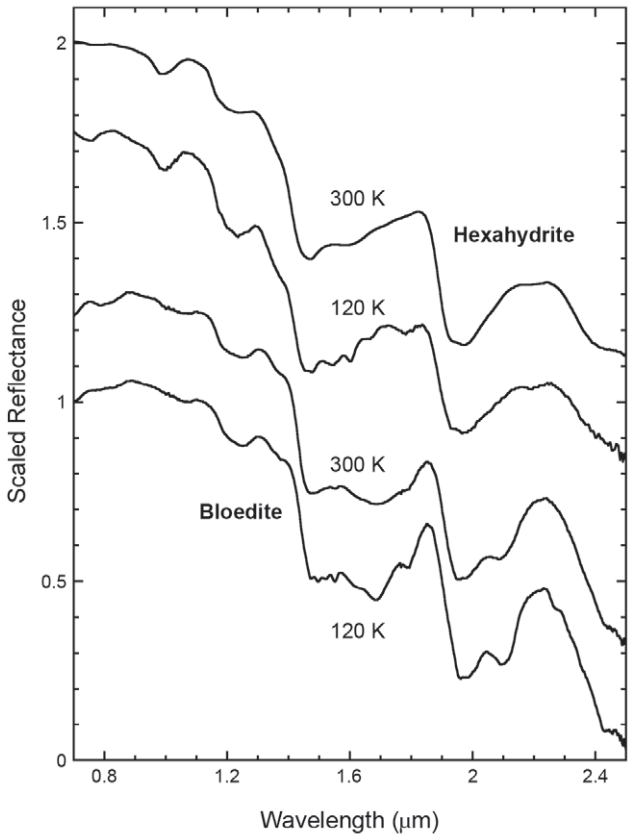

Fig. 6. Laboratory spectra of hexahydrite ($MgSO_4$•$6H_2O$) and bloedite [$Na_2Mg(SO_4)_2$•$4H_2O$] at 300 K and 120 K. At low temperature, the individual vibrational overtones and combinations that make up the broad water absorption features change in frequency, leading to differences in absorption feature position, strength, and width. Additional minor features become apparent and sharpen as the temperature decreases further. Adapted from *Dalton* (2003).

Clark, 1998; *McCord et al.,* 2002; *Dalton et al.,* 2005; *Orlando et al.,* 2005) combine the effects of hydration and small grain size to approximate several of the Europa spectral features. In these frozen brines, mixtures of pure water, anions, cations, and commingled molecules of varying levels of hydration match the overall character and slope of the Europa spectrum, but no perfect match to all the band shapes and positions has yet been obtained.

While magnesium and sodium sulfate hydrates have been studied intensively in the literature, sulfuric acid hydrates also give rise to distorted and asymmetric features in the 1.5- and 2.0-μm range that are strikingly similar to those seen in the spectrum of Europa (*Carlson et al.,* 1999b, 2002, 2005a). Close examination of the spectrum of sulfuric acid hydrate in Fig. 7 (from *Carlson et al.,* 1999b) reveals that the features correspond to those seen in sulfates and other hydrates, at 1.25, 1.5, 1.8, and 2.0 μm. The complex index of refraction of H_2SO_4•$8H_2O$ was subsequently measured and used to generate comparison spectra (*Carlson et al.,* 2005a), showing that the relative strengths and shapes of the laboratory-derived features closely match those seen in Europa spectra. Shifts of the 1.5- and 2.0-μm bands may be due to radiation effects as discussed below.

Similar spectral qualities have also been produced by the addition of acids (HCl, HBr) to water ice, resulting in creation of hydronium (H_3O^+) and altering the ice structure (*Clark,* 2004). Irradiation of water ice may also create H_3O^+ (*Clark,* 2004). These changes in the ice structure may shift spectral absorption feature positions and alter spectral shapes and match Europa's profile (*Clark,* 2004). HCl and HBr also form numerous hydrates whose spectral properties resemble those of Europa (R. Clark, personal communication, 2008).

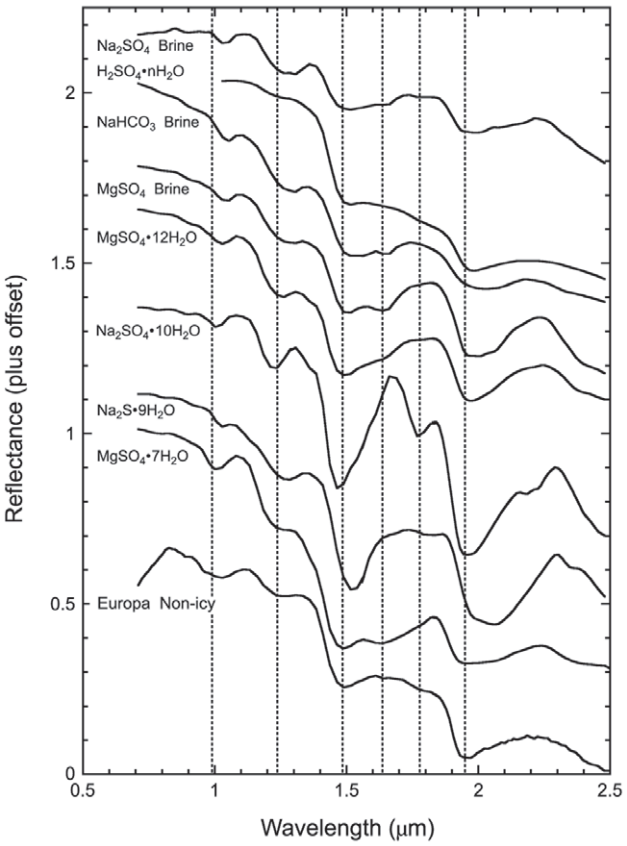

Fig. 7. Cryogenic near-IR reflectance spectra of highly hydrated compounds and frozen brines. Each spectrum has been offset vertically for clarity. All spectra in this figure were measured at 100 K, except sulfuric acid hydrate at 140 K. Spectra were convolved to the NIMS resolution for comparison with the Europa spectrum at bottom. Vertical bars denote band center positions in the Europa spectrum. From bottom, in order of increasing hydration state: epsomite, $MgSO_4$•$7H_2O$; sodium sulfide nonahydrate, Na_2S•$9H_2O$; mirabilite, Na_2SO_4•$10H_2O$; magnesium sulfate hendecahydrate, $MgSO_4$•$11H_2O$; sulfuric acid octahydrate, H_2SO_4•$8H_2O$; $MgSO_4$, $NaHCO_3$, and Na_2SO_4 saturated brines, flash-frozen at 77 K. [Sulfuric acid hydrate spectrum from *Carlson et al.,* (1999b); others from *Dalton et al.* (2005).] The hydration state of $MgSO_4$•$11H_2O$ was established by *Peterson and Wang* (2006).

Biological materials also contain a number of hydrated compounds, and cryogenic spectroscopy of extremophilic organisms has demonstrated that microbes in low-temperature ice provide as close a spectral match to the Europa deposits as any individual material proposed thus far (*Dalton et al.,* 2003). Before such measurements can be considered as potential evidence for extant or extinct biological activity at Europa, however, spectral properties of other candidate materials, including many hydrates, must be investigated.

Midinfrared spectra within the reflected sunlight regime (i.e., for wavelengths greater than ~2.5 μm) may provide anion-specific information. While the fundamental stretching and bending transitions occur at longer wavelengths, combination bands will appear at shorter wavelengths, within the reflected sunlight regime (to ~7 μm for Europa). For example, the frequencies of the fundamental stretching transitions of sulfate anions are in the 1040 to 1210 cm^{-1} region (~8 to 12 μm), and the overtone occurs at about 4.5 μm. Water-of-hydration also can add additional combination bands that can be diagnostic of the anions, and perhaps the cations. However, the added H_2O molecules introduce more absorption and can mute the band structure. Examples are shown in Fig. 8, illustrating that diagnostic information may be gleaned from mid-IR spectra, but such spectra can vary with grain size, measurement geometry, and temperature. NIMS trailing-side measurements (Fig. 4) confirm the low and seemingly featureless reflectance found through groundbased spectrophotemetry by *Lebofsky and Fegely* (1985), consistent with the presence of an acid hydrate or a mixture of salt hydrates, but the amount of radiation noise in NIMS's long-wave channels has discouraged comprehensive investigations. More laboratory work and data analysis needs be performed to make full use of this spectral region.

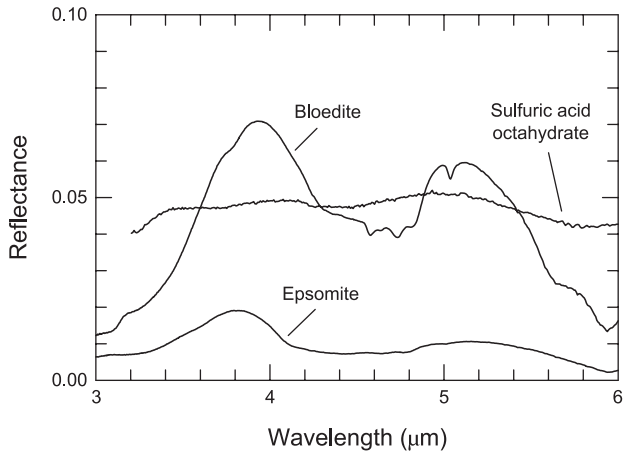

Fig. 8. Reflectance of example sulfate hydrates in the 3- to 6-μm region. Although the reflectance is low, some hydrates exhibit diagnostic structure that may be useful for hydrate identification. The bloedite [$Na_2Mg(SO_4)_2 \cdot 4H_2O$] and epsomite ($MgSO_4 \cdot 7H_2O$) spectra are from the USGS splib06a library (*Clark et al.,* 2007) and are from measurements by *Crowley et al*. (1991). The samples were at room temperature and the grain sizes are about 250 μm (*Crowley et al.,* 1991). Other hydrated salt spectra are presented by *McCord et al*. (1999). The acid hydrate spectrum is for a sample at 77 K (*Carlson et al.,* 1999b). Reflectance spectra are sensitive to grain size, so spectra of other samples may be brighter or darker and exhibit different shapes.

The UV region may be useful in discriminating between various candidate species, using existing spectra from IUE, Hubble, and Galileo (see section 2.3) and future observations, and comparing them with laboratory measurements. Water ice is relatively transparent for wavelengths greater than ~0.2 μm (*Dressler and Schnepp,* 1960; *Onaka and Takahashi,* 1968; *Pipes et al.,* 1974; *Warren,* 1984; *Warren and Brandt,* 2008; *Hapke et al.,* 1981), so features from absorbers such as hydrates may be present in UV spectra of Europa. As an example, two hydrated salts that have been suggested for Europa, mirabilite and epsomite (see section 2.2.5), show potentially diagnostic UV absorption features [see *Clark et al.*'s (2007) splib06a spectral library and *Crowley et al.* (1991)]. These reflectance spectra are compared with Europa measurements in Fig. 9. Mirabilite exhibits UV absorption with an onset at ~0.4 μm and grows in strength as the wavelength decreases. Epsomite has a weak absorption at 0.27 μm and a stronger band at 0.23 μm with a relative band depth of 25%. The position of weaker band coincides with Europa's 0.27-μm absorption band, but the strength may be too low to explain Europa's absorption, generally considered to be due to SO_2 (see section 2.3). The 0.23-μm feature of epsomite is not apparent in Galileo UVS measurements, but the Europa observations are noisy at these short wavelengths due to the low solar flux and the strength of the epsomite band may be muted by Europa's strong UV absorption, thought to arise from sulfur (see section 2.4). Future UV laboratory measurements and analyses such as those by *Hendrix et al.* (2008) can provide useful constraints for Europa's surface composition.

2.2.3. Spectral effects of radiation. Hydrates are susceptible to alteration by radiation, which can remove water molecules (dehydration), damage crystal structure (amorphization), and destroy either the water molecules or the host molecule (decomposition). One result of these processes is to change the H_2O vibrational modes and thus the corresponding spectrum. These spectral changes of irradiated hydrates are not well characterized, but results by *Nash and Fanale* (1977) illustrate the general effect on the spectrum (Fig. 10), which is to shift the positions of the hydrate bands and change their shape. The derived G value for H_2O decomposition of $MgSO_4 \cdot 7H_2O$ and other sulfates is small [$G(H_2) = 0.0027$; see *Huang and Johnson* (1965)], but the results of *Nash and Fanale* (1977) indicate that the loss of H_2O (dehydration) is greater by a factor of about 100 or more. Band shifts of about 1–2% are also found for the fundamental bands of sulfates (*Spitsyn et al.,* 1969) and silicates (*Dybwad,* 1971). Radiation also darkens sulfates in the visible and UV (*Lebofsky and Fegley,* 1976; *Nash and Fanale,* 1977; see also Fig. 2 of *Carlson et al.,* 1999b), presumably by forming sulfur allotropes.

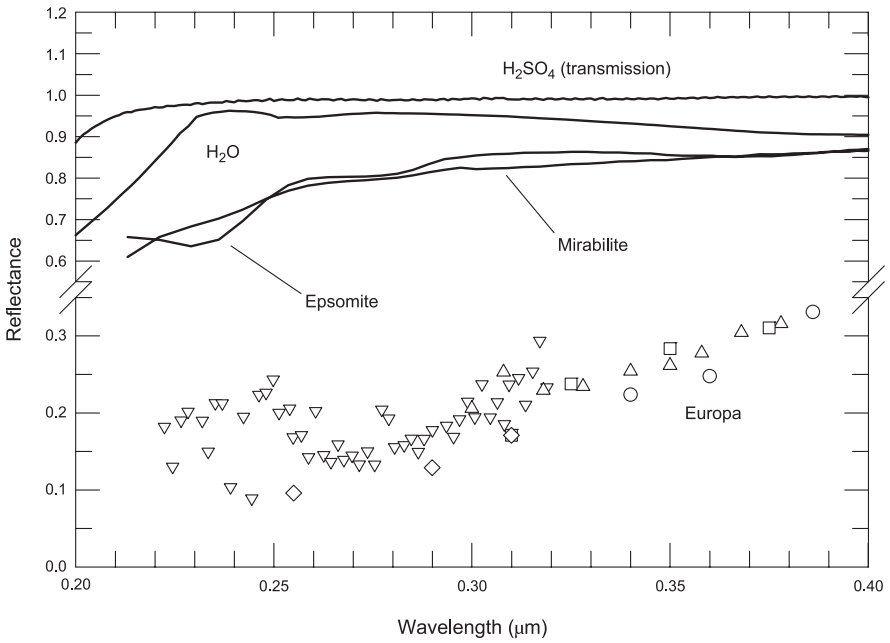

Fig. 9. Ultraviolet spectra of laboratory samples and Europa's trailing hemisphere. Mirabilite (Na_2SO_4•$10H_2O$) and epsomite ($MgSO_4$•$7H_2O$) reflectance spectra are from the USGS splib06a spectral library (*Clark et al.,* 2007) and are from measurements by *Crowley et al*. (1991). The samples were at room temperature and the grain sizes are about 250 μm (*Crowley et al*. 1991). The reflectance of H_2O frost at 77 K measured by *Hapke et al.* (1981) shows the onset of absorption at ~0.23 μm (see also *Pipes et al.,* 1974) as does the transmission spectrum of a 5-mm path-length of liquid sulfuric acid at 20°C, discussed by *Carlson et al*. (1999b). Europa data are from *Johnson* (1970) (○), *Wamsteker* (1972) (△), *McFadden et al.* (1980) (□), *Nelson et al.* (1987) (◇), and *Hendrix et al.* (1998) (▽). See Fig. 13 for extended spectral range and normalization information. Note the vertical scale change.

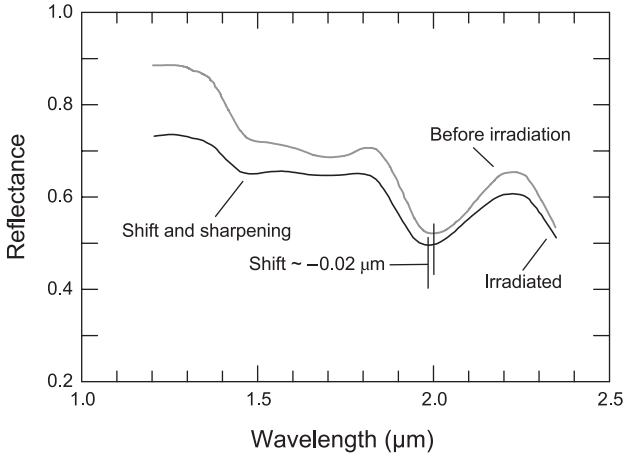

Fig. 10. Radiation-induced spectral shifts. Proton irradiation of bloedite [$Na_2Mg(SO_4)_2$•$4H_2O$] shows hydrate band-center shifts to shorter wavelengths of about 20 nm. Similar shifts to shorter wavelengths are seen in ferric sulfate at doses of ~10 eV/16-amu (*Nash and Fanale,* 1977). Comparisons of laboratory and Europa spectra must allow for radiation-induced shifts of hydrate bands. Measurements from *Nash and Fanale* (1977). The spectrum of the irradiated sample was offset by –0.1 to improve clarity.

2.2.4. Abundance and distribution of Europa's hydrate. The global distribution of hydrated material was initially studied by *McCord et al*. (1999), who chose two endmembers (one mostly ice and the other mostly non-ice hydrated material) and mapped the relative fraction using linear mixing. They found that spectra for the ice-poor areas looked nearly identical for all regions investigated, implying that the hydrate was about the same composition everywhere studied. A subsequent analysis (*Carlson et al.,* 2005a) assumed intimate mixtures of hydrate grains and H_2O ice grains and, using measured values of the optical constants for sulfuric acid octahydrate and water ice, performed a radiative transfer fit for each spectrum in NIMS global observations. The results (Fig. 11b) are similar to those of the earlier work by *McCord et al*. (1999) where the two studies overlap, but the later work encompasses more of Europa and provides information about absolute abundance and grain sizes. The maximum hydrate concentration near the antapex, expressed as hydrate/(hydrate + H_2O) is about 80–90% by volume. For sulfuric acid hydrate, this would be about 1 sulfur atom (or sulfate anion) per 10 water molecules, roughly 2 of which are in H_2O ice grains and about 8 in the hydrate (*Carlson et al.,* 2005a). Hydrate grain sizes

(diameters) are 6–14 μm on the equatorial trailing-side region, and 12–20 μm on the antijovian equatorial side. The grain sizes increase to about 25 μm at 45° to 60°N latitude. Observations during the recent New Horizons flyby produced a low-spatial resolution (180–250 km) hydrate map (Fig. 11a) that has more leading-side and southern hemisphere coverage than obtained with Galileo (*Grundy et al.,* 2007). The hydrate concentration was found to be very low throughout the observed leading hemisphere.

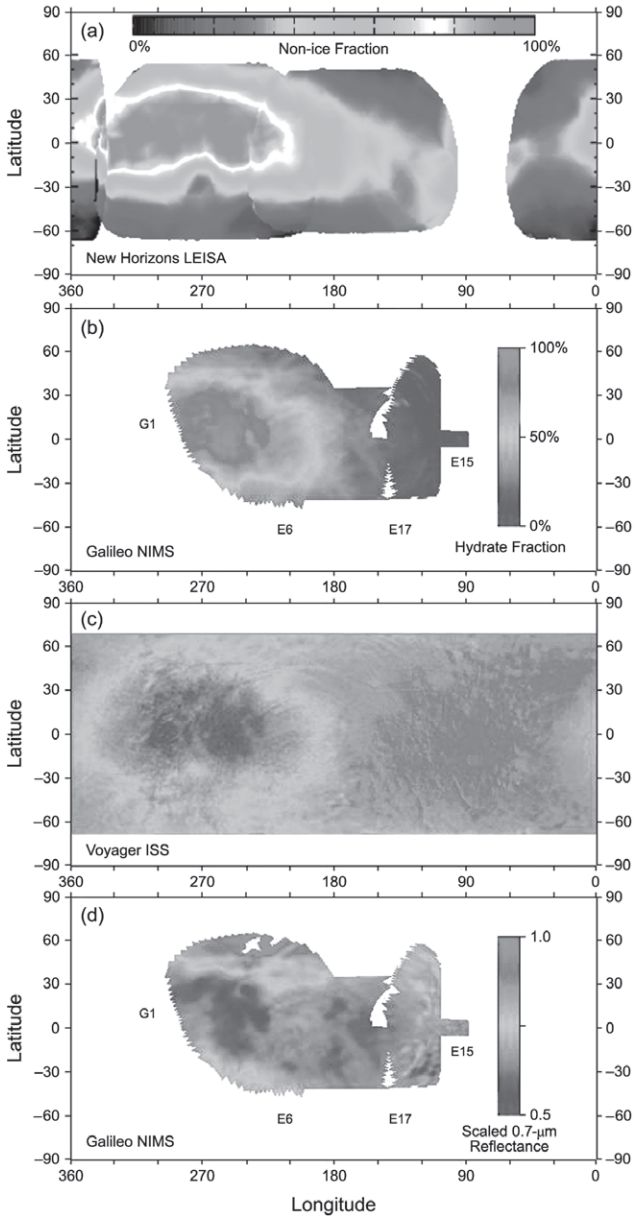

Fig. 11. See Plate 17. Distribution of hydrate and UV and near-IR albedos. **(a)** Non-ice distribution measured from New Horizons (*Grundy et al.,* 2007). **(b)** Molar distribution of hydrate assuming sulfuric acid hydrate, but representative of other hydrates (*Carlson et al.,* 2005a). **(c)** Voyager UV/V map, from *McEwen* (1986). Blue denotes high UV absorption and corresponding low UV reflectance. (d) Galileo NIMS 0.7 μm/1.2 μm ratio map, scaled (*Carlson et al.,* 2005a). Note the correlation of the non-ice hydrate distribution [**(a)** and **(b)**] with both the UV **(c)** and the near-IR absorber **(d)**, and the trailing-side enhancement of all three.

The hydrate distribution correlates with the UV absorber found in Voyager imagery (section 2.4) and with red albedo as measured by NIMS at 0.7 μm (Figs. 11c and 11d, respectively). The correlation of hydrate and decreased visual albedo means that either the hydrated material itself is dark, or that another species with low albedo is intimately associated with the hydrate. Since most hydrated salts and acids are colorless, the second possibility seems the more likely. One interpretation for the dark material is sulfur (S_8 and S_μ, cyclo-octal and polymeric sulfur), produced radiolytically from sulfate, SO_2, and possible sulfide compounds (see below). The hydrate distribution also correlates with Europa's SO_2 as measured in the UV by Galileo (section 2.3).

The hydrated material is least abundant in polar regions, where water ice dominates. The asymmetric spectral effects appear strongest in equatorial regions of the trailing hemisphere, where the iogenic plasma sulfur implantation flux is greatest. This argues for an exogenic origin. In the disrupted chaos regions, and in the immediate vicinity of lineae, the surface is darker and the spectra more asymmetric than in the surrounding terrains, suggesting an endogenic source or an endogenic modification process associated with these features. An endogenic source could be oceanic material introduced to the surface by any of several processes (section 1.3.6). An endogenic modification process could be localized shear or diapiric heating that produces a lag deposit of concentrated hydrate and associated dark material (section 1.3.5). Increasing the grain size can also enhance absorption and darken the surface. There is less hydrate in the leading hemisphere, although there are lineae and chaos regions there as well (*Riley et al.,* 2000). These leading-side features lack the color associated with the trailing "red" hemisphere. The lineae extending from the trailing fade in color in the leading hemisphere (*Nelson et al.,* 1986). Some examples of the hydrate distribution for geological features are shown earlier in Fig. 3 and in *McCord et al*. (1998b), *Fanale et al.* (2000), *McCord et al*. (1999), *Dalton* (2000), *Dalton et al.* (2003), and *Carlson et al*. (2005a).

The trailing-side enhancement suggests sulfur ion implantation as the source of hydrate, but a thin icy shell on the trailing side, allowing surface emplacement of brine, and a thick, impenetratable shell on the leading side might also explain the hemispheric dichotomy.

2.2.5. The hydrated salt hypothesis. *Clark* (1980) first suggested the possibility of hydrated minerals as the source of the asymmetric bands. The more specific hydrated salt explanation was advanced by *McCord et al.* (1998b), who noted a trailing-side enhancement of hydrated material and its association with dark material and geological features such as lineae. They found that sulfate and carbonate hydrates provided a better match to NIMS spectra than ice or hydrous silicate minerals, and that these compounds could be extruded on to the surface from the assumed ocean below. Flash evaporation, freezing, sublimation, and sputter-

ing could concentrate the exposed brine, and leave behind crystallized salt hydrates. The possible existence of salts on the surface could provide evidence for an ocean. This work was expanded to include more mapping and to find possible combinations of minerals that provide good fits to the endmember non-ice spectrum (*McCord et al.,* 1999). Various combinations of natron (Na_2CO_3•$10H_2O$), mirabilite (Na_2SO_4•$10H_2O$), bloedite [$Na_2Mg(SO_4)_2$•$4H_2O$], epsomite ($MgSO_4$•$7H_2O$), and hexahydrate ($MgSO_4$•$6H_2O$) were used to construct the linear mixing modeled reflectance. The hydrate spectra were from room temperature measurements.

The thermal and radiation stability of hydrated salt minerals epsomite, mirabilite, and natron were also investigated at temperatures relevant to Europa (*McCord et al.,* 2001). The thermal stability of epsomite was sufficient for it to remain hydrated at Europa temperatures well over geological timescales, whereas natron and mirabilite would dehydrate significantly in 10^8 and 10^3 yr, respectively. A G value for the destruction of $MgSO_4$•$7H_2O$ by the decomposition of the sulfate anion, producing SO_2, was established as $G(SO_2)$ = 0.004 and is consistent with other measurements [see *Johnson et al.* (2004) and section 1.3.1]. Flash freezing of brines that might occur on Europa if extruded brines condensed on high-thermal conductivity grains (*Baragiola,* 2003) was considered by *Dalton and Clark* (1998, 1999), *Dalton* (2000), *McCord et al.* (2002), and *Orlando et al*. (2005). The rapid freezing used in these experiments (10^4 K/min) results in disordered, glassy ices. Models of extrusion on the surfaces of icy satellites (*Allison and Clifford,* 1987; *Fagents,* 2003) do not predict such rapid cooling, but radiation can also reduce the order of crystalline samples (see section 2.2.3) and flash freezing experiments may simulate radiation-induced amorphization (*McCord et al.,* 2002). Since the crystalline order was reduced in the rapid freezing process, the resulting spectral structure was smoother than that found in crystalline hydrates and the frozen brine spectra, providing a better match to the NIMS spectra than obtained with crystalline salt hydrates. *Orlando et al*. (2005) used five combinations of magnesium sulfate, sodium sulfate, and sulfuric acid and found good fits for $MgSO_4$, Na_2SO_4, and H_2SO_4 in the ranges of 24–50%, 25–40%, and 25–35%, respectively (see section 2.2.7).

If salts were the original source, there will an assemblage of metal sulfates, hydrogen sulfates, and metal oxides and hydroxides (*Johnson,* 2001). Sulfate and other hydrates are destroyed in forming SO_2 and by removal of the metal atoms (e.g., Mg and Na), sometimes in the excited state (*Nash and Fanale,* 1977). Resulting products can be MgO, $Mg(OH)_2$, Na_2O, Na_2O_2, and NaOH, but production rates are not known, and there has been little work on oxide and hydroxide radiolysis in water ice. MgO in pure form is rapidly dissociated (*Wysocki,* 1986) with G = 1–4, but $Mg(OH)_2$ is quite stable with a destruction rate of G < 0.03 (*Glagolev et al.,* 1967). Of these two species, $Mg(OH)_2$ will likely be greater in abundance, but experiments on the initial oxide and hydroxide production rates have not been done, so one cannot predict the equilibrium value. Rough upper limits for the molar fractions of NaOH and $Mg(OH)_2$ have been established at 5% and 3% (*Carlson et al.,* 1999b; *Shirley et al.,* 1999), but it may be fruitful to reexamine spectra for these and other hydroxides (strong oxide features do not occur within the spectral range of current Europa data).

2.2.6. The sulfuric acid hypothesis and the radiolytic sulfur cycle. A different hypothesis was formulated by *Carlson et al*. (1999b), prompted by the efficient radiolytic production of sulfuric acid and the hydrophilic nature of H_2SO_4. In the frozen, crystalline state, the hydrates H_2SO_4•nH_2O with n = 1,2,3,4,6.5, and 8 are formed while in the liquid, and presumably the amorphous solid state, the first hydration shell surrounding the sulfate anion contains 7–12 H_2O molecules, and there are four H_2O molecules in the first hydration shell around each proton [present as the hydronium ion, H_3O^+ (*Ohtaki and Radnai,* 1993)]. Spectra of the hemi-hexahydrate and octahydrate showed good agreement with Europa as measured by Galileo's NIMS (*Carlson et al.,* 1999b, 2005a) (see section 2.2.7). The position of the band minima for the crystalline samples is ~0.02 μm longer than observed on Europa and has been attributed to the amorphous nature of radiolytically produced sulfate compared to the ordered structure of presumed crystalline samples measuered in the laboratory (*Carlson et al.,* 2005a).

The sulfate group, SO_4^{2-}, is a highly oxidized and stable complex and is the end product of numerous photolytic and radiolytic reactions. It is present on Venus as the main cloud particle constituent where it is formed by photolysis, it is present on Earth as acid rain from SO_2 oxidation, and perhaps was present on early Mars. Sulfuric acid is formed with high efficiency by the radiolysis of elemental sulfur in water ice at 77 K (*Carlson et al.,* 2002). H_2SO_4 is also made by sulfur ion implantation into water ice (*Strazzulla et al.,* 2007). When SO_2 in water ice is irradiated by energetic particles or photons, sulfuric acid is formed (*Schriver-Mazzuoli et al.,* 2003b; *Moore et al.,* 2007). The ions that are observed are sulfate, bisulfate (HSO_4^-), and bisulfite (HSO_3^-) (*Moore et al.,* 2007).

Sulfur dioxide and hydrogen sulfide are not produced in measurable quantities in either sulfur ion implantation or by radiolysis of elemental sulfur in water (*DellaGuardia and Johnston,* 1980; *Strazzulla et al.,* 2007). Instead, SO_2 is a product of sulfate destruction (see *Hochanadel et al.,* 1955; summary in *Johnson et al.,* 2004). Elemental sulfur is a minor decomposition product of both SO_2 (*Rothschild,* 1964; *Moore,* 1984) and sulfates (*Sasaki et al.,* 1978), but the efficiency or G value has not been obtained for SO_2 or sulfates in ice. Since sulfate is both produced and destroyed by ionizing radiation, the net result is that, whatever the starting point, an equilibrium mixture of sulfate, SO_2, elemental sulfur, and possibly some H_2S will be produced, with most of the sulfur atoms in the form of sulfate. The observed association of hydrate with dark, reddish material (presumably polymeric sulfur, S_μ; see section 2.4) and with SO_2 (see section 2.3) is consistent with the radiolytic sulfur cycle and supports this hypothesis. The timescale to establish equilibrium on Europa is two to four years (*Moore et al.,* 2007).

2.2.7. Spectral observations and fits. The two explanations discussed above are both plausible, and current analyses are unable to eliminate either of them. Indeed, it may be that both are currently operating on Europa. However, the possible existence of material derived from the ocean is an important question and definitive spectral evidence of endogenic material, such as salts or perhaps derived metal hydroxides, is needed to resolve this question. This is not possible with the current state of analysis, which we illustrate with three spectral fits in Fig. 12. Fits to Europa spectra using only sulfuric acid grains and water ice grains, intimately mixed, are shown (Fig. 12a) for a hydrated region an icy region, and an intermediate case (*Carlson et al.,* 2005a). Flash frozen acidic brines, from *Orlando et al.* (2005), are shown in Fig. 12b for their best match, consisting of 50% $MgSO_4$, 25% Na_2SO_4, and 25% H_2SO_4. An equivalent case using $NaHSO_4$ instead of equal mixtures of Na_2SO_4 and H_2SO_4 shows the same spectral behavior. Using cryogenic laboratory spectra, *Dalton* (2007) found a good match (Fig. 12b) to the Europa spectrum with a linear mixture of 62% sulfuric acid hydrate, 14% hexahydrite, 11% bloedite, and 12% mirabilite. It is not possible to distinguish between competing hypotheses at present.

2.3. Sulfur Dioxide

SO_2 was the second compound identified with any certainty on Europa. *Lane et al*. (1981), using IUE data, found an absorption band centered at 0.28 μm in Europa's trailing-side/leading-side ratio spectrum and attributed it to SO_2 in Europa's ice. These authors made the important suggestion that this compound was produced from implanted sul-

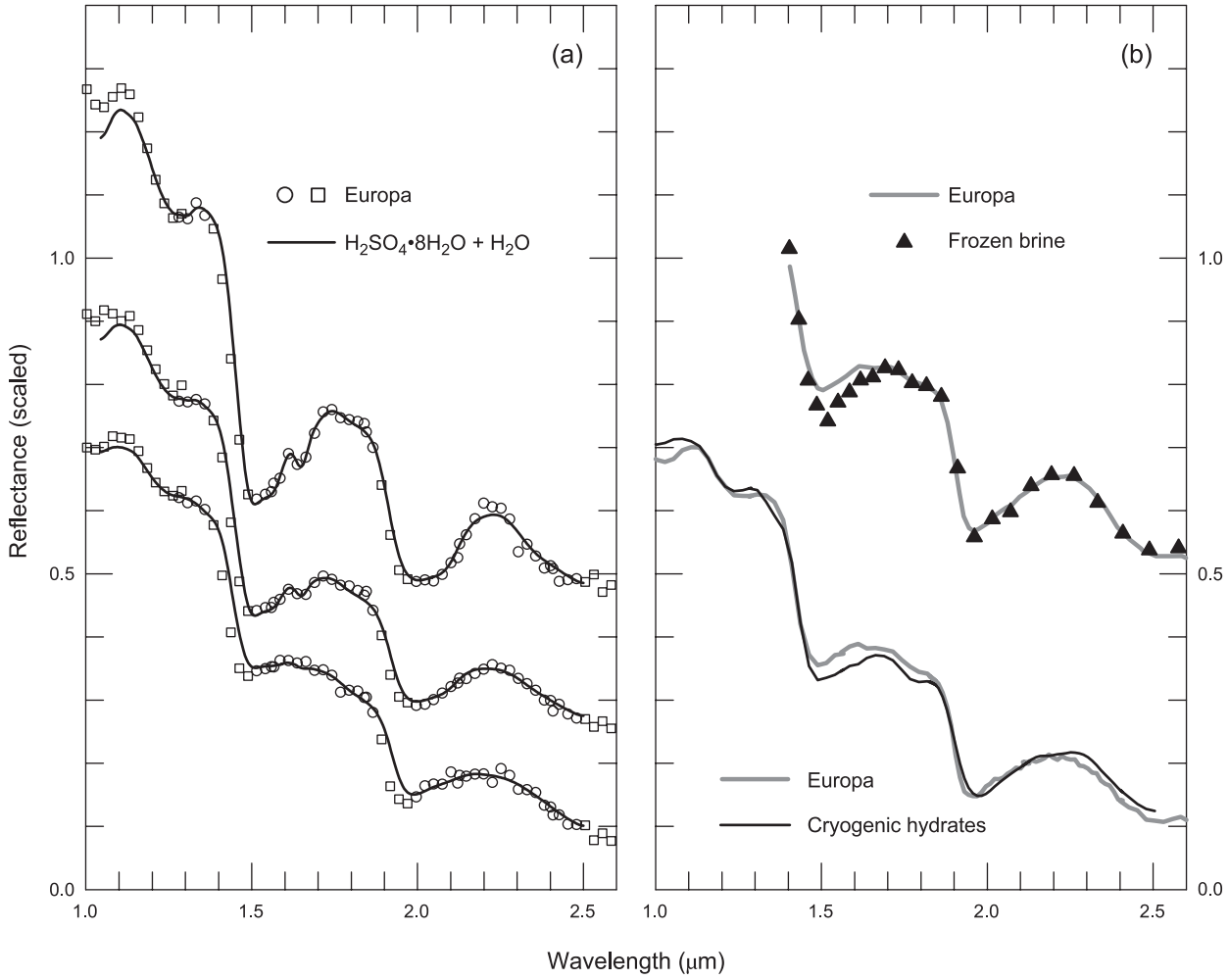

Fig. 12. Examples of the current state of spectral analysis of Europa's hydrate. **(a)** Spectra of intimately mixed sulfuric acid hydrate and water ice grains (black lines) fitted to individual NIMS spectra (symbols) using measured optical constants for H_2SO_4 hydrate and H_2O ice. The hydrate fractions for the three different pixels are, from top to bottom, 30%, 54%, and 89%. From *Carlson et al.* (2005a). **(b)** Hydrated salts and frozen brines compared to NIMS endmember spectra. The upper set compares the spectrum of a frozen brine solution (triangles) with NIMS spectra (gray line). The brine's non-H_2O composition was 50% $MgSO_4$, 25% Na_2SO_4, and 25% H_2SO_4. From *Orlando et al*. (2005). The lower set compares NIMS data (gray line) with spectrum of a numerically fitted linear mixture of individual cryogenic reflectance spectra, using 62% sulfuric acid hydrate, 14% hexahydrite, 11% bloedite, and 12% mirabilite. No H_2O was needed in this fit. From *Dalton* (2007).

fur ions from Io's plasma torus, an exogenic source contemporaneously recognized by *Eviatar et al*. (1981) (see Figs. 9 and 13 for HST and Galileo UV spectra of Europa).

The position and shape of Europa's feature closely matches spectra of condensed SO_2 (*Sack et al.,* 1992) and this molecule is the most stable sulfoxide. While sulfur monoxide, SO, exhibits absorption in the UV (*Jones,* 1950), this molecule and its dimer are extremely reactive and found only in the gas phase or within inert matrices at very low temperature (<31 K) (*Hopkins and Brown,* 1975). Disulfur monoxide, S_2O, is also unstable (see discussion in *Carlson et al*., 2007; *Baklouti et al.,* 2008) and exhibits a UV band that peaks at 0.295 μm (*Phillips et al.,* 1969), inconsistent with Europa's band position. Sulfur trioxide, SO_3, rapidly reacts with H_2O to form H_2SO_4. Other substances absorb in the UV, including sulfur. In particular, S_8 in various solvents and S_8 in the gas phase exhibit absorption maximum at ~0.28 μm, as does polymeric sulfur (*Meyer et al.,* 1971; *Nishijima et al.,* 1976; *Nelson and Hapke,* 1978; *Sill and Clark,* 1982) and irradiated sulfur (*Hapke and Graham,* 1989). In contrast, orthorhombic α-S, the most stable form of cyclo-octal sulfur, has absorption minima at 0.28 μm (*Fuller et al.,* 1998). Therefore, while SO_2 is a plausible and likely candidate, its presence is not unequivocally established.

From IUE ratio spectra, *Lane et al*. (1981) found that the feature was stronger on the trailing side compared to the leading hemisphere (and may have been absent there; see below). The feature was strongest at 277° ± 3°W (*Ockert et al.,* 1987; *Nelson et al.,* 1987). *Sack et al*. (1992) simulated Europa's SO_2 in the laboratory by vapor deposition and found a good fit to observations from *Nelson and Lane* (1987) using reflection data for an SO_2 film about 0.12 μm thick (or about 2×10^{17} cm^{-2} within the sampling depth). *Noll et al*. (1995) obtained a Hubble Space Telescope UV reflectance spectrum of Europa's trailing side and also compared it to *Sack et al.*'s (1992) data, finding good agreement with Europa's absorption feature and laboratory spectra of a slightly thicker film (0.16 μm, or about 3×10^{17} cm^{-2}).

The UV absorption feature was mapped over Europa's surface by *Hendrix et al.* (1998) using Galileo UV data, finding abundances similar to those of *Noll et al*. (1995) and *Sack et al*. (1993). No SO_2 feature was observed on the leading side, as also shown in spectra presented by *Domingue and Lane* (1998). In contrast, *Spencer et al*. (1995) noted, in his in leading-side spectra, a possible absorption edge at ~0.38 μm that could be due to SO_2, but this seems unlikely considering the apparently low leading-

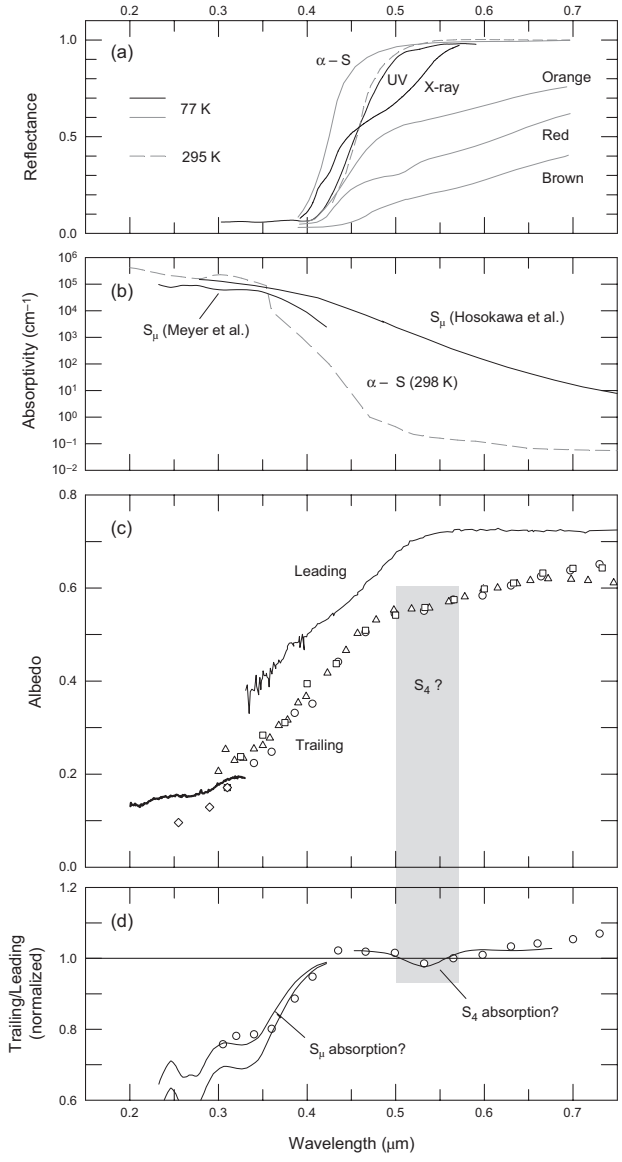

Fig. 13. Europa spectra and sulfur. **(a)** Laboratory reflectance for α-S_8 (orthorhombic cyclo-octal sulfur) at 295 K and 77 K, temperatures for which α-S_8 appears yellow or white, respectively. Spectra of 77 K quenched liquid samples (initially at 382 K, 47 5 K, and 718 K) forming orange, red, and brown sulfur with progressively increasing amounts of polymeric sulfur S_μ and S_4 (in "red sulfur"). These spectra are from *Gradie et al*. (1980). Ultraviolet- and X-ray-irradiated S_8 at 77 K (*Hapke and Graham,* 1989; *Nelson et al.,* 1990), showing S_μ and S_4 photolytic and radiolytic production. Note the shift in the band edge from 0.45 μm to 0.5 μm by UV irradiation and the presumed S_4 absorption from X-ray irradiation and the possible presence of S_3 at ~0.42 μm. **(b)** Absorption coefficients of α-S_8 at room temperature (*Fuller et al.,* 1998); liquid sulfur at 450°C showing S_μ absorption that extends to ~1.5 μm (*Hosokawa et al.,* 1994); and yellow polymeric sulfur from 250°C liquid quenched at 0°C (*Meyer et al.,* 1971) (arbitrary scaling). **(c)** Spectra of Europa. The leading-side spectrum is from *Spencer et al.* (1995). The trailing-side ground-based spectrophotometry measurements are from *Johnson* (1970) (○) and *Wamsteker* (1972) (△), both normalized at 0.56 μm to *McFadden et al.* (1980) (□) [as presented in *Calvin et al.* (1995)]. Note the possible S_4 absorption at ~0.53 μm. The UV spectrum is from *Noll et al.* (1995) (—) and the ◇ points are from *Nelson et al.* (1987). **(d)** The trailing-to-leading-side spectral albedo ratio, normalized at 0.56 μm, is from *Johnson* (1970) (○) and compared to S_μ and S_4 absorption using *Meyer et al.*'s (1971, 1972) absorption profiles for two optical depths.

side SO_2 abundance and the small absorption cross section at this wavelength.

Hendrix et al. (2002, 2008) found that SO_2 linearly correlates with Europa's hydrate, consistent with Europa's radiolytic sulfur cycle. At 80% hydrate concentration, approximately the maximum concentration of hydrate on the trailing side, they found that the SO_2 equivalent column density for a one-way path was 6×10^{17} cm^{-2} based on laboratory reflection measurements by *Sack et al.* (1992). We estimate the photon path length using the continuum reflectivity of R ~ 0.2 at 0.28 μm (Fig. 9) and an average hydrate grain size of 10 μm (section 2.2.4), giving L ~ 120 μm (see section 1.4). The column density of H_2O molecules along this path is ~3.6×10^{20} cm^{-2}, so the SO_2 molar density at high hydrate concentration is about 0.2%. The form of SO_2 is not known. It could exist as a dispersed molecular component in solid solution, as SO_2 inclusions, as hydrates or clusters of $(SO_2)_m(H_2O)_n$ (*Schriver et al.,* 1988; *Schriver-Mazzuoli et al.,* 2003a), or in a mixed clathrate (*Hand et al.,* 2006). Using IUE data, *Ockert et al.* (1987) and *Nelson et al*. (1987) found that the signature was unchanged within 20% over the eight-year span of observations. Combining IUE and Galileo results, *Domingue and Hendrix* (2005) showed that the feature was stable over the 1978–1996 period.

A strong feature in Io's spectra is the SO_2 $\nu_1 + \nu_3$ combination band at 4.07 μm, and has been suggested to be the absorber for a 4-μm band in Ganymede and Callisto's spectra (*McCord et al.,* 1997, 1998a; *Hibbitts et al.,* 2000) as well as for Europa's (*Smythe et al.,* 1998; *Hansen and McCord*, 2008). However, there is an inconsistency between Europa's UV and IR measurements if one assumes they are both due to SO_2. A simple radiative model shows that the relative reflectance decrease at low reflectance is $\Delta R/R = -(2/3)D f\alpha$ where f is the molar concentration of SO_2 and α is its absorption coefficient. Using the above UV derived SO_2 abundance of 0.2% and obtaining a using SO_2 optical constants (*Schmitt et al.,* 1994), then an IR band depth of only 0.1% is expected. If the 4-μm band depth of ~5–10% (*Hansen and McCord,* 2008) were due to SO_2 then the UV feature would be much stronger than observed. The same also applies to Ganymede, which does not exhibit an UV SO_2 feature (*Noll et al.,* 1996; *Hendrix et al.,* 1999), but does show a 4-μm band with a ~4% average absorption depth (*McCord et al.,* 1998a). It may be that the IR absorption strength of SO_2 is greatly enhanced in H_2O ice, or perhaps another absorber is responsible for this band.

Sulfur dioxide, while it could be an outgassing product from the interior (*Noll et al.,* 1996), is more likely a product of surficial chemical reactions. *Lane et al*. (1981) suggested SO_2 formation through implantation of energetic sulfur ions into the icy surface, but this mechanism does not directly produce SO_2 molecules with high efficiency (*Strazzulla et al.,* 2007). Irradiation of ice-coated sulfurous residues is also inefficient in producing SO_2 (*Gomis and Strazzulla,* 2008). SO_2 is produced by irradiation of H_2S:H_2O ices (*Moore et al.,* 2007); however, H_2S is not yet observed on Europa (see section 2.9.4). Sulfur dioxide can also be formed in the decomposition of sulfates [see review by *Johnson et al*. (2004) and the measurements by *Moore et al*. (2007)] and would be an equilibrium species in Europa's radiolytic sulfur cycle. The newly formed SO_2 is then itself photolytically and radiolytically decomposed (*Schriver-Mazzuoli et al.,* 2003b; *Moore et al.,* 2007) with a lifetime of a few years in Europa's top 100 μm (*Moore et al.,* 2007). The decomposition products reform sulfate in a repeating cycle, and a radiolytic equilibrium SO_2 abundance is formed that is sensitive to the total sulfur to water ratio (*Moore et al.,* 2007). For $[\Sigma S]/[H_2O]$ = 1/3, 1/10, and 1/30, the equilibrium SO_2 fractional abundance is found to be $[SO_2]/[H_2O]$ = 8%, 0.35%, and 0.003%, using $[SO_2]/[\Sigma S]$ values obtained by *Moore et al.* (2007) with proton irradiation. The intermediate case simultaneously mimics Europa's UV-derived SO_2 abundance and Europa's hydrate abundance {$[\Sigma S]/[H_2O]$ ~ 0.1 (*Carlson et al.,* 2005a)} within factors of ~3. The predominance of SO_2 on the trailing side suggests sulfur ion implantation as the source but SO_2 can also be produced by radiolysis of sulfate salts. Uniform outgassing of SO_2 over Europa's surface is ruled out by the paucity of SO_2 on the leading side.

2.4. Sulfur Allotropes

Native sulfur has long been a candidate for Europa's dark material. Multispectral photometry of the Galilean satellites (see Fig. 13c) showed an absorption band shortward of 0.5 μm that was suggestive of sulfur compounds. *Johnson and McCord* (1971) noted that polysulfides may be responsible for this UV downturn in the satellite spectra, although other candidates were noted, including radiation-damaged ice and iron compounds (see section 2.9.2). *Wamsteker* (1972) suggested that sulfur may be a common absorber on the icy Galilean satellites and particularly on Io (*Wamsteker et al.,* 1973). Recognition that the Io plasma torus contains sulfur ions that diffuse away from Io's orbit and can strike Europa prompted *Eviatar et al.* (1981) to suggest this exogenic source. Shortly thereafter, *Lane et al*. (1981) found evidence for sulfur implantation through IUE observations of SO_2 on Europa's trailing side.

Johnson et al. (1983) analyzed Voyager color maps and found three prominent spectral units, one being bright in orange light, and two darker regions, one with UV reflectance lower than the other. The low UV reflectance units were predominately on the trailing side and are responsible for the higher trailing-side UV absorption compared to the leading side discovered in groundbased spectrophotometry (Fig. 13c,d). These authors reiterated the suggestion of ion implantation of sulfur, suggesting that differential contamination by this element could produce the UV differences. *Nelson et al.* (1986) analyzed these data and found that all spectral units showed gradual changes with longitude. They suggested that all dark units are related, including the brown lineae, spots, and the two types of mottled terrain (UV dark and UV bright). The UV absorption feature was found to

occur on both hemispheres with a distribution that followed a cosine dependence, with its minimum on the leading apex of orbital motion and maximum in the trailing antapex. *Nelson et al*. (1986) considered this to be a magnetospheric effect, and favored sulfur ion implantation on the trailing and leading sides, the latter due to high-energy ions, with modifications by sputtering redistribution and gardening. Grain size variations were also considered. *McEwen* (1986) similarly found a global pattern suggesting exogenic control, again possibly from sulfur-ion implantation, sputtering, and impact gardening, that could produce compositional and/or grain size gradients and the observed pattern. *Johnson et al*. (1988) and *Pospieszalska and Johnson* (1989) calculated the longitudinal implantation flux of plasma and high-energy sulfur ions and found good agreement with the Voyager UV images. *Spencer et al.* (1995) obtained spectra of Europa's leading side (see Fig. 13c) and found excellent fits, particularly at the 0.5 μm band edge, using α-sulfur, SO_2, and proton-irradiated NaSH. They also found a slope change at about 0.38 μm that may be part of the UV absorption feature prominent on the trailing side (Fig. 13c) and also present on the leading side. Since the 0.5-μm absorption edge is evident on both the trailing and leading sides, *Spencer et al.* (1995) suggested that the sulfur could be endogenic.

Early objections for sulfur being on Io were due to the temperature shift of sulfur's absorption band, shifting the band edge to shorter wavelengths and producing a white compound at low temperatures rather than yellow [see review of Io's surface composition and sulfur properties by *Carlson et al.* (2007)]. However, it was shown by *Steudel et al*. (1986) that UV radiation produced yellow polymeric sulfur at satellite temperatures, with the band edge shifting back to 0.5 μm (*Hapke and Graham,* 1989) and thus sulfur is consistent with Io's spectrum (and Europa's). Other radiation alteration effects may be operative. High-energy irradiation can open the S_8 ring and the products can recombine to produce longer chains and large rings, an allotrope known as polymeric sulfur and denoted S_μ or S_∞ (*Steudel and Eckert,* 2003). Solid polymeric sulfur is yellow or brown (*Meyer et al.,* 1972; *Steudel et al.,* 1986) and can be formed by irradiation and by quenching the liquid. It exhibits an absorption band starting at ~0.4 μm, with a band or shoulder at 0.36 μm seen in liquid sulfur, quenched sulfur, and annealed sulfur photolysis products (*Meyer et al.,* 1971; *Nishijima et al.,* 1976; *Eckert and Steudal,* 2003). It is possible that Europa's UV feature is due to absorption by polymeric sulfur. Figure 13d shows the absorption by this allotrope based on the relative absorption found by *Meyer et al*. (1971), and provides a good fit to *Johnson*'s (1970) trailing-to-leading-side spectral ratios. The preponderance of this feature on the trailing side may be due to enhanced irradiation on this hemisphere by energetic electrons (*Paranicas et al.,* 2001), in addition to there being simply more sulfur.

We estimate the differential amount of S_μ between the leading and trailing hemispheres using *Johnson*'s (1970) measurements (Fig. 13d) with typical S_μ absorption values from *Hosokawa et al*. (1994), finding that the concentration difference, relative to water, is $[S_\mu]/[H_2O] \sim 2 \times 10^{-4}$. This can be regarded as a lower limit for the differential and total sulfur abundance. The absolute abundance is difficult to estimate and will require radiative transfer calculations and spectral fitting with differing proportions of S_8 and S_μ.

Another sulfur feature, found in spectra of Io and perhaps present in Europa's spectrum, is the 0.53 μm band of tetrasulfur, S_4. This molecule is formed during radiolytic decomposition and has two absorption bands in the visible, the stronger one at ~0.53 μm and the weaker isomer band at ~0.63 μm. S_4 is produced in X-ray irradiation (equivalent to electron and proton irradiation) along with the less stable S_3 molecule (*Nelson et al.,* 1990). Tetrasulfur is produced photolytically (*Meyer and Stroyer-Hansen,* 1972) and in electric discharges (*Hopkins et al.,* 1973). The lifetime of photolytic S_4 is ~60 h at 171 K but the molecule may be more stable at europan temperatures (see below). Its possible presence on Europa is hinted at in Fig. 13c, which shows an inflection at ~0.53 μm in the trailing-side spectrophotometry, and in Fig. 13d, where a minimum is seen at the same wavelength. Although *Johnson and McCord* (1970) and *Johnson* (1971) noted no appreciable dip between 0.5 and 0.6 μm, *Wamsteker* (1972) did consider this a possible europan feature in his spectrophotometric data, as did *Nelson and Hapke* (1978) in theirs, and they identified the stronger ionian feature with S_4. *McFadden et al*. (1980) thought this a possible feature too, but not necessarily the same as Io's due to differing widths and positions. The absorption strength measurements of S_4 (*Meyer et al.,* 1972; *Krasnopolsky,* 1987; *Billmers and Smith,* 1991) are too discrepant to make a meaningful estimate of its abundance, but if this molecule is indeed present on Europa it must be continuously produced as its lifetime is probably less than 2 months, based on its apparent lifetime in Io plume ejecta (*Carlson et al.,* 2007). $S_3 + S_5$ are also produced by irradiation, and S_3 has a band at ~0.4 μm that is ~10 times stronger than the S_4 band, but such a feature is not apparent in Io or Europa spectra, probably due to the greater instability of S_3 (*Hopkins et al.,* 1973). There are other possibilities for the 0.53-μm feature, including ferric iron as suggested for Io by *Nash and Fanale* (1977), but the accompanying 0.8-μm Fe^{+++} band is not apparent in Europa's spectrum (see section 2.9.5).

As illustrated in sulfur reflectance and absorbance data (Figs. 13a,b), polymeric sulfur absorption can extend to near-IR wavelengths. An IR leading-trailing-side effect was observed by *Pollack et al*. (1978), who noted a lower albedo at ~1 μm for the trailing side compared to the leading hemisphere. This effect is seen in Galileo NIMS spectra, where the material that is dark in the visible region is absorbing for wavelengths up to 1 μm. This spectral region includes S_μ and sulfur dangling bond absorption (*Hosokawa et al.,* 1994). Figure 11d shows a map of this absorption at 0.7 μm and the strong correlation with the UV absorption feature (Fig. 11c).

Europa's sulfurous matter can arise from the S ion plasma influx, meteoritic and cometary infall, and from endogenic sources, such as SO_2 outgassing, emplacement of oceanic material containing sulfates and sulfides, or from existing sulfurous impurities in the ice crust. The amount brought in by ion impact can be estimated by assuming that the ice crust was emplaced 50 m.y. ago, and that the current plasma flux (Table 1) has been constant over that period. For the synchronous rotation case and with little plasma diversion, the antapex would receive enough sulfur (12 g) to form a 6-cm layer of elemental sulfur, or a 66-cm layer of sulfate hydrate. Gardening will reduce this to a concentration of several percent relative to H_2O, and nonsynchronous rotation will tend to average the distribution, just as it does for the accumulated ionizing dose (see Fig. 2). The implanted sulfur ions do not create elemental sulfur directly, but instead sulfuric acid (which is colorless) is preferentially produced (*Strazzulla et al.,* 2007), followed by decomposition of the sulfate to produce SO_2 (also colorless) and elemental sulfur (see *Johnson et al.,* 2004). Continued radiolysis reforms sulfate in timescales of a few years in a continuing radiolytic sulfur cycle (*Carlson et al.,* 1999b, 2002, 2005a; *Moore et al.,* 2007). Any endogenic sulfurous material will also be rapidly incorporated into the cycle. No matter what the source, the most stable and abundant form is expected to be sulfate, followed by SO_2 and elemental sulfur.

The distribution of the presumed sulfur is variegated and is controlled by the implantation pattern, the emplacement pattern of any endogenic sources, gardening, the random distribution of impacts, and geological processes such as tectonism, mass wasting, brine mobilization, and the production of lag deposits by near-surface heating events. Polymeric sulfur, if the cause of the UV and near-IR absorption, correlates with Europa's hydrated material (Fig. 11) and offers potential for deciphering surface history and source mechanisms.

2.5. Molecular Oxygen

In March and April of 1993 and 1994, telescopic observations uncovered two previously unseen absorption features on Jupiter's moon Ganymede at 0.6275 and 0.5773 μm (*Spencer et al.,* 1995). Subsequent searches identified weaker features on both Europa and Callisto (*Spencer and Calvin,* 2002) and the 0.5773-μm feature may be present on a Kuiper belt object (*Tegler et al.,* 2007). These bands were identified with condensed molecular oxygen based on the precise central wavelength match, the band asymmetry, and the relative strength of the two strongest visible absorptions (*Spencer et al.,* 1995; *Calvin et al.,* 1996). These absorptions arise from the simultaneous excitation of interacting pairs of O_2 molecules, producing the transitions $O_2(^1\Delta_g) + O_2(^1\Delta_g) \leftarrow O_2(^3\Sigma_g^-) + O_2(^3\Sigma_g^-)$, with the observed features being the first two members of the vibrational-excitation progression (*Landau et al.,* 1962). Higher excitation bands occur at shorter wavelengths in laboratory spectra but are too weak to have been observed from the satellites. The band shapes are similar to those of oxygen in the liquid or solid γ phase or a similar dense state.

The electronic absorption spectrum of condensed oxygen has been studied since at least the 1930s. General information on the absorption band positions, shape, and strength in both condensed and high-pressure oxygen can be found in the literature (*Landau et al.,* 1962; *Dianov-Klokov,* 1964, 1966; *Findlay,* 1970; *Greenblatt et al.,* 1990; see review by *Cooper et al.,* 2003a). There have been a number of attempts to model and explain the double electronic transition that results in the blue color of the condensed phase, which are now generally interpreted as collision-induced transitions (*Robinson,* 1967; *Blickensderfer and Ewing,* 1969a,b; *Tsai and Robinson,* 1969; *Long and Kearns,* 1973; *Long and Ewing,* 1973). The four strongest bands in the liquid are also observed in all three crystallographic phases of solid O_2 (*Landau et al.,* 1962; *Dianov-Klokov,* 1966). The central wavelengths of the visible features are similar in the high-pressure gas, the liquid, and the solid; however, there is a marked increase in the band asymmetry in the liquid and solid phases. Absorption band strengths of these collision-induced bands are strongly dependent on the density of O_2 as seen in transmission measurements of liquid O_2 at varying temperatures (W. Calvin et al., unpublished data). The absorption strength of the O_2 IR atmospheric system ($^1\Delta_g \leftarrow {}^3\Sigma_g^-$) is also enhanced by collisions and weak bands at 1.25 and 1.06 μm (v' = 0 and 1, respectively) may be expected to be present in Europa's spectrum, but H_2O has bands at these positions so the O_2 component has not been distinguished. *Cooper et al.* (2003a) has reviewed the spectroscopy of O_2 relevant to its presence and observation on the icy satellites.

This existence of surficial O_2 is surprising, since at the surface temperatures and pressures of the Galilean satellites, O_2 is expected to evaporate into the atmosphere immediately. The oxygen must be trapped in the ice and, since these bands are intrinsically weak, significant quantities of O_2 must be present in concentrated form. Assuming a linear dependence between the observed band strength and density, *Johnson et al.* (2003) estimated Europa's molar O_2 abundance, relative to H_2O, to be 0.017–0.17%. However, since the absorption occurs by excitation of two interacting molecules, a quadratic dependence may be appropriate if O_2 molecules are *randomly* distributed, for which a relative abundance of 1.2–4.6% is estimated (*Hand et al.,* 2006). If O_2 molecules are clustered, trapped within defects for example, then the same absorption could be obtained from a smaller average concentration. In contrast to Ganymede's O_2 features, which are strongest on the trailing hemisphere, Europa's bands are distributed over all longitudes with no significant longitudinal variation (*Spencer and Calvin,* 2002).

O_2 is a product of energetic plasma bombardment of the water ice surface (*Calvin et al.,* 1996; *Johnson and Jesser,* 1997; *Johnson and Quickenden,* 1997; *Sieger et al.,* 1998) and its existence on the surfaces of the icy Galilean satellites provided one of the first definitive indications that ra-

diolysis is an important process on these bodies. Although O_2 formation in irradiated ice has been studied for almost a century, detailed reaction mechanisms have been difficult to determine. In a now-classic experiment, *Reimann et al*. (1984) showed that O_2 production in freshly deposited ice samples increased as the ice became increasing altered by the radiation and appeared to be correlated with the loss of H_2. Both the O_2 and H_2 were formed and trapped at depth in these samples, and not just at the surface layers, with an efficiency that increases with the ice temperature, as recently confirmed by *Teolis et al*. (2005b). They found, using 100-keV Ar^+ bombardment (approximately simulating Europa's oxygen and sulfur ion irradiation), that O_2 concentrations of up to 30% are produced in H_2O ice at 130 K. At 100 K the concentration is less, be-ing <5%. The fluence level to reach equilibrium O_2 concentrations was found by *Teolis et al.* (2005b) to be $1–3 \times 10^{15}$ ions cm^{-2}, which is reached in 3–10 yr on Europa when considering only the energetic O and S ion fluxes (*Cooper et al.,* 2001). Electron and proton irradiation will shorten these timescales. Gardening and condensation of Europa's tenuous water vapor atmosphere will bury the O_2-rich ice, building up an oxidant-rich regolith.

O_2 production in bombarded water ice appears to require the formation of a precursor molecule that is stable at 120 K on timescales on the order of at least 1 h (*Sieger et al.,* 1998; *Orlando and Sieger,* 2003). The precursor is associated with the loss of H_2 (*Reimann et al.,* 1984) and has been suggested to be O trapped in a defect as O-H_2O (*Khriachtchev et al.,* 1997; *Johnson et al.,* 2003, 2005; *Orlando and Sieger,* 2003), a form that can also convert to peroxide under irradiation, or the precursor could be peroxide itself. *Cooper et al.* (2003b) have argued that production of O_2 dimers occurs by a different mechanism, through photolysis or radiolysis of peroxide aggregates, although *Loeffler and Baragiola* (2005) have concluded that H_2O_2 exists on Europa as a solution, rather than as discrete aggregates (see Fig. 15 and section 2.6).

The location and form of the trapped oxygen has been a subject of some debate (*Calvin and Spencer,* 1997; *Vidal et al.,* 1997; *Baragiola and Bahr,* 1998; *Baragiola et al.,* 1999b; *Johnson,* 1999; *Cooper et al.,* 2003b), but recent work (*Teolis et al.,* 2005a,b; *Loeffler et al.,* 2006d) supports the model suggested by *Johnson and Jesser* (1997) that O_2 trapping is facilitated by defect formation by radiation. The O_2 absorption bands are probably associated with multiple O_2 molecules trapped together in inclusions formed from multiple defects. These are often called microbubbles and are formed in a variety of irradiated materials. As discussed in the H_2O section, radiation amorphizes the ice, producing defects — pores and voids — within which the radiolytically produced O_2 can accumulate. Radiation also compacts the ice (*Palumbo,* 2006; *Raut et al.,* 2007), closing the pores and trapping the oxygen at densities of up to ~30% (*Teolis et al.,* 2005b). *Teolis et al.* (2006) simulated an icy satellite with a tenuous H_2O atmosphere that is recondensing on the surface as it is being irradiated. A column of radiolytic O_2 is built up as the compacted ice column replaces the sputtered H_2O, grows, and caps the O_2 below, protecting it from diffusive or sputtering loss. This interesting mechanism holds promise in understanding the O_2 content on the jovian satellites.

Radiation compaction occurs for both ion and electron irradiation and the trapping sites may be similar to clathrate structures (*Grieves and Orlando,* 2005; *Hand et al.,* 2006). Mixed clathrates have been suggested by *Hand et al*. (2006) for Europa's crust that could contain caged O_2 molecules in single and double occupancy, the latter potentially producing the observed O_2 collision pair features. Radiolysis of oxygen-rich ice will enhance the production of H_2O_2 and will produce ozone (O_3) and other reactive oxidants such as hydroperoxyl (HO_2) and hydrogen trioxide (HO_3) (*Cooper et al.,* 2006). Ozone, not yet observed on Europa, is discussed in section 2.9.3.

2.6. Hydrogen Peroxide

H_2O_2 was predicted to be on Europa as a radiolysis product of ice by *Johnson and Quickenden* (1997), and was soon thereafter discovered (*Carlson et al.,* 1999a) on the surface using Galileo IR and UV spectroscopy (Fig. 14). Peroxide is quickly dissociated by UV radiation so the existence and abundance of H_2O_2 dramatically indicated rapid radiolytic production and the importance of radiation effects on the Galilean satellites, especially Europa. This oxidizing molecule, along with O_2, is also of astrobiological interest (see chapter by Hand et al.).

The initial discovery made use of spectra of Europa's leading, and iciest, hemisphere, but subsequent analysis indicates that H_2O_2 is also present on the trailing hemisphere with comparable band depths (*Hansen and McCord,* 2008). The leading side's average molar abundance is about 0.13% (*Carlson et al.,* 1999a) but there are variations over the surface. The leading-side distribution of H_2O_2 (*Carlson,* 2004) seemed to correlate with the abundance of CO_2, possibly related to the production mechanism, discussed below. There may be temporal variations as well. *Domingue and Hendrix* (2005) have noted UV spectral slope decreases and darkening on the leading side, antijovian quadrant that occurred between the IUE era (1979–1984) and Galileo's (1995–1996). Similar changes were observed earlier on both the leading and trailing hemisphere (*Domingue and Lane,* 1998). It was suggested by *Domingue and Hendrix* (2005) that temporal variability of the space environment (e.g., Jupiter's magnetosphere or gardening rates) may have depleted the amount of H_2O_2.

An ionizing particle with energy in the keV to MeV range produces a track of lower-energy secondary electrons as it passes through the H_2O ice. Hydrogen peroxide forms along these tracks through electron-induced dissociation and ionization of H_2O molecules, producing H + OH radicals. The OH radicals can combine: $OH + OH \rightarrow H_2O_2$. Peroxide can be destroyed by electrons produced in a subsequent ionizing particle's avalanche and by UV and visible radia-

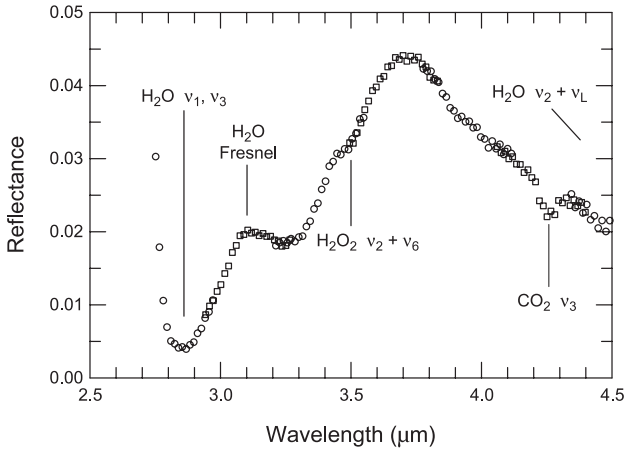

Fig. 14. Spectrum of Europa's leading side in the 2.5- to 4.5-μm region. The hydrogen peroxide combination band is identified at 3.5 μm and shown with continuum removed in Fig. 15. Ultraviolet spectra of Europa corroborate this identification. The CO_2 asymmetric stretch fundamental is at 4.25 ± 0.01 μm and consistent with the 4.258-μm band centers found for Ganymede and Callisto and many saturnian satellites (2.7). The broad, structureless Fresnel reflection peak of H_2O is indicative of amorphous ice. L denotes libration.

tion. The diurnally averaged H_2O_2 photolysis rate, ignoring any reduction from the cage effect, is about 10^{-6} s^{-1} when surface reflection is accounted for, giving a photodissociation lifetime of about 10 d. The cage effect (*Franck and Rabinowitsch,* 1934) can inhibit photodissociation rates by factors of 3 or more (*Schriever et al.,* 1991). The half-life of H_2O_2 in water ice under energetic proton irradiation is ~3 d in the top 100 μm (*Hudson and Moore,* 2006; see also *Loeffler et al.,* 2006c). Thus, to first order we can ignore photodissociation and can consider only particle-induced production and destruction processes. Equilibrium concentrations will be achieved when these rates are equal. Only ions, mainly protons, are thought to strike Europa's leading side (*Paranicas et al.,* 2001) and experimental ion irradiation results are consistent with the concentrations measured on that hemisphere. For example, ices irradiated by 100-keV protons show equilibrium peroxide concentrations of 0.14% and 0.1% for 80 K and 120 K ice samples, respectively (*Loeffler et al.,* 2006b). These results are also in general agreement with the ion irradiation measurements of *Moore and Hudson* (2000) and *Gomis et al.* (2004a,b), although *Moore and Hudson* (2000) found that the addition of electron scavengers such CO_2 increased the yield at Europa-like temperatures and may explain the apparent association of H_2O_2 with CO_2 as noted above.

H_2O_2 production by high-energy electron irradiation has been studied by *Hand* (2007), who found an inverse temperature dependency for the equilibrium values, similar to that for ion irradiation. He found equilibrium values that were about a factor of 3 smaller than for ion irradiation, being 0.04%, 0.03%, and 0.01% for 10-keV electron irradiation of 80 K, 100 K, and 120 K ice, respectively.

It is of interest to know the equilibration time. For both electron and ion irradiation, equilibrium concentrations are achieved at a fluence of about 10^{19} eV cm^{-2} (*Hand,* 2007; *Gomis et al.,* 2004a,b; *Loeffler et al.,* 2006b). Using *Cooper et al.*'s (2001) energy fluxes, an equilibration time on the trailing side is about 2 days, and roughly a week on the leading side. These times pertain to the mean penetration depths of the ionizing particle.

The position and shape of Europa's H_2O_2 band is indicative of the state of H_2O_2 in the ice matrix. *Loeffler and Baragiola* (2005) found different spectral properties for pure crystalline H_2O_2, aggregates of H_2O_2 within the ice, and H_2O_2 dispersed throughout the ice. The absorbance profiles for peroxide produced by proton and electron bombardment are similar to the shape and position observed for Europa's H_2O_2 (Fig. 15), and both are the same as spectra of H_2O_2 dispersed in ice (*Loeffler and Baragiola,* 2005). Using phase diagram information, *Loeffler and Baragiola* (2005) inferred that the dispersed H_2O_2 exists as individual trimers, H_2O-H_2O_2-H_2O, randomly dispersed throughout the H_2O matrix. At high temperatures (150 K), these trimers will precipitate as inclusions of the dihydrate H_2O_2•$2H_2O$, rather than as aggregates of pure H_2O_2. This seems to contradict the O_2 production scheme proposed by *Cooper et al.* (2003b).

2.7. Carbon Dioxide

Carbon dioxide is a common constituent on icy satellites and was first observed on Ganymede and Callisto by Galileo's NIMS using the strong ν_3 absorption band at

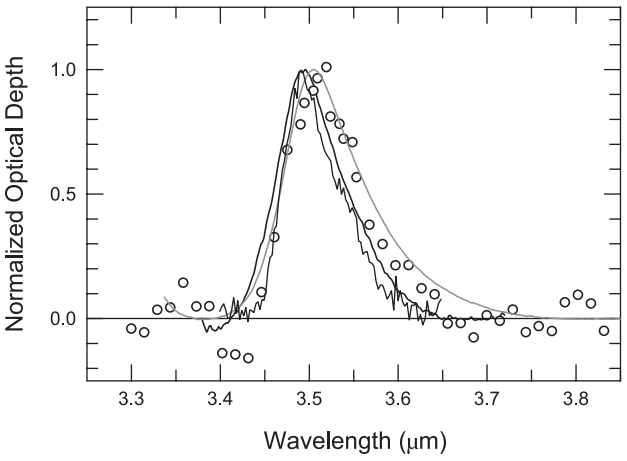

Fig. 15. Comparison of the absorbance profile of H_2O_2 on Europa with that produced in the laboratory by irradiation of H_2O ice. NIMS data are shown as circles and have the underlying continuum subtracted. The thick black line corresponds to H_2O_2 produced by irradiation of ice at 80 K [curve g of Fig. 1 in *Loeffler and Baragiola* (2005)]. Spectra of electron irradiated H_2O at 80 K (thin black line) show a similar profile (*Hand,* 2007). The NIMS profile and the two irradiation profiles are all similar to spectra of H_2O_2 dispersed in water ice (gray line; curve f of Fig. 1 in *Loeffler and Baragiola* (2005)].

4.3 μm (*Carlson et al.,* 1996; *McCord et al.,* 1997, 1998a; *Carlson,* 1999; *Hibbitts et al*., 2000, 2002, 2003). Evidence for the presence of CO_2 on Europa was subsequently obtained for the leading hemisphere using distant observations to avoid radiation noise (*Smythe et al.,* 1998); confirming previous hints of structure near 4.3 μm (*McCord et al.,* 1998a). A recent analysis of NIMS data provides evidence for CO_2 on the trailing side, with large band depths and a nonuniform distribution (*Hansen and McCord,* 2008).

Europa's 2.5–4.5-μm spectrum (Fig. 14) shows absorption due to the CO_2 ν_3 transition. The equivalent width of this feature was used by *Hand et al*. (2007) to estimate the leading-side CO_2 concentration at 360 ppmv. The position of the band is similar to that observed for the other icy Galilean satellites and for many CO_2-rich regions on the saturnian satellites (*Clark et al.,* 2005a,b, 2008b). The leading-side distribution, while obtained with poor spatial resolution (*Carlson,* 2001), shows a correlation with visibly dark material, similar to results for Ganymede and Callisto, and similar to the trailing-side analysis by *Hansen and McCord* (2008).

The existence of CO_2 on the icy satellites presents two puzzles. First, what is its origin — exogenic or endogenic — and second, how can it be stable at the temperatures of the Galilean satellites? The origin may be endogenic. It is now known that condensed CO_2 is widespread in the solar system, being present in icy satellites of Saturn (*Buratti et al.,* 2005; *Clark et al.,* 2005a,b, 2008b; *Brown et al.,* 2006a,b; *Waite et al.,* 2006), three uranian satellites (*Grundy et al.,* 2003, 2006), and Neptune's Triton (*Cruikshank et al.,* 1993). It is also present on Mars and in comets and interstellar grains (*Gibb et al.,* 2004). It is attractive, then, to assume a common, endogenic source for the icy satellites, with the CO_2 being a degassing product of primordial or internally produced volatiles. Since interstellar grains contain CO_2, and are likely to be a component of the initial solar nebula, a common and ubiquitous source of primordial CO_2 seems probable. There is observational evidence from the extent of sublimational erosion that Callisto's CO_2 is internally derived (*Moore et al.,* 1999). Furthermore, Cassini's mass spectrometer has directly measured CO_2 venting from Enceladus's interior through the south pole "tiger stripes" vents (*Waite et al.,* 2006), perhaps due to clathrate exsolvation. At Enceladus, and in other bodies, CO_2 could also be produced through high-temperature oxidation of organic compounds in the interior (see chapter by Zolotov and Kargel for details). Endogenic primordial or internally generated CO_2 seems plausible and likely for icy satellites.

On the other hand, surface photolysis and radiolysis may play a role in producing CO_2 from carbonaceous material. Mapping of Callisto's surficial CO_2 by *Hibbitts et al*. (2000) shows that CO_2 forms a trailing-side "bulls-eye," suggesting an influence by Jupiter's rotating magnetic field and magnetosphere. The correlation with dark material suggests that a carbon-containing material is involved. At Europa, oxidized carbon compounds (CO_3^{2-}, HCO_3^-, carbonates) or organic molecules are possibilities, and meteorites and micrometeoroids are certain sources of carbonaceous material (section 1.2, Table 1, section 2.9.1). Carbon ions are present in the jovian magnetosphere but the fluxes are too low to be of compositional significance (*Cohen et al.,* 2001).

When carbonaceous grains with water ice mantles are irradiated, CO and CO_2 molecules are formed at the interface (*Mennella et al.,* 2004; *Gomis and Strazzulla,* 2005; *Raut et al.,* 2005). Equilibrium surface densities at the interface are ~$0.3–6 \times 10^{15}$ CO_2 molecules cm^{-2}, equivalent to a few monolayers or less. *Gomis and Strazzulla* (2005) have argued that ices with small amounts of ion-irradiated submicrometer carbonaceous particles can contribute sufficient CO_2 to produce the absorptions observed on the Galilean satellites. The energy dose to reach equilibrium is ~100 eV/16-amu (*Gomis and Strazzulla,* 2005), corresponding to times of about 300 and 150 yr on Europa's leading and trailing hemisphere, respectively. Note that the equilibrium concentration is independent of the ionizing flux since production and destruction rates are equal. Consequently, similar processes may be occurring on other solar system bodies by cosmic-ray irradiation, albeit with longer timescales. An objection to this mechanism is that the resulting CO_2 band position [2339 cm^{-1} (*Mennella et al.,* 2004)] is inconsistent with that observed from the Galilean satellites and elsewhere (see discussion of CO_2 stability below).

If the carbonaceous material is mixed in ice on molecular scales, rather than as grains, access to carbon is greatly enhanced, and CO_2 production is increased. Examples of ion-irradiated mixed ices containing hydrocarbons are given in *Moore et al*. (1996), *Palumbo* (1997), *Moore and Hudson* (1998), and *Palumbo et al*. (1998), and for electron irradiation, by *Hand* (2007). Figure 16 shows a typical example of the production curves for the radiolysis products of a mixed ice of isobutane (C_4H_{10}) and H_2O. Carbon dioxide and carbon monoxide are generally produced, irrespective of the original C and O mixture (*Palumbo,* 1997).

Carbon dioxide on Europa's surface, whether it is endogenic, photolytic, or radiolytic, can be destroyed to yield carbonic acid (H_2CO_3) and carbon monoxide (*Moore et al.,* 1991; *Moore and Khanna,* 1991; *DelloRusso et al.,* 1993; *Brucato et al.,* 1997; *Gerakines et al.,* 2000) and these molecules will then be radiolyzed back to CO_2. The major species in this cycle is CO_2, with H_2CO_3 being present at relative molar density of $[H_2CO_3]/[CO_2] \sim 1.7\%$ along with some CO (*Carlson et al.,* 2005b; *Hand,* 2007).

An O–H stretching band of H_2CO_3 was suggested by *Hage et al*. (1998) as a candidate for Ganymede and Callisto's 3.8-μm absorption feature. The relative intensities of the 3.8-μm and CO_2 ν_3 bands are about the same for the Ganymede and Callisto observations and the laboratory radiolysis measurements, lending support for Hage et al.'s suggestion. The H_2CO_3 band is not evident in Fig. 14 but may be just at the limit of detection. The structure of carbonic acid is $(HO)_2CO$ (*Moore and Khanna,* 1991), with the three oxygen atoms bonded to the carbon atom, so there are no C-H bonds. However, the C-H stretching band from alcohols should be present, but these bands are intrinsically

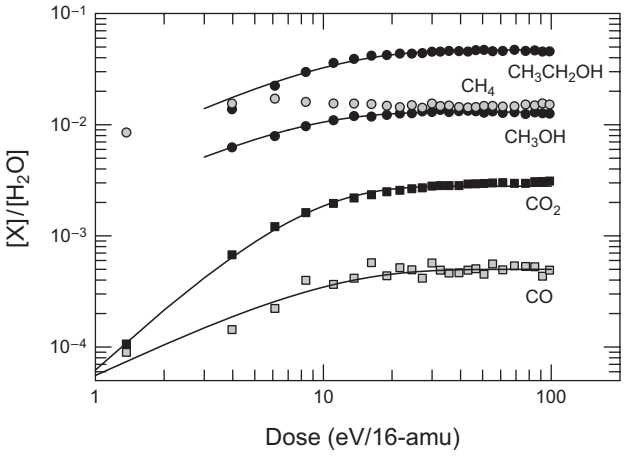

Fig. 16. Production curves for the radiolysis products of a 1:10 C_4H_{10}:H_2O ice at 80 K, illustrating radiolytic equilibrium. The major products are the alcohols methanol (CH_3OH) and ethanol (CH_3CH_2OH) and methane, with minor amounts of CO_2 and CO. The initial slope of the CO_2 curve indicates that this molecule is a secondary product, derived from a radiolytically-generated precursor. Ice containing methanol, when mildly heated in vacuum, forms clathrates that can also trap CO_2 and other molecules. This is one possible explanation for the existence and stability of trapped CO_2 on icy satellites.

weak compared to the CO_2 band, and can be a factor of 10 less intense than the CO_2 feature in spectra of radiolyzed ice containing hydrocarbons (*Moore et al.,* 1996; *Moore and Hudson,* 1998). Carbon monoxide (section 2.9.1) is also produced, but this volatile molecule will rapidly diffuse out of the ice and escape into the atmosphere. The apparent loss of CO_2 and possibly CO, the former indicated by the existence of a CO_2 atmosphere on Callisto (*Carlson,* 1999), implies that carbon is being lost from Europa. The widespread occurrence of CO_2 on icy satellites throughout the solar system suggests that surficial CO_2 is not a transient feature, so there must be continual replenishment of carbon atoms. The crudely estimated CO_2 loss rate from Callisto of 6×10^6 cm^{-2} s^{-1} is close to the meteoritic C atom input rate of 1.2×10^6 cm^{-2} s^{-1} (Table 1) and suggestive of meteoritic infall as the continuing supply.

Carbon dioxide ice is highly volatile, with a vapor pressure of 0.1 mbar at 125 K, so it cannot exist as CO_2 ice on the Galilean satellites. In dilute H_2O ice solutions, CO_2 is more stable, but much of it is lost when amorphous to cubic transitions take place (*Sandford and Allamandola,* 1990). The timescale for these phase changes on Europa is ~10 yr (see section 2.1). Some CO_2 still remains trapped on laboratory timescales, but stability over longer periods probably requires a more effective trapping mechanism. Early suggestions for trapping CO_2 were as clathrates, as fluid inclusions, or trapped in radiation-induced defects and voids (*Carlson et al.,* 1996; *McCord et al.,* 1998a). Many silicates effectively trap CO_2 and some show weaker bands at ~4 μm [see the *Clark et al.* (2007) spectral library] that could be related to the 4-μm feature present on Ganymede, Callisto, and perhaps Europa. The position of the CO_2 band is potentially diagnostic of the trapping mechanism. For example, the band position of CO_2 ice is 2343 cm^{-1}, and is 2340 cm^{-1} for CO_2 molecules in H_2O ice (*Sandford and Allamandola,* 1990), whereas the band lies at 2349 ± 2.2 cm^{-1} for the Galilean satellites (less accurately known for Europa). This position is very close to the 1-0 R-branch rotation-vibration line of the gas, arising from excitation of CO_2 in the nonrotating state (J" = 0). This suggests that the molecules' environment restricts their rotation but otherwise the molecules are nearly free. Hindered rotation of the J = 1 excited state probably broadens the line.

A specific trapping mechanism has not been identified and is the subject of ongoing work. Numerous prior studies of numerous CO_2-rich minerals and ices have shown band positions occurring over a 30-cm^{-1} span, but with few candidates in the interval of interest (2349 ± 2.2 cm^{-1}). Some zeolites provide adequate positions at room temperature, but few studies at relevant temperatures have been performed. *Hibbitts and Szanyi* (2007) have investigated physisorption on various minerals at icy satellite temperatures. Of the samples considered, Ca-montmorillonite, serpentine, goethite, and palagonite, CO_2 adsorbed only on Ca-montmorillonite where it remained for times longer than tens of minutes. The position of the asymmetric stretching band of the adsorbed CO_2 at 125 K was found to be 4.26 μm (2347 cm^{-1}), in excellent agreement with the Galilean satellites' CO_2 band position. While this remains a plausible candidate, the long-term stability needs to be studied. Alteration of the physisorbing medium by irradiation may be an important component in trapping CO_2 on the Galilean satellites (*Hibbitts and Szanyi,* 2007).

Trapping of CO_2 in clathrate structures is also a possibility (*Carlson and Hand,* 2006; *Hand et al.,* 2006). In particular, when hydrocarbons in ice are irradiated, methanol (CH_3OH) is produced, along with CO_2 and other species (Fig. 16). Water ice that contains methanol, when heated to about 120–125 K, transforms to a clathrate at vacuum (*Blake et al.,* 1991), and if other molecules are present, they can be incorporated into the clathrate cages, forming a mixed clathrate. The band position of enclathrated CO_2 shifts to 2346 cm^{-1} (*Blake et al.,* 1991; *Fleyfel and Devlin,* 1991), noticed earlier in mixed ice experiments (*Sandford and Allamandola,* 1990; *Ehrenfreund et al.,* 1999). Interactions between CO_2 and CH_3OH may also produce shifts in position (*Chaban et al.,* 2007). The band center for clathrate-trapped CO_2 is encouragingly close to observed values. Further work on clathrate production, physisorption on mineral grains, and other CO_2 production and trapping mechanisms is needed in order to understand the origin of CO_2 on Europa and icy satellites in general.

2.8. Sodium and Potassium Compounds

Although sodium and potassium compounds have not been directly detected on Europa's surface, these atoms have been observed in the atmosphere and are thought to be introduced there by sputtering (see chapters by McGrath

et al. and Johnson et al.). The initial source of these atoms could be exogenic or endogenic, from Io's plasma torus or alkali-containing salts from Europa's putative ocean, therefore their detection is of great interest.

Potassium has been identified once (*Brown,* 2001), whereas sodium has been observed a few times (*Brown,* 1999, 2001; *Leblanc et al.,* 2002, 2005). An emission peak reported by *Porco et al*. (2003) when Europa was in Jupiter's shadow has been also associated with sodium (*Cassidy et al.,* 2008). Modeling of these observations has given insight into the transport and loss of sodium, as described in more detail in the chapter by McGrath et al. Such processes apply to other trace species ejected from Europa's surface, but not yet detected in the gas phase. There are also reports of alkali pickup ions observed near Europa (Table 2).

Alkali elements on Europa's surface could exist in the form of salts, hydroxides (*Johnson,* 2001), solvated ions, or neutral atoms (*Yakshinskiy and Madey,* 2001). Sputtering simulations showed that there may be considerable redistribution of sodium and potassium across the surface of Europa, which would also be the case for other trace species that are sputtered. Therefore, a significant fraction of the observed gas-phase alkalis are from previously sputtered atoms, adsorbed on the surface and again ejected into the atmosphere. Most are not directly ejected from an intrinsic salt mineral. Observations and modeling suggest that the dark region on the trailing hemisphere of Europa is likely the initial source (*Leblanc et al.,* 2005; *Cassidy et al.,* 2008).

Assuming sodium in an ice matrix is carried off with the sputtered water products, theoretical models indicated that the average molar surface sodium concentration, relative to H_2O, was ~0.5–1% (*Johnson et al.,* 2002; *Leblanc et al.,* 2002) and that the present escape rate is 5×10^6–12×10^6 Na atoms cm^{-2} s^{-1} (*Leblanc et al.,* 2002, 2005). *Cipriani et al*. (2008) have considered models that include orbital or temporal nonuniformities in the magnetospheric flux that sputters the Na, and infer Na escape rates of 3×10^6 atoms cm^{-2} s^{-1} or greater. If one assumes a plasma implantation reduction factor (*Saur et al.,* 1998) of $r_{Europa} = 0.1$ to 0.2 (i.e., implantation flux reduced by a factor of either 10 or 5), then the sodium implantation rate could not account for the loss rate implied by the observations (*Johnson,* 2000; *Leblanc et al.,* 2002). That implantation is not the principal source was also suggested by the different Na/K ratios at Europa (25 ± 3) and at Io (10 ± 3) (*Brown,* 2001; *Johnson et al.,* 2002; *Leblanc et al.,* 2005). A meteoroid source would have a Na/K ratio of ~13, whereas *Zolotov and Shock*'s (2001) model predicts that Europa's ocean will have a ratio of ~14–19. Since freezing of upwelling oceanic water may increase the Na/K ratio, material originating from Europa's ocean could produce a ratio at the surface consistent with the observations (*Zolotov and Shock,* 2001). Note that Na is predicted by geochemical models to be a major constituent of Europa's ocean, but that the K abundance depends strongly of the H_2 and CO_2 fugacities (*Zolotov,* 2008).

A critical assumption of the above discussion is that plasma is significantly deflected at Europa, implying that plasma implantation provides too little Na to satisfy the inferred ejection rate, and that an endogenic source is necessary. While there does seems to be diversion of flow on the jovian face of Europa (*Paterson et al.,* 1999b), the plasma reduction factor could be much less than considered above. *Ip* (1996) derives a reduction factor of $r_{Europa} = 0.8$, while analysis of combined magnetic field and energetic particle data (*Paranicas et al.,* 2002; *Volwerk et al.,* 2004) yields $r_{Europa} = 0.9$. In these high values of r_{Europa}, the rate of Na plasma input ($>5.3 \times 10^6$ Na atoms cm^{-2} s^{-1}, Table 1) could balance Europa's loss rate noted above and an endogenic source is not be required. The source location, the trailing-side dark material, is also consistent with plasma implantation, which occurs primarily on the trailing hemisphere. In addition, the surface density of Na can be independently estimated by assuming S and Na ions are supplied in the flux ratio from Table 1 and using *Carlson et al.*'s (2005a) estimate of $[S]/[H_2O] \sim 0.1$ on Europa's trailing side (S as sulfate), giving a surface concentration of $[Na]/[H_2O] \geq 0.4\%$. This is comparable to the 0.5–1% estimate for Na from the model fits noted above. Better models and understanding of Europa's plasma interaction are being developed (see chapter by Kivelson et al.) and soon we may be able to better estimate endogenic and exogenic contributions.

The different values of [Na]/[K] for Io and Europa are often used to state that Europa's alkalis are endogenic. However, fractionation occurs in the various sputtering processes and in the escape process, and sputtering of ice mixtures has not been adequately studied. As an example, for low cascade density sputtering (*Johnson,* 1990), Europa's distant Na/K ratio can be estimated as follows: If gardening is more rapid than loss by sputtering, then Europa's Na and K surface densities would be expected to be in the same ratio as Io's escaping Na and K, consistently estimated to be 10 ± 3 (*Brown,* 2001) and 10 ± 5 (*McGrath et al.,* 2004), although higher values (20–30) have been reported (*Trafton,* 1981). The low cascade density sputtering yield Y for a minor species with concentration c in ice is $Y = c(U_{H_2O}/U)\,Y_{H_2O}$, where U is a characteristic cohesion energy (*Johnson,* 1990). The escape fraction is proportional to $U/(\frac{1}{2}Mv_{esc}^2)$, with M being the mass and v_{esc} the escape velocity. The escape fraction is therefore independent of the cohesion energy and fractionation will occur inversely proportional to mass. For an iogenic input with [Na]/[K] = 5–15, we find Europa's escape flux ratio to be 8.5 to 25.5. This upper value is consistent with Brown's observations. Other sputtering processes (e.g., thermal spikes) can exhibit different fractionation effects. We conclude that definitive conclusions about the endogenic or exogenic nature of Europa's alkalis cannot be made at the present.

2.9. Other Possible or Suggested Species

2.9.1. Carbon compounds.

2.9.1.1. Carbon-oxygen compounds: Carbonate minerals have been suggested as possible candidates for Ganymede and Callisto's 4-μm feature (*Johnson et al.,* 2004) but further analysis is needed to establish the potential of CO_3^{2-}

compounds to explain the icy satellite's feature. Since carbon dioxide is present on Europa, one might expect related compounds such as carbon monoxide to be present. CO could be an endogenic outgassing product, or produced by radiolysis of CO_2 (*Moore et al.,* 1991; *Moore and Khanna,* 1991; *Brucato et al.,* 1997; *Strazzulla et al.,* 2005) or hydrocarbons (*Strazzulla et al.,* 1995; *Moore et al.,* 1996; *Moore and Hudson,* 1998; *Strazzulla and Moroz,* 2005). CO_2 is a back reaction product of CO radiolysis, and at equilibrium, the ratio of CO to CO_2 for various initial compounds is about unity (*Strazzulla et al.,* 1995). CO is very volatile, so any outgassed or radiolytically produced CO may rapidly escape, resulting in a low surface concentration. We can place a conservative limit on the leading-side concentration by assuming a band depth of less than 5% for possible CO 1-0 band absorption at 4.67 μm, giving a limit to the equivalent width of ~0.6 cm^{-1} (using NIMS' 0.025-μm resolution). Using the band strength determined by *Gerakines et al*. (1995), we find $<5 \times 10^{16}$ CO molecules cm^{-2} in the photon path L. Using a reflectance of 2% to derive the MOPL = αL, and using the absorption coefficient for H_2O, we determine L and the corresponding column density of H_2O molecules. This procedure gives $[CO]/[H_2O] <$ 250 ppm. Limits on the trailing-side abundance are higher due to higher noise levels in the available spectra.

CO radiolysis produces carbon suboxide, C_3O_2, and formaldehyde, H_2CO. In light of the CO upper limit, neither is expected in great quantities, but H_2CO merits discussion as it can be derived from hydrocarbons (*Moore and Hudson,* 1998) and is of astrobiological interest (*Chyba,* 2000; chapter by Hand et al.). The positions of formaldehyde's absorption bands depend on the matrix and the H_2CO concentration; for low concentrations in H_2O the CH symmetric and asymmetric stretch bands occur at 2785 and 2853 cm^{-1} (3.59 and 3.51 μm), respectively (*va der Zwet et al.,* 1985). The asymmetric stretch band is close to Europa's H_2O_2 feature, but the symmetric stretch band is isolated and one can estimate an upper limit for the leading side. Assuming a detectable integrated band intensity that is one-third that for Europa's H_2O_2 band (Fig. 14), and using the H_2CO band strength (*va der Zwet et al.,* 1985) relative to that of CH_4 (*d'Hendecourt and Allamandola,* 1986) with *Loeffler et al.*'s (2006b) value for H_2O_2, we find a limit of $[H_2CO]/[H_2O] <$ 0.25% for the leading side.

2.9.1.2. Hydrocarbons: The aliphatic hydrocarbon CH stretching band has been reported in Callisto spectra (*McCord et al.,* 1997) but is not yet observed on Europa. An upper limit to the hydrocarbon content is given in the chapter by Hand et al. as the number of methylene groups per water molecule, $[CH_2]/[H_2O]$, being $<1.5 \times 10^{-3}$. The number expected for meteoritic infall and burial by gardening, if all the C atoms are associated with methylene, is about 500 ppm or about one-third of this upper limit (see Table 1).

2.9.2. Nitrogen compounds.

2.9.2.1. Nitriles: A feature at 4.57 μm is found in spectra of both Ganymede and Callisto (*McCord et al.,* 1997, 1998a) and was suggested to be due to absorption by molecules containing the nitrile, C≡N, group. The fundamental C≡N stretch band occurs in the 4.4- to 4.9-μm region (*Bernstein et al.,* 1997; *Lowenthal et al.,* 2002; *Raunier et al.,* 2003; *Gerakines et al.,* 2004). The well-known interstellar XCN feature [now known to be due to OCN^- (*Hudson et al.,* 2001)] occurs at 4.62 μm. Polymeric HCN and some tholins possess absorption features in the 4.53- to 4.61-μm region that may be consistent with the suggestion of cyanogens (*Cruikshank et al.,* 1991; *Khare et al.,* 1994). Whichever molecule(s) the Ganymede and Callisto features are due to, it is reasonable to expect it to also be present on Europa if the material emanates from meteoritic and cometary infall. However, Europa's surface age is young compared to Ganymede and Callisto, so the amount that has accumulated is less by perhaps by a factor of about 100. Therefore it is not surprising that the abundance is too low to be detected on Europa.

2.9.2.2. Ammonia: Noting possible features at 1.8, 2.1, 2.2, and 2.3 μm in spectra obtained by R. Clark in 1980, *Brown et al*. (1988) subsequently searched the 2.0- to 2.5-μm region using improved instrumentation. They found weak absorptions at 2.2 and 2.3 μm in 1985, but not in measurements a year later. They considered sources of systematic error and noted that, while transient $NH_3 \bullet H_2O$ features could explain the features, they were skeptical of invoking transient phenomena as an explanation. *Calvin et al*. (1995) obtained telescopic spectra in 1989 and found none of the reported 2.1-, 2.2-, and 2.3-μm features. They noted that incomplete cancellation of the stellar Brackett line, or interference by atmospheric gases, could introduce spurious features at these wavelengths. They also noted that the 1.8-μm feature in the 1980 measurements could be real, or could be an artifact caused by incomplete atmospheric water vapor removal. Ammonia is rapidly destroyed by radiation, forming N_2 and H_2 (*Loeffler et al.,* 2006a), both of which will rapidly escape the surface.

2.9.2.3. Amides: *Dalton et al*. (2003) examined IR methods for detection capabilities of biological molecules and found two possible features (at 2.05 and 2.17 μm) in NIMS spectra that could be due N–H-related combination bands of an amide. While intriguing, these features are close to the noise level, and there are other possibilities for lines at these positions. If amide functional groups can survive the radiation environment at Europa they could serve as potential biomarkers; however, more laboratory work is needed to assess their stability and to investigate other, abiotic sources for these features.

2.9.3. Ozone and oxygen compounds. There have been considerable experimental advances in understanding the production of ozone in ice. *Baragiola et al.* (1999a) used the Hartley UV absorption band to study ozone production in H_2O:O_2 ices and successfully described ozone production using the classic Chapman atmospheric reaction scheme. Recent laboratory work by *Cooper et al*. (2008), using thin films of oxygen aggregates in water ice, has confirmed the suggestion that ozone is created through the irradiation of O_2 inclusions, as suggested earlier by *Johnson and Jesser* (1997). Starting only with water ice at satellite-like temperatures, *Teolis et al*. (2006) formed O_2 and O_3 using heavy

ion bombardment (section 2.5). The key element of this experiment was the simultaneous deposition of H_2O to simulate recondensation of a satellite's tenuous H_2O atmosphere. They found that the temperature, radiation, and recondensation conditions for O_3 production are met on the jovian and saturnian satellites. Therefore it is not surprising that O_3 is found on Ganymede (*Noll et al.,* 1996; *Hendrix et al.,* 1999) and might be expected on Europa and Callisto, where O_2 is also present [but in lesser amounts; see *Spencer and Calvin* (2002)]. This molecule is, surprisingly, also present on the surfaces of saturnian satellites (*Noll et al.,* 1997), where a less-intense magnetosphere would be expected to produce less precursor O_2.

Radiolysis of $H_2O + O_2$ produces H_2O_2, O_3, OH, HO_2, and HO_3 at exposures levels of only a few eV/16-amu. As the temperature of the radiolyzed $H_2O + O_2$ ices is raised, the amount of O_3 was found to decrease (*Cooper et al.,* 2008). This inverse temperature dependence may partly explain the existence of O_3 on the saturnian satellites even though their radiation environment is less intense than that of the jovian system. Ozone is also produced by irradiation of $H_2O + CO_2$ ice mixtures (*Strazzulla et al.,* 2005).

Ganymede's O_3 abundance in the observed column was measured by *Noll et al*. (1996) and *Hendrix et al.* (1999) as 4.5×10^{16} and 4.6×10^{16} cm^{-2}, respectively. Europa does not show an ozone-like feature (*Hendrix et al.,* 1998) in the UV, so the upper limit must be some fraction of Ganymede's abundance. Searches for a 4.8-μm O_3 band on the Galilean satellites with NIMS data have so far been unsuccessful, in part due to the low intrinsic absorption strength for this transition (P. Cooper, personal communication, 2007).

Oxides and hydroxides related to hydrated salts are discussed in section 2.2.5. The hydroxyl radical, OH, and other radicals are expected to be present in trace amounts (*Johnson and Quickenden,* 1997) but are below the detection limits of current datasets.

2.9.4. Sulfur compounds.

2.9.4.1. Hydrosulfides and hydrogen sulfide: A feature at 3.88 μm is observed on Ganymede and Callisto and suggested to arise from absorption by the SH stretch transition of a hydrosulfide (*McCord et al.,* 1997, 1998a). If this feature were present on Europa, then H_2S would be a candidate since the ocean, if nonoxidizing, could be rich in hydrogen sulfide. However, such an ocean arises if it remains reducing because of little hydrogen loss, implying weak communication to the surface and minimal surface emplacement of H_2S. Radiolytic H_2S was predicted in sulfate hydrate-rich regions at relative molar concentrations of 2×10^{-4} (*Carlson et al.,* 2002), neglecting UV destruction. However, Europa's oxidizing surface can effectively destroy H_2S. H_2S is very volatile and escapes from H_2O:H_2S ices at 132 K in laboratory timescales (*Moore et al.,* 2007). The band position for H_2S in H_2O ice is 3.90 μm. This species is not observed on Europa, but no limits have been established since the band strength in H_2O ice is not established. If it is present, it might be associated with sulfur and preferentially distributed on the trailing side.

2.9.4.2. Sulfanes: Sulfur chains with an H atom attached to the ends are termed sulfanes. Since polymeric sulfur containing long sulfur chains is possibly present on Europa's trailing hemisphere, then sulfanes might be present there as well. Sulfanes will exhibit the SH stretch band, but the exact positions and strengths are not known.

2.9.4.3. Polysulfur oxides: *Spencer et al*. (1995) noted the likelihood of sulfur compounds on Europa and followed *Sill and Clark*'s (1982) suggestion for Io, suggesting polymers of disulfur monoxide (S_2O) with SO_2 as coloring agents. Pure, concentrated S_2O can polymerize to form polysulfur oxides (PSO); however, the red color associated with S_2O and PSOs on Io is now thought to be due to the decomposition product S_4 (*Steudel and Steudel,* 2004). If S_2O or polysulfur oxides are present in significant amounts, they will produce overtone absorption bands at approximately 4.5 μm (*Baklouti et al.,* 2008). These bands are not seen in Europa's spectrum but upper limits to S_2O and PSO abundances cannot be calculated because the band strengths are not yet known.

2.9.4.4. Sulfurous acid: Aqueous solutions of SO_2 produces H^+ and HSO_3^-, an acidic solution termed sulfurous acid. In contrast to H_2SO_4 and H_2CO_3, the free molecule H_2SO_3 has not been found in nature. *Voegele et al*. (2004) calculated that, while pure H_2SO_3 molecules might have a long lifetime, the presence of H_2O greatly decreases the stability of the molecule. At 100 K, and with a 1:2 H_2SO_3:H_2O ratio, the computed lifetime is about 1 d. The molecule has not been found following proton implantation in frozen SO_2 (*Garozzo et al.,* 2008). H_2SO_3 molecules will persist on Europa in vanishingly small quantities, far below the detection limit.

2.9.5. Iron compounds. Ferric (Fe^{3+}) iron oxides and oxyhydroxides show strong absorption in the UV and blue, extending to about 0.55 μm, due to charge transfer between oxygen and Fe^{3+}. Electronic crystal field transitions in the Fe^{3+} ion produce a series of absorption bands. An excellent description of these electronic transitions is given in *Burns* (1993). For oxides and oxyhydroxides these band positions (and assignments) are 0.43 μm ($^6A_{1g} \rightarrow {}^4A_{1g}$, ^4E_g), 0.63 μm ($^6A_{1g} \rightarrow {}^4T_{2g}$), and 0.87 μm ($^6A_{1g} \rightarrow {}^4T_{1g}$) (*Morris et al.,* 1985). Additionally, there is a double electron transition at 0.5 μm ($2^6A_{1g} \rightarrow 2^4T_{1g}$) (*Morris et al.,* 1997). The positions of these bands are independent of temperature, at least for hematite, but the bands sharpen somewhat as the temperature is reduced (*Morris et al.,* 1997). Even though these four bands correspond to spin-forbidden transitions, they all can be quite strong. The combined effect of these absorptions is to produce a very reddish spectrum for ferric oxides and oxyhydroxides. The positions and strengths of electronic transitions depend on the site symmetry and the mineral composition. For example, ferric sulfate nonahydrate, $Fe_2(SO_4)_3 \bullet 9H_2O$ – coquimbite, exhibits bands at 0.42–0.43 μm ($^6A_{1g} \rightarrow {}^4A_{1g}$, ^4E_g), 0.56 μm ($^6A_{1g} \rightarrow {}^4T_{2g}$), and 0.78 μm ($^6A_{1g} \rightarrow {}^4T_{1g}$), giving this mineral a gray-green tinge (*Rossman,* 1975).

Ferrous iron (Fe^{2+}) has spin-allowed crystal field transitions that produce the well known iron silicate absorption

bands in the 1- and 2-μm regions, as well as spin-forbidden transitions at 0.45 μm ($^5T_{2g} \rightarrow {}^3T_{2g}$), 0.51 μm ($^5T_{2g} \rightarrow {}^1A_{1g}$), and 0.55 μm ($^5T_{2g} \rightarrow {}^3T_{1g}$) (*Hunt and Salisbury,* 1970; *Hunt et al.,* 1971b).

Iron compounds have been suggested for the Galilean satellites in general, based on the general red appearance of their spectra and those of iron compounds (*Johnson,* 1970; *Johnson and McCord,* 1970; *Sill and Clark,* 1982; *McEwen,* 1986), but no features are found in groundbased 0.9- to 1.1-μm spectra (*Johnson and Pilcher,* 1977) and none have been found in later telescopic or spacecraft spectra, indicating a lack of ferrous silicates.

Given the oxidizing nature of Europa's surface, ferric oxides and oxyhydroxides are possible candidates. *Clark* (1980) noted 0.87-μm absorption features in spectra of Europa, Ganymede, and Callisto that he suggested were due to absorption by ferric iron compounds. The absorption was weakest for Europa, for which the band was about 4% deep and had a full width at half maximum of ~0.1 μm. This position and width is consistent with Fe^{3+} absorption, although there were questions about the accuracy of the lunar reference spectrum in this spectral region (*Clark,* 1980). This band is not apparent in NIMS spectra at about the 2% level. Nanophase ferric oxides, and such minerals as ferrihydrite, goethite, hematite, maghemite, and lepidocrocite, have been extensively studied for Mars application and representative spectra are given in *Morris et al*. (1993, 2000). Ferric oxides show the 0.87-μm band, sometimes centered at longer wavelengths. Just shortward of this band, generally at about 0.7–0.8 μm, the reflectivity drops quickly due to the stronger 0.63-μm band, and at ~0.6 μm, another shoulder is reached, below which the reflectivity drops even more quickly. In many cases this second shoulder is absent, and the break-point in the spectrum is between 0.7 and 0.8 μm. At low temperature, the 0.6-μm shoulder becomes a local maximum, with the minimum at 0.63 μm. Thus, the turnover point in the spectrum occurs at a longer wavelength compared to either the leading or trailing-side spectra of Europa (Fig. 13c). We conclude that there is no strong evidence for ferric oxide or hydroxide compounds at observable amounts on Europa.

Ferric sulfate is worthy of consideration, since concentrated ferric sulfate aqueous solutions possess low freezing points, possibly as low as ~200 K (*Chevrier and Altheide,* 2008). *Nash and Fanale* (1977) obtained spectra of $Fe_2(SO_4)_3 \bullet xH_2O$ [see also *Rossman* (1975), *Crowley et al.* (2003), *Clark et al.*'s (2007) splib06 spectral library] and they suggested that the absorption bands at 0.5 and 0.8 μm might be responsible for two bands in Io's spectra. Although it is now thought that the 0.53-μm band in Io's spectrum is due to S_4 (*Carlson et al.,* 2007) and tetrasulfur is possible on Europa, it is appropriate to consider ferric sulfate. The depth of Europa's potential 0.53-μm band is about 4% (Fig. 13D) and *Rossman's* (1975) absorbance measurement suggests equal strengths for the 0.56- and 0.78-μm features, whereas *Nash and Fanale*'s (1977) measurements indicate that the 0.8-μm band should be about five times stronger in band depth than the 0.5-μm feature. However, NIMS spectra show less than a 2% feature at 0.8 μm. In addition, Europa's 0.4-μm reflectance (Fig. 13c) of ~40% is much higher than would be expected based on *Nash and Fanale*'s (1977) and *Crowley et al.*'s (2003) reflectance spectra, both of which show reflectance values at 0.4 μm of ~2%. While we cannot rule out some iron compounds on Europa's surface, any amount present is constrained to trace levels.

3. FUTURE MEASUREMENTS AND EXPERIMENTS

There are several avenues to pursue to improve understanding of Europa's surface composition in general and the hydrate question in particular. First, we need better understanding of the exogenic and endogenic sources. Source rates for material emanating from the small outer satellites and Ganymede and Callisto need quantification. We also need to understand Europa's plasma interaction better in order to verify (or refute) Europa as an endogenic source of the escaping Na and K. This understanding may be developed by further analysis theoretical modeling and analysis of Galileo particles and magnetic field data, as well as continued observations and analysis of Europa's extended Na and K atmosphere.

Additionally, the age and evolution of the surface needs to be understood. Does the ~50-m.y. cratering age imply that entire crust was replenished then, or has the ice that forms the crust remained in the crust since formation of the satellite? How pure was the pristine crust?

Telescopic measurements, both from the ground and by orbiting telescopes, can continue near-IR searches for hydrated salt features as well as searching for hydroxide features to identify any metals and nonmetals. Low light level luminescence emissions from Europa observed when in eclipse may allow detection of species such as magnesium, as emissions from neutral Mg are produced by ion bombardment (e.g., the Mg I lines $^3P^0$–^3S λλ5167 Å–5183 Å and ^1S–$^1P^0$ λ2852 Å as observed by irradiating $MgSO_4 \bullet 7H_2O$ (*Nash and Fanale,* 1977)). Telescopic observations of the atmosphere near Europa, as well as of the neutral torus, may provide identifications of new species that may have originated from the surface (e.g., Cl). Mapping of Europa's surficial O_2 may lead to better understanding of the oxygen production and trapping mechanism. For that matter, except for the observations by *Spencer et al*. (1995), there have been no spatially resolved imaging spectroscopy measurements of Europa in the visible region. Such measurements could provide better evidence for S_4 and possibly other absorbers and coloring agents. Further analysis of existing UV and IR data may be fruitful; a search for metal hydroxide features is one area of interest.

More laboratory spectra with extended wavelength coverage are needed for candidate materials. Many of the published spectra of candidate icy satellite surface materials were recorded during investigations of the properties and chemistry of the interstellar medium and comets. In many cases, such published spectra are from thin films (0.1–10 μm) measured in the mid-IR region at a few kelvins in

temperature. However, the data needed for quantitative comparisons to spectra from Europa and other icy satellites often require different experimental conditions. Laboratory measurements for all candidate materials are needed, ideally with the following characteristics: First, spectra must be recorded in either diffuse reflectance or presented in terms of optical constants — quantities that enable quantitative abundance modeling. For diffuse reflectance, different grain sizes must be investigated. Second, laboratory measurements are needed across the full spectral range of typical and future spacecraft instruments (0.1–7 μm). Third, measurements must be conducted with samples sufficiently thick to produce useful absorption features, particularly the shapes and strengths of weak bands, such as in the near-IR region. Fourth, measurements must be temperature-appropriate for the bodies of interest, since many candidate compounds (especially ices) display marked spectral changes with temperature. For the specific case of Europa, laboratory measurements in the 80–130-K range are critical.

There have few laboratory studies of how radiation-induced dehydration, amorphization, and decomposition can alter hydrate band positions and profiles. Such measurements should be carried out for both ion and electron irradiation, as collision effects may be different for the two cases. The vapor pressure of radiation-produced amorphous ice is needed to accurately describe Europa's sublimational atmosphere and transport. Continued study of the radiolytic production and trapping of O_2, CO_2, and other volatiles will tell us how much O_2 is stored in Europa's regolith and if clathrates are important features of the icy shell.

The logical next stage of exploration would be an orbiter around Europa, instrumented with remote-sensing IR and UV spectrometers. The IR spectrometer should have a longer wavelength capability than NIMS had, in order to measure important functional groups such as C=O, C=C, N=O, NO_2, CO_2^-, and C-O, and the deformation transitions of N-H, NH_2, and O-H. Classes of molecules such as carbonates, carboxylic acid and their salts, nitrates, alcohols, esters, ketones, aldehydes, aromatic molecules, amines, and amides would be observable in this extended wavelength interval. Sufficient spatial resolution to acquire spectra of distinct geological regions will be critical to identify and discriminate surface materials and assessing their roles in evolution of the surface. Europa's sputter atmosphere provides another means of indirectly determining surface composition. An orbiting ion mass spectrometer or rotational line microwave spectrometer could respectively measure the ion or neutral component and provide new insights into Europa's surface composition. Concepts for a future landed mission to Europa require knowledge of the surface composition and structure. While many data sets are now available, there remains much work to be done in order to further explore this fascinating world and determine its habitability.

Acknowledgments. We thank R. Clark and C. Hibbits for their important and insightful reviews, and W. Grundy, K. Hand, M. Loeffler, W. McKinnon, U. Raut, J. Shirley, K. Zahnle, and M. Zolotov for their comments, data, and discussions. A portion of the research described in this chapter was carried out at the Jet Propulsion Laboratory, California Institute of Technology, and was done so under a contract with the National Aeronautics and Space Administration.

REFERENCES

Allamandola L. J., Sandford S. A., and Valero G. J. (1988) Photochemical and thermal evolution of interstellar/precometary ice analogs. *Icarus, 76,* 225–252.

Allison M. L. and Clifford S. M. (1987) Ice-covered water volcanism on Ganymede. *J. Geophys. Res., 92,* 7865–7876.

Alvarellos J. L., Zahnle K. J., Dobrovolskis A. R., and Hamill P. (2008) Transfer of mass from Io to Europa and beyond due to cometary impacts. *Icarus, 194,* 636–646, DOI: 10.1016/j.icarus.2007.09.025.

Anders E. and Grevasse N. (1989) Abundances of the elements: Meteoritic and solar. *Geochim. Cosmochim. Acta, 53,* 197–214.

Bagenal F. (1994) Empirical-model of the Io plasma torus — Voyager measurements. *J. Geophys. Res., 99,* 11043–11062.

Baklouti D., Schmitt B., and Brissaud O. (2008) S_2O, polysulfur oxide and sulfur polymer on Io's surface? *Icarus, 194,* 647–659.

Baragiola R. A. (2003) Water ice on outer solar system surfaces: Basic properties and radiation effects. *Planet. Space Sci., 51,* 953–961.

Baragiola R. A. and Bahr D. A. (1998) Laboratory studies of the optical properties and stability of oxygen on Ganymede. *J. Geophys. Res., 103,* 25865–25872.

Baragiola R. A., Atteberry C. L., Bahr D. A., and Jakas M. M. (1999a) Solid-state ozone synthesis by energetic ions. *Nucl. Instr. Meth. Phys. Res. B, 157,* 233–238.

Baragiola R. A., Atteberry C. L., Bahr D. A., and Peters M. (1999b) Comment on "Laboratory studies of the optical properties and stability of oxygen on Ganymede" by Raul A. Baragiola and David A. Bahr — Reply. *J. Geophys. Res., 104,* 14183–14187.

Baragiola R. A., Loeffler M. J., Raut U., Vidal R. A., and Wilson C. D. (2005) Laboratory studies of radiation effects in water ice in the outer solar system. *Rad. Phys. Chem., 72,* 187–191.

Baratta G. A., Leto G., Spinella F., Strazzulla G., and Foti G. (1991) The 3.1 μm feature in ion-irradiated ice. *Astron. Astrophys., 252,* 421–424.

Baratta G. A., Castorina A. C., Leto G., Palumbo M. E., Spinella F., and Strazzulla G. (1994) Ion irradiation experiments relevant to the physics of comets. *Planet. Space Sci., 42,* 759–766.

Bauer W. H. (1964) On the crystal chemistry of salt hydrates II: A neutron diffraction study of $MgSO_4 \cdot 4H_2O$. *Acta Crystallogr., 17,* 863–869.

Bergren M. S., Shuh D., Sceats M. G., and Rice S. A. (1978) The OH stretching region infrared spectra of low density amorphous solid water and polycrystalline ice I_h. *J. Chem. Phys., 69,* 3477–3482.

Bernstein M. P., Sandford S. A., and Allamandola L. J. (1997) The infrared spectra of nitriles and related compounds frozen in Ar and H_2O. *Astrophys. J., 476,* 932–942.

Bertie J. E. and Jacobs S. M. (1977) Far-infrared absorption by ices Ih and Ic at 4.3 K and the powder diffraction pattern of ice I_c. *J. Chem. Phys., 67,* 2445–2448.

Bertie J. E. and Whalley E. (1964) Infrared spectra of ices I_h and I_c in the range 4000 to 350 cm^{-1}. *J. Chem. Phys., 40,* 1637–1645.

Bertie J. E. and Whalley E. (1967) Optical spectra of orientationally disordered crystals. II. Infrared spectra of ice I_h and I_c from 360 to 50 cm^{-1}. *J. Chem Phys., 46,* 1271–1284.

Bertie J. E., Labbe H. J., and Whalley E. (1969) Absorptivity of ice I in the range 4000–30 cm^{-1}. *J. Chem. Phys., 50,* 1271–1284.

Billmers R. I. and Smith A. L. (1991) Ultraviolet-visible absorption spectra of equilibrium sulfur vapor: Molar absorptivity spectra of S_3 and S_4. *J. Phys. Chem., 95,* 4242–4245.

Blake D., Allamandola L., Sandford S., Hudgins D., and Freund F. (1991) Clathrate hydrate formation in amorphous cometary ice analogs in vacuo. *Science, 254,* 548–551.

Blickensderfer R. P. and Ewing G. E. (1969a) Collision-induced absorption spectrum of gaseous oxygen at low temperatures and pressures. II. Simultaneous transitions $^1\Delta_g + {}^1\Delta_g \leftarrow {}^3\Sigma_g^- + {}^3\Sigma_g^-$ and $^1\Delta_g + {}^3\Sigma_g^+ \leftarrow {}^3\Sigma_g^- + {}^3\Sigma_g^-$. *J. Chem. Phys., 51,* 5284–5289.

Blickensderfer R. P. and Ewing G. E. (1969b) Collision-induced absorption spectrum of gaseous oxygen at low temperatures and pressures. I. The $^1\Delta_g - {}^3\Sigma_g$ system. *J. Chem. Phys., 51,* 873–883.

Brown M. E. (1999) Trace elements in the atmosphere of Europa as a probe of surface composition (abstract). *Eos Trans. AGU, 80,* F604.

Brown M. E. (2001) Potassium in Europa's atmosphere. *Icarus, 151,* 190–195.

Brown R. H., Cruikshank D. P., Tokunaga A. T., Smith R. G., and Clark R. N. (1988) Search for volatiles on icy satellites I. Europa. *Icarus, 74,* 262–271.

Brown R. H., Baines K. H., Belluci G., Buratti B. J., Cappaccioni F., et al. (2006a) Observations in the Saturn system during approach and orbital insertion, with Cassini's visual and infrared mapping spectrometer (VIMS). *Astron. Astrophys., 446,* 707–716.

Brown R. H., Clark R. N., Buratti B. J., Cruikshank D. P., Barnes J. W., et al. (2006b) Composition and physical properties of Enceladus' surface. *Science, 311,* 1425–1428.

Brucato J. R., Palumbo M. E., and Strazzulla G. (1997) Carbonic acid by ion implantation in water/carbon dioxide ice mixtures. *Icarus, 125,* 135–144.

Buratti B. J., Cruikshank D. P., Brown R. H., Clark R. N., Bauer J. M., et al. (2005) Cassini infrared and visual mapping spectrometer observations of Iapetus: Detection of CO_2. *Astrophys. J., 622,* L149–L152.

Burchell M. J., Cole M. J., and Ratcliff P. R. (1996) Light flash and ionization from hypervelocity impacts on ice. *Icarus, 122,* 359–365.

Burns J. A. (1968) Jupiter's decametric radio emission and the radiation belts of its galilean satellites. *Science, 159,* 971–972.

Burns R. G. (1993) Origin of electronic spectra of minerals in the visible and near-infrared region. In *Remote Geochemical Analysis* (C. M. Pieters and P. A. J. Englert, eds.), pp. 3–29. Cambridge Univ., Cambridge.

Buxton G. V. (1987) Radiation chemistry of the liquid state, 1, Water and homogeneous aqueous solutions. In *Radiation Chemistry* (M. A. Farhataziz and J. Rodgers, eds.), pp. 321–349. Wiley, New York.

Calvin W. M. and Spencer J. R. (1997) Latitudinal distribution of O_2 on Ganymede: Observations with the Hubble Space Telescope. *Icarus, 130,* 505–516.

Calvin W. M., Clark R. N., Brown R. H., and Spencer J. R. (1995) Spectra of the icy Galilean satellites from 0.2 to 5 μm — A compilation, new observations, and a recent summary. *J. Geophys. Res., 100,* 19041–19048.

Calvin W. M., Johnson R. E., and Spencer J. R. (1996) O_2 on Ganymede: Spectral characteristics and plasma formation mechanisms. *Geophys. Res. Lett., 23,* 673–676.

Carlson R. W. (1999) A tenuous carbon dioxide atmosphere on Jupiter's moon Callisto. *Science, 283,* 820–821.

Carlson R. W. (2001) Spatial distribution of carbon dioxide, hydrogen peroxide, and sulfuric acid on Europa (abstract). *Bull. Am. Astron. Soc., 33,* 1125.

Carlson R. W. (2003) Europa's radiation processed regolith (abstract). *Bull. Am. Astron. Soc., 35,* 17.01.

Carlson R. W. (2004) Distribution of hydrogen peroxide, carbon dioxide, and sulfuric acid in Europa's icy crust. In *Workshop on Europa's Icy Shell: Past, Present and Future,* p. 15. LPI Contribution No. 1195, Lunar and Planetary Institute, Houston.

Carlson R. W. and Hand K. P. (2006) The mystery of carbon dioxide on icy satellites: A mixed clathrate hydrate? (abstract). *Bull. Am. Astron. Soc., 38,* 38.30.13.

Carlson R. W., Weissman P. R., Smythe W. D., Mahoney J. C., Aptaker I., Bailey G., Baines K., Burns R., Carpenter E., Curry K., Danielson G., Encrenaz T., Enmark H., Fanale F., Gram M., Hernandez M., Hickok R., Jenkins G., Johnson T., Jones S., Kieffer H., Labaw C., Lockhart R., Macenka S., Marino J., Masursky H., Matson D., McCord T., Mehaffey K., Ocampo A., Root G., Salazar R., Sevilla D., Sleigh W., Smythe W., Soderblom L., Steimle L., Steinkraus R., Taylor F., and Wilson D. (1992) Near–Infrared mapping spectrometer experiment on Galileo. *Space Sci. Rev., 60,* 457–502.

Carlson R. W., Smythe W., Baines K., Barbinis E., Becker K., Burns R., Calcutt S., Calvin W., Clark R., Danielson G., Davies A., Drossart P., Encrenaz T., Fanale F., Granahan J., Hansen G., Herrera P., Hibbitts C., Hui J., Irwin P., Johnson T., Kamp L., Kieffer H., Leader F., Lellouch E., Lopes-Gautier R., Matson D., McCord T., Mehlman R., Ocampo A., Orton G., Roos-Serote M., Segura M., Shirley J., Soderblom L., Stevenson A., Taylor F., Torson J., Weir A., and Weissman P. (1996) Near-infrared spectroscopy and spectral mapping of Jupiter and the Galilean satellites: Results from Galileo's initial orbit. *Science, 274,* 385–388.

Carlson R. W., Anderson M. S., Johnson R. E., Smythe W. D., Hendrix A. R., Barth C. A., Soderblom L. A., Hansen G. B., McCord T. B., Dalton J. B., Clark R. N., Shirley J. H., Ocampo A. C., and Matson D. L. (1999a) Hydrogen peroxide on the surface of Europa. *Science, 283,* 2062–2064.

Carlson R. W., Johnson R. E., and Anderson M. S. (1999b) Sulfuric acid on Europa and the radiolytic sulfur cycle. *Science, 286,* 97–99.

Carlson R. W., Anderson M. S., Johnson R. E., Schulman M. B., and Yavrouian A. H. (2002) Sulfuric acid production on Europa: The radiolysis of sulfur in water ice. *Icarus, 157,* 456–463.

Carlson R. W., Anderson M. S., Mehlman R., and Johnson R. E. (2005a) Distribution of hydrate on Europa: Further evidence for sulfuric acid hydrate. *Icarus, 177,* 461–471.

Carlson R. W., Hand K. P., Gerakines P. A., Moore M. H., and Hudson R. L. (2005b) Radiolytic production of carbonic acid and applications to Jupiter's icy satellites (abstract). *Bull. Am. Astron. Soc., 37,* 751–752.

Carlson R. W., Kargel J. S., Doute S., Soderblom L. A., and Dalton B. (2007) Io's surface composition. In *Io after Galileo* (R. M. C. Lopes and J. R. Spencer, eds.), pp. 193–229. Springer-Praxis, Chichester.

Cassidy T. A., Johnson R. E., McGrath M. A.., Wong M. C., and Cooper J. E. (2007) The spatial morphology of Europa's near-surface O_2 atmosphere. *Icarus, 191,* 755–764.

Cassidy T. A., Johnson R. E., Geissler P., and Leblanc F. (2008) Simulation of Na D emission near Europa during eclipse. *J. Geophys. Res., 113,* E02005, DOI: 10.1029/2007/je002955.

Chaban G. M., Huo W. M., and Lee T. J. (2002) Theoretical study of infrared and Raman spectra of hydrated magnesium sulfate salts. *J. Chem. Phys., 117,* 2532–2537.

Chaban G. M., Bernstein M. P., and Cruikshank D. P. (2007) Carbon dioxide on planetary bodies: Theoretical and experimental studies of molecular complexes. *Icarus, 187,* 592–599.

Chevrier V. F. and Altheide T. S. (2008) Low temperature aqueous ferric sulfate solutions on the surface of Mars. *Geophys. Res. Lett., 35,* L22101, DOI: 10.1029/2008GL035489.

Christensen P. R., Bandfield J. L., Hamilton V. E., Howard D. A., Lane M. D., Piatek J. L., Russ S. W., and Stefanov W. L. (2000) A thermal emission spectral library of rock-forming minerals. *J. Geophys. Res., 105,* 9735–9740.

Chyba C. F. (2000) Energy for microbial life on Europa. *Nature, 403,* 381–382.

Cipriani F., Leblanc F., Witasse O., and Johnson R. E. (2008) Sodium recycling at Europa: What do we learn from the sodium cloud variability? *Geophys. Res. Lett., 35,* L19201, DOI: 10.1029/2008gl035061.

Clark R. N. (1980) Ganymede, Europa, Callisto, and Saturn's rings — Compositional analysis from reflectance spectroscopy. *Icarus, 44,* 388–409.

Clark R. N. (1981a) Water frost and ice — The near–infrared spectral reflectance 0.65–2.5 microns. *J. Geophys. Res., 86,* 3087–3096.

Clark R. N. (1981b) The spectral reflectance of water-mineral mixtures at low-temperatures. *J. Geophys. Res., 86,* 3074–3086.

Clark R. N. (2004) The surface composition of Europa: Mixed water, hydronium, and hydrogen peroxide ice. In *Workshop on Europa's Icy Shell: Past, Present, and Future,* Abstract #7057. LPI Contribution 1195, Lunar and Planetary Institute, Houston.

Clark R. N. and Lucey P. G. (1984) Spectral properties of ice-particulate mixtures and implications for remote sensing 1. Intimate mixtures. *J. Geophys. Res., 89,* 6341–6348.

Clark R. N. and Roush T. L. (1984) Reflectance spectroscopy: Quantitative analysis techniques for remote sensing applications. *J. Geophys. Res., 89,* 6329–6340.

Clark R. N., Fanale F. P., and Zent A. P. (1983) Frost grain-size metamorphism: Implications for remote-sensing of planetary surfaces. *Icarus, 56,* 233–245.

Clark R. N., King T. V. V., Klejwa M., Swayze G. A., and Vergo N. (1990) High spectral resolution reflectance spectroscopy of minerals. *J. Geophys. Res., 95,* 12653–12680.

Clark R. N., Swayze G. A., Gallagher A., King T. V. V., and Calvin W. M. (1993) *USGS Digital Spectral Library, Version 1: 0.2 to 3.0 μm.* U.S. Geol. Surv. Open File Report 93 592, U.S. Geological Survey, Flagstaff, Arizona. 1340 pp. Available online at http://speclab.cr.usgs.gov.

Clark R. N., Swayze G. A., Wise R., Livo K. E., Hoefen T. M., Kokaly R. F., and Sutley S. J. (2003) *USGS Digital Spectral Library splib05a.* USGS Open File Report 03-395, U.S. Geological Survey, Flagstaff, Arizona.

Clark R. N., Brown R., Baines K., Belluci G., Bibring J.-P., et al. (2005a) Cassini VIMS compositional mapping of surfaces in the Saturn system and the role of water, cyanide compounds and carbon dioxide. *Bull. Am. Astron. Soc., 37,* 705.

Clark R. N., Brown R. H., Jaumann R., Cruikshank D. P., Nelson R. M., Buratti B. J., et al. (2005b) Compositional maps of Saturn's moon Phoebe from imaging spectroscopy. *Nature, 435,* 66–69.

Clark R. N., Swayze G. A., Wise R., Livo E., Hoefen T., Kokaly R., and Sutley S. J. (2007) *USGS Digital Spectral Library splib06a.* Digital Data Series 231, U.S. Geological Survey, Flagstaff, Arizona.

Clark R. N., Curchin J. M., Hoefen T. M., and Swayze G. A. (2008a) Reflectance spectroscopy of organic compounds I: Alkanes. *J. Geophys. Res.–Planets.,* in press.

Clark R. N., Curchin J. M., Jaumann R., Cruikshank D. P., Brown R. H., Hoefen T. M., Stephan K., Moore J. M., Buratti B. J., Baines K. H., Nicholson P. D., and Nelson R. M. (2008b) Compositional mapping of Saturn's satellite Dione with Cassini VIMS and implications of dark material in the Saturn system. *Icarus, 193,* 372–386.

Cloutis E. A., Hawthorne F. C., Mertzman S. A., Krenn K., Craig M. A., Marcino D., Methot M., Strong J., Mustard J. F., Blaney D. L., Bell J. F., and Vilas F. (2006) Detection and discrimination of sulfate minerals using reflectance spectroscopy. *Icarus, 184,* 121–157, DOI: 10.1016/j.icarus.(2006)04.003.

Cohen C. M. S., Stone E. C., and Selesnick R. S. (2001) Energetic ion observations in the middle jovian magnetosphere. *J. Geophys. Res., 106,* 29871–29881.

Collins G. C., Head J. W., Pappalardo R. T., and Spaun N. A. (2000) Evaluation of models for the formation of chaotic terrain on Europa. *J. Geophys. Res., 105,* 1709–1716.

Cooper J. F., Johnson R. E., Mauk B. H., Garrett H. B., and Gehrels N. (2001) Energetic ion and electron irradiation of the icy Galilean satellites. *Icarus, 149,* 133–159.

Cooper P. D., Johnson R. E., and Quickenden T. I. (2003a) Hydrogen peroxide dimers and the production of O_2 in icy satellite surfaces. *Icarus, 166,* 444–446.

Cooper P. D., Johnson R. E., and Quickenden T. I. (2003b) A review of possible optical absorption features of oxygen molecules in icy surfaces of outer solar system bodies. *Planet. Space Sci., 51,* 183–192.

Cooper P. D., Moore M. H., and Hudson R. L. (2006) Infrared detection of HO_2 and HO_3 radicals in water ice. *J. Phys. Chem. A., 110,* 7985–7988.

Cooper P. D., Moore M. H., and Hudson R. L. (2008) Radiation chemistry of $H_2O + O_2$ ices. *Icarus, 194,* 379–388.

Crowley J. K. (1991) Visible and near-infrared (0.4–2.5 μm) reflectance spectra of playa evaporite minerals. *J. Geophys. Res., 96,* 16231–16240.

Crowley J. K., Williams D. E., Hammarstrom J. M., Piatek N., Chou I.-M., and Mars J. C. (2003) Spectral reflectance properties (0.4–2.5 μm) of secondary Fe-oxide, Fe-hydroxide, and Fe-sulfate-hydrate minerals associated with sulphide-bearing mine wastes. *Geochemistry, 3,* 219–228.

Cruikshank D. P., Allamandola L. J., Hartmann W. K., Tholen D. J., Brown R. H., Mathews C. N., and Bell J. F. (1991) Solid C≡N bearing material on outer solar system bodies. *Icarus, 94,* 345–353.

Cruikshank D. P., Roush T. L., Owen T. C., Geballe T. R., Debergh C., Schmitt B., Brown R. H., and Bartholomew M. J. (1993) Ices on the surface of Triton. *Science, 261,* 742–745.

Curtis D. B., Rajaram B., Toon O. B., and Tolbert M. A. (2005) Measurement of the temperature-dependent optical constants of water ice in the 15–200 μm range. *Appl. Optics, 44,* 4102–4118.

Dalton J. B. and Clark R. N. (1998) Laboratory spectra of Europa candidate materials at cryogenic temperatures (abstract). *Bull. Am. Astron. Soc., 30,* 1081.

Dalton J. B. and Clark R. N. (1999) Observational constraints on Europa's surface composition from Galileo NIMS. In *Lunar and Planetary Science XXX,* Abstract #2064. Lunar and Planetary Institute, Houston (CD–ROM).

Dalton J. B. (2000) Constraints on the surface composition of Jupiter's moon Europa based on laboratory and spacecraft data. Ph.D. thesis, University of Colorado, Boulder, 253 pp.

Dalton J. B. (2003) Spectral behavior of hydrated sulfate salts: Implications for Europa mission spectrometer design. *Astrobiology, 3,* 771–784. DOI: 10.1089/153110703322736097.

Dalton J. B. (2007) Linear mixture modeling of Europa's non-ice material using cryogenic laboratory spectroscopy. *Geophys. Res. Lett., 34,* L21205, DOI: 10.1029/2007GL031497.

Dalton J. B., Mogul R., Kagawa H. K., Chan S. L., and Jamieson C. S. (2003) Near-infrared detection of potential evidence for microscopic organisms on Europa. *Astrobiology, 3,* 505–529, DOI: 10.1089/153110703322610618.

Dalton J. B., Prieto-Ballesteros O., Kargel J. S., Jamieson C. S., Jolivet J., and Quinn R. C. (2005) Spectral comparison of heavily hydrated salts with disrupted terrains on Europa. *Icarus, 177,* 472–490.

DellaGuardia R. A. and Johnston F. J. (1980) Radiation-induced reaction of sulfur and water. *Rad. Res., 84,* 259–264.

DelloRusso N., Khanna R. K., and Moore M. H. (1993) Identification and yield of carbonic acid and formaldehyde in irradiated ices. *J. Geophys. Res., 98,* 5505–5510.

d'Hendecourt L. and Allamandola L. (1986) Time dependent chemistry in dense molecular clouds. III. Infrared band cross sections of molecules in the solid state at 10 K. *Astron. Astrophys. Suppl., 64,* 453–467.

Dianov-Klokov V. I. (1964) Absorption spectrum of oxygen at pressures from 2 to 35 atmospheres in the region 12600–3600 Å. *Optika I Spektroskopiya, 16,* 409–416.

Dianov-Klokov V. I. (1966) Absorption spectrum of condensed oxygen in 1.26–0.3 μm region. *Optics and Spectroscopy-USSR, 20,* 530.

Domingue D. and Allamandola L. (2001) Introduction to the special section: Photolysis and radiolysis of outer solar system ices (PROSSI). *J. Geophys. Res.–Planets, 106,* 33273–33273.

Domingue D. and Hendrix A. (2005) A search for temporal variability in the surface chemistry of the icy Galilean satellites. *Icarus, 173,* 50–65.

Domingue D. L. and Lane A. L. (1998) IUE views Europa: Temporal variations in the UV. *Geophys. Res. Lett., 25,* 4421–4424.

Dowell L. G. and Rinfret A. P. (1960) Low-temperature forms of ice as studied by X-ray diffraction. *Nature, 188,* 1144–1148.

Dressler K. and Schnepp O. (1960) Absorption spectra of solid methane, ammonia, and ice in the vacuum ultraviolet. *J. Chem. Phys., 33,* 270–274.

Dybwad J. P. (1971) Radiation effects on silicates (5-keV H^+, D^+, He^+, H^{2+}). *J. Geophys. Res., 76,* 4023–4029.

Eckert B. and Steudal R. (2003) Molecular spectra of sulfur molecules and solid sulfur allotropes. *Topics Curr. Chem., 231,* 31–98.

Ehrenfreund P., Kerkhof O., Schutte W. A., Boogert A. C. A., Gerakines P. A., Dartois E., d'Hendecourt L., Tielens A. G. G. M., van Dishoeck E. F., and Whittet D. C. B. (1999) Laboratory studies of thermally processed H_2O-CH_3OH-CO_2 ice mixtures and their astrophysical implications. *Astron. Astrophys., 350,* 240–253.

Eichhorn K. and Grun E. (1993) High-velocity impacts of dust particles in low-temperature water ice. *Planet. Space Sci., 41,* 429–433.

Encrenaz T. (2008) Water in the solar system. *Annu. Rev. Astron. Astrophys., 46,* 57–87.

Eviatar A., Siscoe G. L., Johnson T. V., and Matson D. L. (1981) Effects of Io ejecta on Europa. *Icarus, 47,* 75–83.

Fagents S. A. (2003) Considerations for effusive cryovolcanism on Europa: The post-Galileo perspective. *J. Geophys. Res., 108(E12),* 5139.

Fagents S. A., Greeley R., Sullivan R. J., Pappalardo R. T., and Prockter L. M. (2000) Cryomagmatic mechanisms for the formation of Rhadamanthys linea, triple band margins, and other low-albedo features on Europa. *Icarus, 144,* 54–88.

Fanale F. P., Granahan J. C., Greeley R., Pappalardo R., Head J., Shirley J., Carlson R., Hendrix A., Moore J., McCord T. B., and Belton M. (2000) Tyre and Pwyll: Galileo orbital remote sensing of mineralogy versus morphology at two selected sites on Europa. *J. Geophys. Res., 105,* 22647–22655.

Feldman P. D., Ake T. B., Berman A. F., Moos H. W., Sahnow D. J., Strobel D. F., Weaver H. A., and Young P. R. (2001) Detection of chlorine ions in the Far Ultraviolet Explorer spectrum of the Io plasma torus. *Astrophys. J. Lett., 554,* L123–L126.

Feldman P. D., Strobel D. F., Moos H. W., and Weaver H. A. (2004) The far ultraviolet spectrum of the Io plasma torus. *Astrophys. J., 601,* 583–591.

Findlay F. D. (1970) Visible emission bands of molecular oxygen. *Can. J. Phys., 48,* 2107.

Fink U., Dekkers N. H., and Larson H. P. (1973) Infrared spectra of the Galilean satellites of Jupiter. *Astrophys. J. Lett., 179,* L155–L159.

Fleyfel F. and Devlin J. P. (1991) Carbon-dioxide clathrate hydrate epitaxial-growth — Spectroscopic evidence for formation of the simple Type-II CO_2 hydrate. *J. Phys. Chem., 95,* 3811–3815.

Franck J. and Rabinowitsch E. (1934) Some remarks about free radicals and the photochemistry of solutions. *Trans. Faraday Soc., 30,* 0120–0130.

Fuller K. A., Downing H. D., and Querry M. R. (1998) Orthorhombic sulfur (α-S). In *Handbook of Optical Constants of Solids III* (E. D. Palik, ed.), p. 899. Academic, San Diego.

Gaffey S. J., McFadden L. A., Nash D., and Pieters C. M. (1993) Ultraviolet, visible, and near–infrared reflectance spectroscopy: Laboratory spectra of geologic materials. In *Remote Geochemical Analysis* (C. M. Pieters and P. A. J. Englert, eds.), pp. 43–77. Cambridge Univ., Cambridge.

Garozzo M., Fulvio D., Gomis O., Palumbo M. E., and Strazzulla G. (2008) H-implantation in SO_2 and CO_2 ices. *Planet. Space Sci., 56,* 1300–1308.

Geissler P. E., Greenberg R., Hoppa G., McEwen A., Tufts R., Phillips C., Clark B., Ockert–Bell M., Helfenstein P., Burns J., Veverka J., Sullivan R., Greeley R., Pappalardo R. T., Head J. W., Belton M. J. S., and Denk T. (1998) Evolution of lineaments on Europa: Clues from Galileo multispectral imaging observations. *Icarus, 135,* 107–126.

Gerakines P. A., Schutte W. A., Greenberg J. M., and van Dishoeck E. F. (1995) The infrared band strengths of H_2O, CO, and CO_2 in laboratory simulations of astrophysical ice mixtures. *Astron. Astrophys., 296,* 810–818.

Gerakines P. A., Moore M. H., and Hudson R. L. (2000) Carbonic

acid production in H_2O:CO_2 ices — UV photolysis vs. proton bombardment. *Astron. Astrophys., 357,* 793–800.

Gerakines P. A., Moore M. H., and Hudson R. L. (2004) Ultraviolet photolysis and proton irradiation of astrophysical ice analogs containing hydrogen cyanide. *Icarus, 170,* 202–213.

Gerakines P. A., Bray J. J., Davis A., and Richey C. R. (2005) The strengths of near-infrared absorption features relevant to interstellar and planetary ices. *Astrophys. J., 620,* 1140–1150.

Gibb E. L., Whittet D. C. B., Boogert A. C. A., and Tielens A. G. G. M. (2004) Interstellar ice: The Infrared Space Observatory Legacy. *Astrophys. J. Suppl. Ser., 151,* 35–73.

Glagolev V. L., Gordeeva V. A., Zhabrova G. M., and Kadenatsi B. M. (1967) On the radiation decomposition of aluminum and magnesium hydroxides. *High Energy Chem., 1,* 247–248.

Gomis O. and Strazzulla G. (2005) CO_2 production by ion irradiation of H_2O ice on top of carbonaceous material and its relevance to the Galilean satellites. *Icarus, 177,* 570–576.

Gomis O. and Strazzulla G. (2008) Ion irradiation of H_2O ice on top of sulfurous solid residue and its relevance to the Galilean satellites. *Icarus, 194,* 146–152.

Gomis O., Leto G., and Strazzulla G. (2004a) Hydrogen peroxide production by ion irradiation of thin water ice films. *Astron. Astrophys., 420,* 405–410.

Gomis O., Satorre M. A., Strazzulla G., and Leto G. (2004b) Hydrogen peroxide formation by ion implantation in water ice and its relevance to the Galilean satellites. *Planet. Space Sci., 52,* 371–378.

Gradie J., Thomas P., and Veverka J. (1980) The surface composition of Amalthea. *Icarus, 44,* 373–387.

Greenblatt G. D., Orlando J. J., Burkholder J. B., and Ravishankara A. R. (1990) Absorption-measurements of oxygen between 330 nm and 1140 nm. *J. Geophys. Res., 95,* 18577–18582.

Grieves G. A. and Orlando T. M. (2005) The importance of pores in the electron stimulated production of D_2 and O_2 in low temperature ice. *Surface Sci., 593,* 180–186.

Grundy W. M. and Schmitt B. (1998) The temperature-dependent near-infrared absorption spectrum of hexagonal ice. *J. Geophys. Res., 103,* 25809–25822.

Grundy W. M. and Stansberry J. A. (2000) Solar gardening and the seasonal evolution of nitrogen ice on Triton and Pluto. *Icarus, 148,* 340–346.

Grundy W. M., Buie M. W., Stansberry J. A., Spencer J. R., and Schmitt B. (1999) Near-infrared spectra of icy outer solar system surfaces: Remote determination of H_2O ice temperatures. *Icarus, 142,* 536–549.

Grundy W. M., Doute S., and Schmitt B. (2000) A Monte Carlo ray-tracing model for scattering and polarization by large particles with complex shapes. *J. Geophys. Res., 105,* 29291–29314.

Grundy W. M., Young L. A., and Young E. F. (2003) Discovery of CO_2 ice and leading-trailing spectral asymmetry on the uranian satellite Ariel. *Icarus, 162,* 222–229.

Grundy W. M., Young L. A., Spencer J. R., Johnson R. E., Young E. F., and Buie M. W. (2006) Distributions of H_2O and CO_2 ices on Ariel, Umbriel, Titania, and Oberon from IRTF/SpeX observations. *Icarus, 184,* 543–555.

Grundy W. M., Buratti B. J., Cheng A. F., Emery J. P., Lunsford A., McKinnon W. B., Moore J. M., Newman S. F., Olkin C. B., Reuter D. C., Schenk P. M., Spencer J. R., Stern S. A., Throop H. B., Weaver H. A., and the New Horizons Team (2007) New Horizons mapping of Europa and Ganymede. *Science, 318,* 234–237, DOI: 10.1126/science.1147623.

Hage W., Liedl K. R., Hallbrucker A., and Mayer E. (1998) Carbonic acid in the gas phase and its astrophysical relevance. *Science, 279,* 1332–1335.

Hagen W., Tielens A. G. G. M., and Greenberg J. M. (1981) The infrared spectra of amorphous solid water and ice I_c between 10 and 140 K. *Chem. Phys., 56,* 367–379.

Hall D. T., Gladstone G. R., Moos H. W., Bagenal F., Clarke J. T., Feldman P., McGrath M. A., Schneider N. M., Shemansky D. E., Strobel D. F., and Waite J. H. (1994) Extreme ultraviolet Explorer satellite observation of Jupiter's Io plasma torus. *Astrophys. J. Lett., 426,* L51–L54.

Hand K. P. (2007) On the physics and chemistry of the ice shell and sub-surface ocean of Europa. Ph.D. thesis, Stanford University, Stanford, California.

Hand K. P., Chyba C. F., Carlson R. W., and Cooper J. F. (2006) Clathrate hydrates of oxidants in the ice shell of Europa. *Astrobiology, 6,* 463–482, DOI: 10.1089/ast.(2006)6.463.

Hand K. P., Carlson R. W., and Chyba C. F. (2007) Energy, chemical disequilibrium, and geological constraints on Europa. *Astrobiology, 7,* 1006–1022.

Handa Y. P., Klug D. D., and Whalley E. (1988) Energies of phases of ice at low temperature and pressure relative to ice I_h. *Can. J. Chem., 66,* 919–924.

Hansen C. J., Shemansky D. E., and Hendrix A. R. (2005) Cassini UVIS observations of Europa's oxygen atmosphere and torus. *Icarus, 176,* 305–315.

Hansen G. B. and McCord T. B. (2004) Amorphous and crystalline ice on the Galilean satellites: A balance between thermal and radiolytic processes. *J. Geophys. Res., 109,* E01012, 1–19, DOI: 10.1029/2003JE002149.

Hansen G. B. and McCord T. B. (2008) Widespread CO_2 and other non-ice compounds on the anti-Jovian and trailing sides of Europa from Galileo/NIMS observations. *Geophys. Res. Lett., 35,* L01202.

Hapke B. (2001) Space weathering from Mercury to the asteroid belt. *J. Geophys. Res., 106,* 10039–10073.

Hapke B. and Graham F. (1989) Spectral properties of condensed phases of disulfur monoxide, polysulfur oxide, and irradiated sulfur. *Icarus, 79,* 47–55.

Hapke B., Wells E., Wagner J., and Partlow W. (1981) Far-UV, visible, and near-IR reflectance spectra of frosts of H_2O, CO_2, NH_3 and SO_2. *Icarus, 47,* 361–367.

Head J. W. and Pappalardo R. T. (1999) Brine mobilization during lithospheric heating on Europa: Implications for formation of chaos terrain, lenticula texture, and color variations. *J. Geophys. Res., 104,* 27143–27155.

Head J. W., Pappalardo R. T., and Sullivan R. (1999) Europa: Morphological characteristics of ridges and triple bands from Galileo data (E4 and E6) and assessment of a linear diapirism model. *J. Geophys. Res., 104,* 24223–24236.

Hendrix A. R., Barth C. A., Hord C. W., and Lane A. L. (1998) Europa: Disk-resolved ultraviolet measurements using the Galileo ultraviolet spectrometer. *Icarus, 135,* 79–94.

Hendrix A. R., Barth C. A., and Hord C. W. (1999) Ganymede's ozone-like absorber: Observations by the Galileo ultraviolet spectrometer. *J. Geophys. Res., 104,* 14169–14178.

Hendrix A. R., Carlson R. W., Mehlman R., and Smythe W. D. (2002) Europa as measured by Galileo NIMS and UVS (abstract). In *Jupiter after Galileo and Cassini,* p. 108. Observa-

torio Astronomico de Lisboa, Lisbon.
Hendrix A., Carlson R., and Johnson R. E. (2008) Europa's ultraviolet absorption feature: Correlation with endogenic surface features on the trailing hemisphere (abstract). *Bull. Am. Astron. Soc., 40,* Abstract No. 59.07.
Henning T., Il'in V. B., Krivova N. A., Michel B., and Voshchinnikov N. V. (1999) WWW database of optical constants for astronomy. *Astron. Astrophys. Suppl., 136,* 405–406.
Herzberg G. (1945) *Molecular Spectra and Molecular Structure II: Infrared and Raman Spectra of Polyatomic Molecules.* Van Nostrand, Princeton.
Herzberg G. (1950) *Molecular Spectra and Molecular Structure I: Spectra of Diatomic Molecules.* Van Nostrand, Princeton.
Hibbitts C. A. and Szanyi J. (2007) Physisorption of CO_2 on non-ice materials relevant to icy satellites. *Icarus, 191,* 371–380.
Hibbitts C. A., McCord T. B. and Hansen G. B. (2000) The distributions of CO_2 and SO_2 on the surface of Callisto. *J. Geophys. Res., 105,* 22541–22557.
Hibbitts C. A., Klemaszewski J. E., McCord T. B., Hansen G. B., and Greeley R. (2002) CO_2-rich impact craters on Callisto. *J. Geophys. Res., 107,* 14-1 to 14-12, 5084, DOI: 1029/2000JE001412.
Hibbits C. A., Pappalardo R. T., Hansen G. B., and McCord T. B. (2003) Carbon dioxide on Ganymede. *J. Geophys. Res., 108,* 2-1 to 2-21, 5036, DOI: 1029/2002JE001956.
Hinrichs J. I. and Lucey P. G. (2002) Temperature-dependent near-infrared spectral properties of minerals, meteorites, and lunar soil. *Icarus, 155,* 169–180.
Hobbs P. V. (1974) *Ice Physics.* Oxford Univ., London.
Hochanadel C. J., Ghormley J. A., and Sworski T. J. (1955) The decomposition of sulfuric acid by cobalt γ rays. *J. Am. Chem. Soc., 77,* 3215.
Hopkins A. G. and Brown C. W. (1975) Infrared spectrum of sulfur monoxide. *J. Chem. Phys., 62,* 2511–12.
Hopkins A. G., Tang S.-Y., and Brown C. W. (1973) Infrared and Raman spectra of the low-temperature products from discharged sulfur dioxide. *J. Am. Chem. Soc., 95,* 3486–3490.
Hosokawa S., Matsuoka T., and Tamura K. (1994) Optical absorption spectra of liquid sulphur over a wide absorption range. *J. Phys. Condens. Matter, 6,* 5273–5282.
Huang S. and Johnson E. R. (1965) The radiation-induced decomposition of some inorganic sulfates. In *Effects of High Energy Radiation on Inorganic Substances,* pp. 121–138. Special Tech. Publ. No. 400, ASTM, Seattle.
Hudson R. L. and Moore M. H. (2006) infrared spectra and radiation stability of H_2O_2 ices relevant to Europa. *Astrobiology, 6,* 483–489.
Hudson R. L., Moore M. H., and Gerakines P. A. (2001) The formation of cyanate ion (OCN–) in interstellar ice analogs. *Astrophys. J., 550,* 1140–1150.
Hunt G. R. (1977) Spectral signatures of particulate minerals in the visible and near infrared. *Geophysics, 42,* 501–533.
Hunt G. R. and Ashley R. P. (1979) Spectra of altered rocks in the visible and near infrared. *Econ. Geol., 74,* 1613–1629.
Hunt G. R. and Salisbury J. W. (1970) Visible and near-infrared spectra of minerals and rocks: I Silicate minerals. *Mod. Geol., 1,* 283–300.
Hunt G. R., Salisbury J. W., and Lenhoff C. J. (1971a) Visible and near-infrared spectra of minerals and rocks: III. Oxides and hydroxides. *Mod. Geol., 2,* 195–205.
Hunt G. R., Salisbury J. W., and Lenhoff C. J. (1971b) Visible and near-infrared spectra of minerals and rocks: IV. Sulphides and sulphates. *Mod. Geol., 3,* 1–14.
Hunt G. R., Salisbury J. W., and Lenhoff C. J. (1973) Visible and near-infrared spectroscopy of minerals and rocks: VI. Additional silicates. *Mod. Geol., 4,* 85–106.
ICRU (1984) *Stopping Powers for Electrons and Positrons.* ICRU Report 37, International Commission on Radiation Units and Measurements. Available online at http://physics.nist.gov/PhysRefData/Star/Text/ESTAR.html.
Ip W. H. (1996) Europa's oxygen exosphere and its magnetospheric interaction. *Icarus, 120,* 317–325.
Jenniskens P., Blake D. F., and Kouchi A. (1998) Amorphous water ice. In *Solar System Ices* (B. Schmitt et al., eds.), pp. 199–240. Kluwer, Boston.
Johnson R. E. (1990) *Energetic Charged-Particle Interactions with Atmospheres and Surfaces.* Springer-Verlag, Berlin.
Johnson R. E. (1999) Comment on "Laboratory studies of the optical properties and stability of oxygen on Ganymede" by Raul A. Baragiola and David A. Bahr. *J. Geophys. Res., 104,* 14179–14182.
Johnson R. E. (2000) Sodium at Europa. *Icarus, 143,* 429–433.
Johnson R. E. (2001) Surface chemistry in the jovian magnetosphere radiation environment. In *Chemical Dynamics in Extreme Environments* (R. A. Dressler, ed.), World Scientific, Singapore.
Johnson R. E. and Jesser W. A. (1997) O_2/O_3 microatmospheres in the surface of Ganymede. *Astrophys. J. Lett., 480,* L79–L82.
Johnson R. E. and Quickenden T. I. (1997) Photolysis and radiolysis of water ice on outer solar system bodies. *J. Geophys. Res., 102,* 10985–10996.
Johnson R. E., Nelson M. L., McCord T. B., and Gradie J. C. (1988) Analysis of Voyager images of Europa — Plasma bombardment. *Icarus, 75,* 423–436.
Johnson R. E., Leblanc F., Yakshinskiy B. V., and Madey T. E. (2002) Energy distributions for desorption of sodium and potassium from ice: The Na/K ratio at Europa. *Icarus, 156,* 136–142.
Johnson R. E., Quickenden T. I., Cooper P. D., McKinley A., and Freeman C. G. (2003) The production of oxidants in Europa's surface. *Astrobiology, 3,* 823–850.
Johnson R. E., Carlson R. W., Cooper J. F., Paranicas C., Moore M. H., and Wong M. (2004) Radiation effects on the surfaces of the Galilean satellites. In *Jupiter: The Planets, Satellites and Magnetosphere* (F. Bagenal et al., eds.), pp. 485–512. Cambridge Univ., Cambridge.
Johnson R. E., Cooper P. D., Quickenden T. I., Grieves G. A., and Orlando T. M. (2005) Production of oxygen by electronically induced dissociations in ice. *J. Chem. Phys., 123,* 184715-1-8.
Johnson T. V. (1970) Albedo and spectral reflectivity of the Galilean satellites of Jupiter. Ph.D. thesis, California Institute of Technology, Pasadena.
Johnson T. V. (1971) Galilean satellites: Narrowband photometry 0.3–1.1 microns. *Icarus, 14,* 94–111.
Johnson T. V. and McCord T. B. (1970) Galilean satellites: The spectral reflectivity 0.30–1.10 microns. *Icarus, 13,* 37–42.
Johnson T. V. and McCord T. B. (1971) Spectral geometric albedo of the Galilean satellites 0.3–2.5 microns. *Astrophys. J., 169,* 589–593.
Johnson T. V. and Pilcher C. B. (1977) Satellite spectrophotometry and surface compositions. In *Planetary Satellites* (J. A. Burns, ed.), pp. 232–268. Univ. of Arizona, Tucson.

Johnson T. V., Soderblom L. A., Mosher J. A., Danielson G. E., Cook A. F., and Kupferman P. (1983) Global multispectral mosaics of the icy galilean satellites. *J. Geophys. Res., 88,* 5789–5805.

Jones A. V. (1950) Infra-red and ultraviolet spectra of sulfur monoxide. *J. Chem. Phys., 18,* 1263–1268.

Kargel J. S., Kaye J., Head J. W. I., Marion G., Sassen R., Crowley J., Prieto O., and Hogenboom D. (2000) Europa's crust and ocean: Origin, composition, and prospects for life. *Icarus, 94,* 368–390.

Kerkhof O., Schutte W. A., and Ehrenfreund P. (1999) The infrared band strengths of CH_3OH, NH_3 and CH_4 in laboratory simulations of astrophysical ice mixtures. *Astron. Astrophys., 346,* 990–994.

Khare B. N., Sagan C., Thompson W. R., Arakawa E. T., Meisse C., and Tuminello P. S. (1994) Optical properties of poly-HCN and their astronomical applications. *Can. J. Chem., 72,* 678–694.

Khriachtchev L., Pettersson M., Tuominen S., and Rasanen M. (1997) Photochemistry of hydrogen peroxide in solid argon. *J. Chem. Phys., 107,* 7252–7259.

Kieffer H. H. (1970) Spectral reflectance of CO_2-H_2O frosts. *J. Geophys. Res., 75,* 501–509.

Kieffer H. H. and Smythe W. D. (1974) Frost spectra: Comparison with Jupiter's satellites. *Icarus, 21,* 506–512.

Kissel J. and Krueger F. R. (1987) Ion formation by impact of fast dust particles and comparison with related techniques. *Appl. Phys. A., 42,* 69–85.

Kouchi A. (1987) Vapor-pressure of amorphous H_2O ice and its astrophysical implications. *Nature, 330,* 550–552.

Kouchi A. and Kuroda T. (1990) Amorphization of cubic ice by ultraviolet-irradiation. *Nature, 344,* 134–135.

Kouchi A., Yamamoto T., Kozasa T., Kuroda T., and Greenberg J. M. (1994) Conditions for condensation and preservation of amorphous ice and crystallinity of astrophysical ices. *Astron. Astrophys., 290,* 1009–1018.

Krasnopolsky V. A. (1987) S_3 and S_4 absorption cross sections in the range of 340 to 600 nm and evaluation of the S_3 abundance in the lower atmosphere of Venus. *Adv. Space. Res., 7,* (12)25–(12)27.

Kruger H., Geissler P., Horanyi M., Graps A. L., Kempf S., Srama R., Moragas-Klostermeyer G., Moissl R., Johnson T. V., and Grun E. (2003) Jovian dust streams: A monitor of Io's volcanic plume activity. *Geophys. Res. Lett., 30,* 3-1 to 3-4.

Kuiper G. P. (1957) Infrared observations of planets and satellites (abstract). *Astron. J., 62,* 245.

Kuppers M. and Schneider N. M. (2000) Discovery of chlorine in the Io torus. *Geophys. Res. Lett., 27,* 513–516.

Landau A., Allin E. J., and Welsh H. L. (1962) The absorption spectrum of solid oxygen in the wavelength region from 12,000 Å to 3300 Å. *Spectrochim. Acta., 18,* 1–19.

Lane A. L., Nelson R. M., and Matson D. L. (1981) Evidence for sulfur implantation in Europa's UV absorption band. *Nature, 292,* 38–39.

Lange M. A. and Ahrens T. J. (1987) Impact experiments in low-temperature ice. *Icarus, 69,* 506–518.

Leblanc F., Johnson R. E., and Brown M. E. (2002) Europa's sodium atmosphere: An ocean source? *Icarus, 159,* 132–144.

Leblanc F., Potter A. E., Killen R. M., and Johnson R. E. (2005) Origins of Europa Na cloud and torus. *Icarus, 178,* 367–385.

Lebofsky L. A. and Fegley M. B. Jr. (1976) Laboratory reflection spectra for the determination of chemical composition of icy bodies. *Icarus, 28,* 379–387.

Lebofsky L. A. and Feierberg M. A. (1985) 2.7-μm to 4.1-μm spectrophotometry of icy satellites of Saturn and Jupiter. *Icarus, 63,* 237–242.

Leto G. and Baratta G. A. (2003) Ly-α photon induced amorphization of I_c water ice at 16 Kelvin. Effects and quantitative comparison with ion irradiation. *Astron. Astrophys., 397,* 7–13.

Leto G., Gomis O., and Strazzulla G. (2005) The reflectance spectrum of water ice: Is the 1.65 μm peak a good temperature probe? *Mem. Soc. Astron. Ital. Suppl., 6,* 57–62.

Loeffler M. J. and Baragiola R. A. (2005) The state of hydrogen peroxide on Europa. *Geophys. Res. Lett., 32,* L17202 1–4.

Loeffler M. J., Raut U., and Baragiola R. A. (2006a) Enceladus: A source of nitrogen and an explanation for the water vapor plume observed by Cassini. *Astrophys. J. Lett., 649,* L133–L136.

Loeffler M. J., Raut U., Vidal R. A., Baragiola R. A., and Carlson R. W. (2006b) Synthesis of hydrogen peroxide in water ice by ion irradiation. *Icarus, 180,* 265–273.

Loeffler M. J., Teolis B. D., and Baragiola R. A. (2006c) Decomposition of solid amorphous hydrogen peroxide by ion irradiation. *J. Chem. Phys., 124,* DOI: 10470210.1063/1.2171967.

Loeffler M. J., Teolis B. D., and Baragiola R. A. (2006d) A model study of the thermal evolution of astrophysical ices. *Astrophys. J. Lett., 639,* L103–L106.

Long C. A. and Ewing G. E. (1973) Spectroscopic investigation of van der waals molecules. 1. Infrared and visible spectra of $(O_2)_2$. *J. Chem. Phys., 58,* 4824–4834.

Long C. and Kearns D. R. (1973) Selection-rules for intermolecular enhancement of spin forbidden transitions in molecular-oxygen. *J. Chem. Phys., 59,* 5729–5736.

Lowenthal M. S., Khanna R. K., and Moore M. H. (2002) Infrared spectrum of solid isocyanic acid (HNCO): Vibrational assignments and integrated band intensities. *Spectrochim. Acta A., 58,* 73–78.

Marion G. M. (2002) A molal-based model for strong acid chemistry at low temperatures (187 to 298 K). *Geochim. Cosmochim. Acta, 66,* 2499–2516.

Marion G. M. and Kargel J. S. (2008) *Cold Aqueous Planetary Geochemistry with FREZCHEM.* Springer-Verlag, Berlin.

Mastrapa R. M. E. and Brown R. H. (2006) Ion irradiation of crystalline H_2O-ice: Effect on the 1.65-μm band. *Icarus, 183,* 207–214.

Mastrapa R. M. and Sandford S. A. (2008) New optical constants of amorphous and crystalline ice, 3–20 micrometers. *Eos Trans. AGU, 89,* Fall Meet. Suppl., Abstract MR13A-1700.

Mastrapa R. M., Bernstein M. P., Sandford S. A., Roush T. L., Cruikshank D. P., and Ore C. M. D. (2008) Optical constants of amorphous and crystalline H_2O-ice in the near infrared from 1.1 to 2.6 μm. *Icarus, 97,* 307–320.

Mauk B. H., Mitchell D. G., Krimigis S. M., Roelof E. C., and Paranicas C. P. (2003) Energetic neutral atoms from a trans-Europa gas torus at Jupiter. *Nature, 421,* 920–922.

Mayer E. (1985) New method for vitrifying water and other liquids by rapid cooling of their aerosols. *J. Appl. Phys., 58,* 663–667.

McCord T. B., Carlson R. W., Smythe W. D., Hansen G. B., Clark R. N., Hibbitts C. A., Fanale F. P., Granahan J. C., Segura M., Matson D. L., Johnson T. V., and Martin P. D. (1997) Organics and other molecules in the surfaces of Callisto and Ganymede. *Science, 278,* 271–275.

McCord T. B., Hansen G. B., Clark R. N., Martin P. D., Hibbits

C. A., Fanale F. P., Granahan J. C., Segura M., Matson D. L., Johnson T. V., Carlson R. W., Smythe W. D., Danielson G. E., and the NIMS Team (1998a) Non-water-ice constituents in the surface material of the icy Galilean satellites from the Galileo near infrared mapping spectrometer investigation. *J. Geophys. Res., 103,* 8603–8626.

McCord T. B., Hansen G. B., Fanale F. P., Carlson R. W., Matson D. L., Johnson T. V., Smythe W. D., Crowley J. K., Martin P. D., Ocampo A., Hibbitts C. A., and Granahan J. C. (1998b) Salts an Europa's surface detected by Galileo's Near Infrared Mapping Spectrometer. *Science, 280,* 1242–1245.

McCord T. B., Hansen G. B., Matson D. L., Johnson T. V., Crowley J. K., Fanale F. P., Carlson R. W., Smythe W. D., Martin P. D., Hibbitts C. A., Granahan J. C., Ocampo A., and the NIMS Team (1999) Hydrated salt minerals on Europa's surface from the Galileo NIMS investigation. *J. Geophys. Res., 104,* 11827–11851.

McCord T. B., Orlando T. M., Teeter G., Hansen G. B., Sieger M. T., Petrik N. K., and Van Keulen L. (2001) Thermal and radiation stability of the hydrated minerals epsomite, mirabilite, and natron under Europa environmental conditions. *J. Geophys. Res., 106,* 3311–3319.

McCord T. B., Teeter G., Hansen G. B., Sieger M. T., and Orlando T. M. (2002) Brines exposed to Europa surface conditions. *J. Geophys. Res., 107,* 4-1 to 4-6.

McEwen A. S. (1986) Exogenic and endogenic albedo and color patterns on Europa. *J. Geophys. Res., 91,* 8077–8097.

McFadden L. A., Bell J. F., and McCord T. B. (1980) Visible spectral reflectance measurements (0.33–1.1 μm) of the Galilean satellites at many orbital phase angles. *Icarus, 44,* 410–430.

McGrath M. A., Lellouch E., Strobel D. F., Feldman P. D., and Johnson R. E. (2004) Satellite atmospheres. In *Jupiter: The Planet, Satellites, and Magnetosphere* (F. Bagenal et al., eds.), pp. 457–483. Cambridge Univ., Cambridge.

McKinnon W. B. and Zolensky M. E. (2003) Sulfate content of Europa's ocean and shell: Evolutionary considerations and some geological and astrobiological implications. *Astrobiology, 3,* 879–897.

McNutt R. L. (1993) Possible in situ detection of K^{2+} in the jovian magnetosphere. *J. Geophys. Res., 98,* 21221–21229.

Mennella V., Palumbo M. E., and Baretta G. A. (2004) Formation of CO and CO_2 molecules by ion irradiation of water ice-covered hydrogenated carbon grains. *Astrophys. J., 615,* 1073–1080.

Meyer B. and Stroyer-Hansen T. (1972) Infrared spectrum of S_4. *J. Phys. Chem., 76,* 3968–3969.

Meyer B., Oommen T. V., and Jensen D. (1971) The color of liquid sulfur. *J. Phys. Chem., 75,* 912–917.

Meyer B., Stroyer-Hansen T., and Oommen T. V. (1972) The visible spectrum of S_3 and S_4. *J. Molec. Spectrosc., 42,* 335–343.

Mills F. P. and Brown M. E. (2000) Thermal infrared spectroscopy of Europa and Callisto. *J. Geophys. Res., 105,* 15051–15059.

Moore J. M., Asphaug E., Morrison D., Spencer J. R., Chapman C. R., Bierhaus B., Sullivan R. J., Chuang F. C., Klemaszewski J. E., Greeley R., Bender K. C., Geissler P. E., Helfenstein P., and Pilcher C. B. (1999) Mass movement and landform degradation on the icy Galilean satellites: Results of the Galileo nominal mission. *Icarus, 140,* 294–312.

Moore M. H. (1984) Studies of proton-irradiated SO_2 at low-temperatures — Implications for Io. *Icarus, 59,* 114–128.

Moore M. H. and Hudson R. L. (1992) Far-infrared spectral studies of phase changes in water ice induced by proton irradiation. *Astrophys. J., 401,* 353–360.

Moore M. H. and Hudson R. L. (1998) Infrared study of ion-irradiated water-ice mixtures with hydrocarbons relevant to comets. *Icarus, 135,* 518–527.

Moore M. H. and Hudson R. L. (2000) IR detection of H_2O_2 at 80 K in ion-irradiated laboratory ices relevant to Europa. *Icarus, 145,* 282–288.

Moore M. H. and Khanna R. K. (1991) Infrared and mass spectral studies of proton irradiated $H_2O + CO_2$ ice: Evidence for carbonic acid. *Spectrochim. Acta, 47A,* 255–262.

Moore M. H., Khanna R., and Donn B. (1991) Studies of proton irradiated $H_2O + CO_2$ and $H_2O + CO$ ices and analysis of synthesized molecules. *J. Geophys. Res., 96,* 17541–17545.

Moore M. H., Ferrante R. F., and Nuth J. A. (1996) Infrared spectra of proton irradiated ices containing methanol. *Planet. Space Sci., 44,* 927–935.

Moore M. H., Hudson R. L., and Ferrante R. F. (2003) Radiation products in processed ices relevant to Edgeworth-Kuiper-belt objects. *Earth Moon Planets, 92,* 291–306.

Moore M. H., Hudson R. L., and Carlson R. W. (2007) The radiolysis of SO_2 and H_2S in water ice: Implications for the icy jovian satellites. *Icarus, 189,* 409–423.

Moroz V. I. (1965) Infrared spectrophotometry of satellites: The Moon and the Galilean satellites of Jupiter. *Astron. Zh., 42,* 1287, trans. in *Soviet Astron.–AJ, 9,* 999–1006.

Morris R. V., Lauer H. V. Jr., Lawson C. A., Gibson E. K. Jr., Nace G. A., and Stewart C. (1985) Spectral and other physicochemical properties of submicron powders of hematite (α-Fe_2O_3), maghemite (γ-Fe_2O_3), magnetite (Fe_3O_4), goethite (α-FeOOH), and lepidocrocite (γ-FeOOH). *J. Geophys. Res., 90,* 3126–3144.

Morris R. V., Golden D. C., Bell J. F., Lauer H. V., and Adams J. B. (1993) Pigmenting agents in martian soils — inferences from spectral, Mossbauer, and magnetic-properties of nanophase and other iron-oxides in Hawaiian palagonitic soil PN-9. *Geochim. Cosmochim. Acta, 57,* 4597–4609.

Morris R. V., Golden D. C., and Bell J. F. III (1997) Low-temperature reflectivity spectra of red hematite and the color of Mars. *J. Geophys. Res., 102,* 9125–9133.

Morris R. V., Golden D. C., Bell J. F., Shelfer T. D., Scheinost A. C., Hinman N. W., Furniss G., Mertzman S. A., Bishop J. L., Ming D. W., Allen C. C., and Britt D. T. (2000) Mineralogy, composition, and alteration of Mars Pathfinder rocks and soils: Evidence from multispectral, elemental, and magnetic data on terrestrial analogue, SNC meteorite, and Pathfinder samples. *J. Geophys. Res., 105,* 1757–1817.

Morrison D. and Burns J. A. (1976) The jovian satellites. In *Jupiter* (T. Gehrels, ed.), pp. 991–1034. Univ. of Arizona, Tucson.

Mozumder A. (1999) *Fundamentals of Radiation Chemistry.* Academic, San Diego.

Na C. Y., Trafton L. M., Barker E. S., and Stern S. A. (1998) A search for new species in Io's extended atmosphere. *Icarus, 131,* 449–452.

Nash D. B. and Fanale F. P. (1977) Io's surface composition based on reflectance spectra of sulfur/salt mixtures and proton irradiation experiments. *Icarus, 31,* 40–80.

Nelson M. L., McCord T. B., Clark R. N., Johnson T. V., Matson D. L., Mosher J. A., and Soderblom L. A. (1986) Europa: Characterization and interpretation of global spectral surface units. *Icarus, 65,* 129–151.

Nelson R. M. and Hapke B. W. (1978) Spectral reflectivities of the Galilean satellites and Titan, 0.32 to 0.86 micrometers. *Icarus, 36,* 304–329.

Nelson R. M. and Lane A. L. (1987) Planetary satellites. In *Scientific Accomplishments of IUE* (Y. Kondo, ed.), pp. 67–99. Reidel, Dordrecht.

Nelson R. M., Lane A. L., Matson D. L., Veeder G. J., Buratti B. J., and Tedesco E. F. (1987) Spectral geometric albedos of the Galilean satellites from 0.24 to 0.34 micrometers: Observations with the International Ultraviolet Explorer. *Icarus, 72,* 358–380.

Nelson R. M., Smythe W. D., Hapke B. W. and Cohen A. J. (1990) On the effect of X-rays on the color of elemental sulfur: Implications for Jupiter's satellite Io. *Icarus, 85,* 326–334.

Nimmo F. and Gaidos E. (2002) Strike-slip motion and double ridge formation on Europa. *J. Geophys. Res., 107,* Article No. 5021.

Nimmo F., Pappalardo R., and Cuzzi J. (2007) Observational and theoretical constraints on plume activity at Europa. AGU Fall Meeting, Abstract #P51E-05.

Nishijima C., Kanamuru N., and Titmura K. (1976) Primary photochemical processes of sulfur in solution. *Bull. Chem. Soc. Japan., 49,* 1151–1152.

Nna-Mvondo D., Khare B., Ishihara T. and McKay C. P. (2008) Experimental impact shock chemistry on planetary icy satellites. *Icarus, 194,* 816–829. DOI: 10.1016/j.icarus.(2007)11.001.

Noll K. S. and Knacke R. F. (1993) Titan: 1–5 μm photometry and spectrophotometry and a search for variability. *Icarus, 101,* 272–281.

Noll K. S., Weaver H. A., and Gonnella A. M. (1995) The albedo spectrum of Europa from 2200 angstrom to 3300 angstrom. *J. Geophys. Res., 100,* 19057–19059.

Noll K. S., Johnson R. E., Lane A. L., Domingue D. L., and Weaver H. A. (1996) Detection of ozone on Ganymede. *Science, 273,* 341–343.

Noll K. S., Roush T. L., Cruikshank D. P., Johnson R. E., and Pendleton Y. J. (1997) Detection of ozone on Saturn's satellites Rhea and Dione. *Nature, 388,* 45–47.

O'Donnell J. H. and Sangster D. F. (1970) *Principles of Radiation Chemistry.* American Elsevier, New York.

Ockert M. E., Nelson R. M., Lane A. L., and Matson D. L. (1987) Europa's ultraviolet absorption band (260 to 320 nm): Temporal and spatial evidence from IUE. *Icarus, 70,* 499–505.

Ockman N. (1958) The infra-red and Raman spectra of ice. *Philos. Mag. Suppl., 7,* 199–220.

Ohtaki H. and Radnai T. (1993) Structure and dynamics of hydrated ions. *Chem. Rev., 93,* 1157–1204.

Onaka R. and Takahashi T. (1968) Vacuum UV absorption of liquid water and ice. *J. Phys. Soc. Japan., 24,* 548–550.

Orlando T. M. and Sieger M. T. (2003) The role of electron-stimulated production of O_2 from water ice in the radiation processing of outer solar system surfaces. *Surf. Sci., 528,* 1–7.

Orlando T. M., McCord T. B., and Grieves G. A. (2005) The chemical nature of Europa surface material and the relation to a subsurface ocean. *Icarus, 177,* 528–533.

Palumbo M. E. (1997) Production of CO and CO_2 after ion irradiation of ices. *Adv. Space. Res., 20,* 1637–1645.

Palumbo M. E. (2006) Formation of compact solid water after ion irradiation at 15 K. *Astron. Astrophys., 453,* 903–909.

Palumbo M. E., Baratta G. A., Brucato J. R., Castorina A. C., Satorre M. A., and Strazzulla G. (1998) Profile of the CO_2 bands produced after ion irradiation of ice mixtures. *Astron. Astrophys., 334,* 247–252.

Paranicas C., Carlson R. W., and Johnson R. E. (2001) Electron bombardment of Europa. *Geophys. Res. Lett., 28,* 673–676.

Paranicas C. P., Vollmer M., and Kivelson M. G. (2002) Flow diversion at Europa. AGU Spring Meeting, Abstract #P21B-07.

Paterson W. R., Frank L. A., and Ackerson K. L. (1999a) Galileo plasma observations at Europa: Ion energy spectra and moments. *J. Geophys. Res., 104,* 22779–22791.

Paterson W. R., Frank L. A., and Ackerson K. L. (1999b) Galileo plasma observations at Europa: Ion energy spectra and moments. *J. Geophys. Res., 104,* 22779–227791.

Pauling L. (1935) The structure and entropy of ice and other crystals with some randomness of atomic arrangement. *J. Am. Chem. Soc., 57,* 2680–2684.

Pearl J., Hanel R., Kunde V., Maguire W., Fox K., Gupta S., Ponnamperuma C., and Raulin F. (1979) Identification of gaseous SO_2 and new upper limits for other gases on Io. *Nature, 280,* 755–758.

Peterson R. C. and Wang R. Y. (2006) Crystal molds on Mars: Melting of a possible new mineral species to create martian chaotic terrain. *Geology, 34,* 957–960. 10.1130/g22678a.1

Phillips C. B. and Chyba C. F. (2001) Impact gardening rates on Europa: Comparison with sputtering. In *Lunar and Planetary Science XXXII,* Abstract #2111. Lunar and Planetary Institute, Houston (CD-ROM).

Phillips C. B. and Chyba C. F. (2004) Impact gardening, sputtering, mixing, and surface–subsurface exchange on Europa. In *Workshop on Europa's Icy Shell,* pp. 70–71. LPI Contribution No. 1195, Lunar and Planetary Institute, Houston.

Phillips L. F., Smith J. J., and Meyer B. (1969) The ultraviolet spectra of matrix isolated disulfur monoxide and sulfur dioxide. *J. Molec. Spectrosc., 29,* 230–243.

Pilcher C. B., Ridgeway S. T., and McCord T. B. (1972) Galilean satellites: Identification of water frost. *Science, 178,* 1087–1089.

Pipes J. G., Browell E. V., and Anderson R. C. (1974) Reflectance of amorphous-cubic NH_3 frosts and amorphous-hexagonal frosts at 77 K from 1400 to 3000 A. *Icarus, 21,* 283–291.

Pollack J. B., Witteborn F. C., Erickson E. F., Strecker D. W., Baldwin B. J., and Bunch T. E. (1978) Near-infrared spectra of the Galilean satellites: Observations and compositional implications. *Icarus, 36,* 271–303.

Porco C. C., West R. A., McEwen A., Genio A. D. D., Ingersoll, A. P., Thomas P., Squyres S., Dones L., Murray C. D., Johnson T. V., Burns J. A., Brahic A., Neukum G., Veverka J., Barbara J. M., Denk T., Evans M., Ferrier J. J., Geissler P., Helfenstein P., Roatsch T., Throop H., Tiscareno M., and Vasavada A. R. (2003) Cassini imaging of Jupiter's atmosphere, satellites, and rings. *Science, 299,* 1541–1547.

Pospieszalska M. K. and Johnson R. E. (1989) Magnetospheric ion-bombardment profiles of satellites — Europa and Dione. *Icarus, 78,* 1–13.

Postberg F., Kempf S., Srama R., Green S. F., Hillier J. K., McBride N., and Grun E. (2006) Composition of jovian dust stream particles. *Icarus, 183,* 122–134. DOI: 10.1016/j.icarus.(2006)02.001.

Prieto-Ballesteros O., Kargel J. S., Fernandez-Sampedro M., Selsis F., Martinez E. S., and Hogenboom D. L. (2005) Evaluation of the possible presence of clathrate hydrates in Europa's icy shell or seafloor. *Icarus,* 491–505.

Prinn R. G. and Fegley B. (1981) Kinetic inhibition of CO and N_2 reduction in circumplanetary nebulae — Implications for satellite compositions. *Astrophys. J., 249,* 308–317.

Prinn R. G. and Fegley B. Jr. (1989) Origin of planetary, satellite, and cometary volatiles. In *Origin and Evolution of Planetary and Satellite Atmospheres* (S. K. Atreya et al., eds.), pp. 8–136. Univ. of Arizona, Tucson.

Prockter L. M., Head J. W., Pappalardo R. T., Sullivan R. J., Clifton A. E., Giese B., Wagner R., and Neukum G. (2002) Morphology of europan bands at high resolution: A mid-ocean ridge-type rift mechanism. *J. Geophys. Res., 107,* DOI: 10.1029/2000JE001458.

Raunier S., Chiavassa T., Allouche A., Marinelli F., and Aycard J.-P. (2003) Thermal reactivity of HNCO with water ice: An infrared and theoretical study. *Chem. Phys., 288,* 197–210.

Raut U., Loeffler M. J., Vidal R. A., and Baragiola R. A. (2004) The OH stretch infrared band of water and its temperature and radiation dependence. In *Lunar and Planetary Science XXXV,* Abstract #1922. Lunar and Planetary Institute, Houston (CD-ROM).

Raut U., Loeffler M. J., Teolis B. D., Vidal R. A., and Baragiola R. A. (2005) Radiation synthesis of carbon dioxide in ice coated grains (abstract). *Bull. Am. Astron. Soc., 37,* 755.

Raut U., Teolis B. D., Loeffler M. J., Vidal R. A., Fama M., and Baragiola R. A. (2007) Compaction of microporous amorphous solid water by ion irradiation. *J. Chem. Phys., 126,* 244511.

Reimann C. T., Boring J. W., Johnson R. E., Garrett J. W., Farmer K. R., and Brown W. L. (1984) Ion induced molecular ejection from D_2O ice. *Surf. Sci., 147,* 227.

Riley J., Hoppa G. V., Greenberg R., and Tufts B. R. (2000) Distribution of chaotic terrain on Europa. *J. Geophys. Res., 105,* 22599–22615.

Robinson G. W. (1967) Intensity enhancement of forbidden electronic transitions by weak intermolecular interactions. *J. Chem. Phys., 46,* 572–585.

Rossman G. R. (1975) Spectroscopic and magnetic studies of ferric iron hydroxy sulfates: Intensification of color in ferric iron clusters bridged by a single hydroxide ion. *Am. Mineral., 60,* 698–704.

Rothschild W. G. (1964) γ-ray decomposition of pure liquid sulfur dioxide. *J. Am. Chem. Soc., 86,* 1307–1309.

Sack N. J. and Baragiola R. A. (1993) Sublimation of vapor-deposited water ice below 170 K and its dependence on growth conditions. *Phys. Rev. B, 48,* 9973–9978.

Sack N. J., Johnson R. E., Boring J. W., and Baragiola R. A. (1992) The effect of magnetospheric ion bombardment on the reflectance of Europa's surface. *Icarus, 100,* 534–540.

Sack N. J., Baragiola R. A., and Johnson R. E. (1993) Effect of plasma ion bombardment on the reflectance of Io's trailing and leading hemispheres. *Icarus, 104,* 152–154.

Sandford S. A. and Allamandola L. J. (1990) The physical and infrared spectral properties of CO_2 in astrophysical ice analogs. *Astrophys. J., 355,* 357–372.

Sasaki T., Williams R. S., Wong J. S., and Shirley D. A. (1978) Radiation damage studies by X-ray photoelectron spectroscopy. I. Electron irradiated $LiNO_3$ and Li_2SO_4. *J. Chem. Phys., 68,* 2718–2724.

Saur J., Strobel D. F., and Neubauer F. M. (1998) Interaction of the jovian magnetosphere with Europa: Constraints on the neutral atmosphere. *J. Geophys. Res., 103,* 19947–19962.

Scattergood T. W., McKay C. P., Borucki W. J., Giver L. P., Vanghyseghem H., Parris J. E., and Miller S. L. (1989) Production of organic-compounds in plasmas — A comparison among electric-sparks, laser-induced plasmas, and uv-light. *Icarus, 81,* 413–428.

Schaefer L. and Fegley B. (2004) A thermodynamic model of high temperature lava vaporization on Io. *Icarus, 169,* 216–241.

Schaefer L. and Fegley B. Jr. (2005) Predicted abundances of carbon compounds in volcanic gases on Io. *Icarus, 618,* 1079–1085.

Schmitt B., de Bergh C., Lellouch E., Maillard J.-P., Barbe A., and Doute S. (1994) Identification of three absorption bands in the 2-μm spectrum of Io. *Icarus, 111,* 79–105.

Schmitt B., Quirica E., Trotta F., and Grundy W. M. (1998) Optical properties of ices from the UV to infrared. In *Solar System Ices* (B. Schmitt et al., eds.), pp. 199–240. Kluwer, Dordrecht.

Schriever R., Chergui M., and Schwentner N. (1991) Cage effect on the photodissociation of H_2O in Xe matrices. *J. Phys. Chem., 95,* 6124–6128.

Schriver A., Schriver L., and Perchard J. P. (1988) Infrared matrix isolation studies of complexes between water and sulfur dioxide: Identification and structure of the 1:1, 1:2, and 2:1 species. *J. Molec. Spectrosc., 127,* 125–142.

Schriver-Mazzuoli L., Chaabouni H., and Schriver A. (2003a) Infrared spectra of SO_2 and SO_2: H_2O ices at low temperature. *J. Mol. Struct., 644,* 151–164.

Schriver-Mazzuoli L., Schriver A., and Chaabouni H. (2003b) Photo-oxidation of SO_2 and of SO_2 trapped in amorphous water ice studied by IR spectroscopy: Implications for Jupiter's satellite Europa. *Can. J. Phys., 81,* 301–309.

Schubert G., Anderson J. D., Spohn T., and McKinnon W. B. (2004) Interior composition, structure, and dynamics of the Galilean satellites. In *Jupiter: The Planet, Satellites and Magnetosphere* (F. Bagenal et al., eds.), pp. 281–306. Cambridge Univ., Cambridge.

Shi M., Baragiola R. A., Grosjean D. E., Johnson R. E., Jurac S., and Schou J. (1995) Sputtering of water ice surfaces and the production of extended neutral atmospheres. *J. Geophys. Res., 100,* 26387–26395.

Shirley J. H., Carlson R. W., and Anderson M. S. (1999) Upper limits for sodium and magnesium hydroxides on Europa (abstract). *Eos Trans. AGU, 80,* F604.

Shoemaker E. M. and Wolfe R. F. (1982) Cratering time scales for the Galilean satellites. In *Satellites of Jupiter* (D. Morrison, ed.), pp. 277–339. Univ. of Arizona, Tucson.

Shoemaker E. M., Lucchitta B. K., Wilhems D. E., Plescia J. B., and Squyres S. W. (1982) The geology of Ganymede. In *The Satellites of Jupiter* (D. Morrison, ed.), pp. 435–520. Univ. of Arizona, Tucson.

Sieger M. T., Simpson W. C. and Orlando T. M. (1998) Production of O_2 on icy satellites by electronic excitation of low-temperature water ice. *Nature, 394,* 554–556.

Sill G. T. and Clark R. N. (1982) Composition of the surfaces of the Galilean satellites. In *Satellites of Jupiter* (D. Morrison, ed.), pp. 174–212. Univ. of Arizona, Tucson.

Smythe W. D., Carlson R. W., Ocampo A., Matson D., Johnson T. V., McCord T. B., Hansen G. E., Soderblom L. A., and Clark R. N. (1998) Absorption bands in the spectrum of Europa detected by the Galileo NIMS instrument. In *Lunar and Planetary Science XXIX,* Abstract #1532. Lunar and Planetary Institute, Houston (CD-ROM).

Spencer J. R. (1987a) The surfaces of Europa, Ganymede, and Callisto: An investigation using Voyager IRIS thermal infra-

red spectra. Ph.D. thesis, University of Arizona, Tucson.
Spencer J. R. (1987b) Thermal segregation of water ice on the galilean satellites. *Icarus, 69,* 297–313.
Spencer J. R. and Calvin W. M. (2002) Condensed O_2 on Europa and Callisto. *Astron. J., 124,* 3400–3403.
Spencer J. R., Calvin W. M., and Person M. J. (1995) Charge-coupled-device spectra of the galilean satellites: Molecular-oxygen on Ganymede. *J. Geophys. Res., 100,* 19049–19056.
Spencer J. R., Tampari L. K., Martin T. Z., and Travis L. D. (1999) Temperatures on Europa from Galileo photopolarimeter-radiometer: Nighttime thermal anomolies. *Science, 284,* 1514–1516.
Spencer J. R., Carlson R. W., Becker T. L., Blue J. S. (2004) Maps and spectra of Jupiter and the Galilean satellites. In *Jupiter: The Planet, Satellites and Magnetosphere* (F. Bagenal et al., eds.), pp. 689–698. Cambridge Univ., Cambridge.
Spencer J. R., Grundy W. M., Dumas C., Carlson R. W., and McCord T. B. (2005) The nature of Europa's non-ice surface components: High spatial and spectral resolution spectroscopy from the Keck telescope. *Icarus, 182,* 202–210.
Spinks J. W. T. and Woods R. J. (1990) *An Introduction to Radiation Chemistry.* Wiley and Sons, New York.
Spitsyn V. I., Mikhailenko I. E., and Morozova T. V. (1969) Use of infrared spectroscopy for studying the change in the nature of the bond in the SO_4^{2-} ion of the radioactive sulfates of some group I and II elements. *Dokl. Phys. Chem., 186,* 358–361.
Steudel R. and Eckert B. (2003) Solid sulfur allotropes. *Topics Curr. Chem., 230,* 1–79.
Steudel R. and Steudel Y. (2004) The thermal decomposition of S_2O forming SO_2, S_3, S_4, and S_5O — An ab initio MO study. *Eur. J. Inorg. Chem., 2004,* 3513–3521.
Steudel R., Holdt G., and Young A. T. (1986) On the colors of Jupiter's satellite Io: Irradiation of solid sulfur at 77 K. *J. Geophys. Res., 91,* 4971–4977.
Strazzulla G. and Moroz L. (2005) Ion irradiation of asphaltite as an analogue of solid hydrocarbons in the interstellar medium. *Astron. Astrophys., 434,* 593–598.
Strazzulla G., Baratta G. A., Leto G., and Foti G. (1992) Ion-beam-induced amorphization of crystalline water ice. *Europhys. Lett., 18,* 517–522.
Strazzulla G., Castorina A. C., and Palumbo M. E. (1995) Ion irradiation of astrophysical ices. *Planet. Space Sci., 43,* 1247–1251.
Strazzulla G., Leto G., Spinella F., and Gomis O. (2005) Production of oxidants by ion irradiation of water/carbon dioxide frozen mixtures. *Astrobiology, 5,* 612–621.
Strazzulla G., Baratta G. A., and Gomis O. (2007) Hydrate sulfuric acid after ion implantation in water ice. *Icarus, 192,* 623–628.
Swallow A. J. (1973) *Radiation Chemistry.* Wiley and Sons, New York.
Tegler S. C., Grundy W. M., Romanishin W., Consolmagno G. J., Mogren K., Vilas F. (2007) Optical spectroscopy of the large Kuiper Belt objects 136472 (2005 FY_9) and 136108 (2003 EL_{61}). *Astron. J., 133,* 526–530.
Teolis B. D., Vidal R. A., Loeffler M. J., and Baragiola R. A. (2005a) Radiolysis and trapping of O_2 and O_3 in water ice. *Bull. Am. Astron. Soc., 37,* 774.
Teolis B. D., Vidal R. A., Shi J., and Baragiola R. A. (2005b) Mechanisms of O_2 sputtering from water ice by keV ions. *Phys. Rev. B, 72,* 245422-1-9.
Teolis B. D., Loeffler M. J., Raut U., Famá M., and Baragiola R. A. (2006) Ozone synthesis on the icy satellites. *Astrophys. J. Lett., 644,* L141–L144.
Tiscareno M. S. and Geissler P. E. (2003) Can redistribution of material by sputtering explain the hemispheric dichotomy of Europa? *Icarus, 161,* 90–101.
Trafton L. (1981) A survey of Io's potassium cloud. *Astrophys. J., 247,* 1125–1140.
Tsai S. C. and Robinson G. W. (1969) Why is condensed oxygen blue? *J. Chem. Phys., 51,* 3559–3568.
van der Zwet G. P., Allamandola L. J., Baas F., and Greenberg J. M. (1985) Laboratory identification of the emission features near 3.5 μm in the pre-main-sequence star HD97048. *Astron. Astrophys., 145,* 262–268.
Varnes E. S. and Jakosky B. M. (1999) Lifetime of organic molecules at the surface of Europa. In *Lunar and Planetary Science XXX,* Abstract #1082. Lunar and Planetary Institute, Houston (CD-ROM).
Vidal R. A., Bahr D., Baragiola R. A., and Peters M. (1997) Oxygen on Ganymede: Laboratory studies. *Science, 276,* 1839–1842.
Voegele A. F., Loerting T., Tautermann C. S., Hallbrucker A., Mayer E., and Liedl K. R. (2004) Sulfurous acid (H_2SO_3) on Io? *Icarus, 169,* 242–249.
Volwerk M., Kivelson M., and Khurana K. K. (2001) Wave activity in Europa's wake: Implications for ion pickup. *J. Geophys. Res., 106,* 26033–26048.
Volwerk M., Paranicas C., Kivelson M. G., and Khurana K. K. (2004) Europa's interaction with Jupiter's magnetosphere. *35th COSPAR Scientific Assembly,* Paris, p. 313.
Waite J. H., Combi M. R., Ip W.-H., Cravens T. E., McNutt R. L. J., and others (2006) Cassini ion and neutral mass spectrometer: Enceladus plume composition and structure. *Science, 311,* 1419–1422.
Wamsteker W. (1972) Narrowband photometry of the galilean satellites. *Comm. Lunar Planet. Lab., 167,* 171–177.
Wamsteker W., Kroes R. L., and Fountain J. A. (1973) On the surface composition of Io. *Icarus, 23,* 417–424.
Warren S. G. (1984) Optical constants of ice from the ultraviolet to the microwave. *Appl. Optics, 23,* 1206–1225.
Warren S. G. and Brandt R. E. (2008) Optical constants of ice from the ultraviolet to the microwave: A revised compilation. *J. Geophys. Res., 113,* D14220, DOI: 10.1029/2007JD009744.
Whalley E. (1968) Structures of ice and water as investigated by infrared spectroscopy. *Dev. Appl. Spectrosc., 6,* 277–296.
Whalley E. and Bertie J. E. (1967) Optical spectra of orientationally-disordered crystals I. Theory for translational lattice vibrations. *J. Chem. Phys., 46,* 1264–1270.
Wood B. E. and Roux J. A. (1982) Infrared optical properties of thin H_2O, NH_3, and CO_2 cryofilms. *J. Opt. Soc. Am., 72,* 720–728.
Wysocki S. (1986) γ-radiolysis of polycrystalline magnesium oxide. *J. Chem. Soc. Faraday Trans., 182,* 715–721.
Yakshinskiy B. V. and Madey T. E. (2001) Electron-and photon-stimulated desorption of K from ice surfaces. *J. Geophys. Res., 106,* 33303–33307.
Zahnle K., Dones L., and Levison H. F. (1998) Cratering rates on the galilean satellites. *Icarus, 136,* 202–222.
Zahnle K., Schenk P., Levison H., and Dones L. (2003) Cratering rates in the outer solar system. *Icarus, 163,* 263–289.
Zahnle K., Alvarellos J. L., Dobrovolskis A., and Hamill P. (2008)

Secondary and sesquinary craters on Europa. *Icarus, 194,* 660–674. DOI: 10.1016/j.icarus.(2007)10.024.

Zeleznik F. J. (1991) Thermodynamic properties of the aqueous sulfuric acid system to 350-K. *J. Phys. Chem. Ref. Data., 20,* 1157–1200.

Ziegler J. F., Biersack J. P., and U. Littmark (1985) *The Stopping and Range of Ions in Matter.* Pergamon, New York. Available online at http://www.srim.org/.

Zolotov M. (2008) Oceanic composition on Europa: Constraints from mineral solubilities. In Lunar and Planetary Science Conference XXXIX, Abstract #2349. Lunar and Planetary Institute, Houston (CD-ROM).

Zolotov M. Y. and Mironenko M. V. (2007) Chemical evolution of an early ocean on Europa: A kinetic-thermodynamic modeling. In *Workshop on Ices, Oceans, and Fire: Satellites of the Outer Solar System,* pp. 157–158. LPI Contribution No. 1357, Lunar and Planetary Institute, Houston.

Zolotov M. Y. and Shock E. L. (2001) Composition and stability of salts on the surface of Europa and their oceanic origin. *J. Geophys. Res., 106,* 32815–32827.

Zolotov M. Y. and Shock E. L. (2003) Energy for biologic sulfate reduction in a hydrothermally formed ocean on Europa. *J. Geophys. Res., 108,* 3-1 5022, DOI: 10.1029/2002JE001966.